UC Davis
UC Davis Electronic Theses and Dissertations

Title
Broad Spectrum Antiviral Activities of Recombinant Enhanced Antiviral Restrictors (REAVRs)

Permalink
https://escholarship.org/uc/item/7xv087p1

Author
Megawati, Anak Agung Dewi

Publication Date
2021

Peer reviewed|Thesis/dissertation

eScholarship.org Powered by the California Digital Library
University of California

Broad Spectrum Antiviral Activities of Recombinant Enhanced Antiviral Restrictors (REAVRs)

By

ANAK AGUNG DEWI MEGAWATI

DISSERTATION

Submitted in partial satisfaction of the requirements for the degree of

DOCTOR OF PHILOSOPHY

in

Microbiology

in the

OFFICE OF GRADUATE STUDIES

of the

UNIVERSITY OF CALIFORNIA

DAVIS

Approved:

Stefan Rothenburg, Chair

Priya Shah

Samuel L. Díaz-Muños

Committee in Charge

2021

Copyright

ANAK AGUNG DEWI MEGAWATI 2021

Dedication

This work is dedicated to my husband Alit, my daughter Nasya, my dad and my mentor Stefan

Acknowledgement

I would like to express my sincerest gratitude to all of the people who have helped me get to where I am today. First and foremost, I would like to thank my major professor, Dr. Stefan Rothenburg, for providing a good environment in the lab that allows me to work from a place of joy and love to science. His leadership style gave me opportunity to learn and grow, which led me to love science even more. I have great respect and love for Dr. Rothenburg, and I am looking forward to continuing working with him from Missouri. I would like to thank my committee members Dr. Priya Shah and Dr. Samuel L. Díaz-Muños, for their tremendous support and supervision during my studies. I am grateful for having them as my committee members. I would like to thank Dr. Priya Shah for providing the dengue virus and cell lines for my studies. Dr. Qizhi Gong for providing vesicular stomatitis virus and helping me to set up VSV infection and plaque assay. Dr. Pei Shi UTMB for providing SARS-CoV-2 mNeonGreen, Dr. Lark Coffey for providing Zika virus, and Dr. Thomas Dever NIH for providing GyrB-PKR constructs.

I would like to thank Rothenburg lab members for their support and friendship. I thank Dr. Greg Brennan for his guidance and friendship throughout my studies, Ryan and Jeannine for helping me with my writing, Ana and Shefali for helping with the SARS-CoV-2 infection, Julhasur, Chorong, Huibin and Chi for the friendship and all the fun together. We have so many happy memories which I will forever treasure.

I also would like to take this opportunity to thank MGG students, the Indonesian student association at UC Davis, the Indonesian community at Davis (Mas Bambang, Mbak Yanti, Mbak Irna, Bang Eben and Dea), and the Indonesian student association of

the University of Idaho and Washington State University, particularly Mbak Kiki, Mas Edwin, Andrew, Vivi, Bli Alit and Mbak Tri for their tremendous support during my lowest point when I was in Idaho. Their love and friendship warmed my heart and helped me get through the rough patch throughout my studies.

I also would like to thank the Rector of Warmadewa University (Prof. Widjana), Dean and Associate deans of School of Medicine (dr. Murdhana, dr. Darwata, dr. Sarmadi, and Kartika), department chair of Microbiology and Parasitology (Prof. Sutisna), and all my colleagues at the Warmadewa University. Thank you so much for your support throughout my studies. I would like to thank Sharon and Haywood Gray for always having my back since I was a kid. Woody is like a dad to me who guide me through this life journey. I would like to thank my Dad, my Mom, my brothers (Agung Widnyana and Agung Darmawan) and my sisters (Agung Cahya and Agung Putri) for their tremendous support and love. Lastly, I'd like to thank my husband Alit and my daughter Nasya. We have been through thick and thin together. No matter how hard life is, we always have each other's back. I am forever grateful for having both of you in my life.

Lastly, I like to thank the Indonesia endowment fund for education (LPDP) and the UC Davis graduate research award for providing funding for my studies and research.

Abstract

Broad Spectrum Antiviral Activities of Recombinant Enhanced Antiviral Restrictors (REAVRs)

Most virus families produce double-stranded (ds) RNA during their lifecycles, which can be sensed by multiple dsRNA-dependent innate immune sensors, including two potent host restriction factors OAS/RNase L and PKR. PKR mainly restricts replication of viruses that are dependent on eIF2, and RNase L inhibits viral replication via degradation of host and viral RNAs. However, while PKR is directly activated by dsRNA, RNase L activation depends on the OAS to both bind dsRNA and synthesize 2'-5' oligoadenylate (2-5A). We hypothesized that engineering proteins to combine the dsRNA sensor domain of PKR with the effector domain of RNase L would bypass the need for OAS activation, making them less susceptible to inhibition by viral molecules, and preserve their potent antiviral activity. To test this, we generated **R**ecombinant **E**nhanced **A**nti**v**iral **R**estrictors (REAVRs) by combining dsRNA-binding domains of PKR from different species with the effector domain of human RNase L. We show that REAVRs led to RNA degradation and decreased the activity of a luciferase reporter, suggesting the REAVRs are functionally active. To investigate whether REAVRs could restrict viral replication, we generated T-REx 293 cells containing a single REAVR copy under the control of a doxycycline-inducible promoter. Some REAVRs exerted potent antiviral activities against five tested viruses: vaccinia virus, dengue virus, Zika virus, SARS-CoV-2, and vesicular stomatitis virus. Importantly, these REAVRs were also effective against viruses that are resistant to

PKR activation, for example, SARS CoV-2 and flaviviruses. This study provides proof-of-concept that REAVRs are active *in vitro* and exhibit antiviral effects on various families of viruses. We envision that REAVRs can be used to generate transgenic organisms with increased viral resistance and represent promising candidates as therapeutics for viral infections.

Table of Contents

Acknowledgement iii

Abstract v

Table of Contents vii

List of Figures ix

List of Tables x

Chapter 1: Diverse strategies used by viruses to evade PKR and OAS/RNase L pathways 1

ABSTRACT 1
1. INTRODUCTION 1
2. DOUBLE STRANDED RNA-INDUCED PKR ACTIVATION 5
3. STRATEGIES DEVELOPED BY VIRUSES TO INHIBIT PKR 8
   a. Expression of viral antagonists *8*
      Class 1 antagonists: reduce dsRNA levels 9
      Class 2 antagonists: prevent PKR homodimerization by dsRNA binding and direct binding to PKR 9
      Class 3 antagonists: induce PKR degradation 10
      Class 4 antagonists: interfere with eIF2α phosphorylation 11
      Class 5 antagonists: induce dephosphorylation of p-eIF2α by recruiting the cellular phosphatase PP1 12
      Class 6 antagonists: inhibit p-eIF2α and eIF2B interaction. 13
   b. Non-canonical cap-independent viral protein synthesis *14*
4. DOUBLE STRANDED RNA-INDUCED OAS/RNASE L ACTIVATION 15
5. STRATEGIES DEVELOPED BY VIRUSES TO EVADE THE OAS/RNASE L PATHWAY 18
   a. Reducing dsRNA availability for OAS activation *19*
   b. 2-5A degradation *19*
   c. Inhibiting RNase L dimerization and activation *20*
   d. Viral genome adaptation *21*
   e. Escape from RNase L cleavage through unknown mechanism *22*
6. CONCLUDING REMARKS 23
REFERENCES 24

Chapter 2: Broad Spectrum Antiviral Activity of Recombinant Enhanced Antiviral Restrictors (REAVRs) 41

ABSTRACT 41
SIGNIFICANCE 42
INTRODUCTION 43
MATERIALS AND METHODS 47
   Cell lines *47*
   Plasmids *48*
   Luciferase-based reporter assays *49*
   Virus and infections *50*

Immunoblot analyses *52*
Flow Cytometry *54*
RNA degradation assay *55*
Cell viability test *55*
Statistical analysis and fold-change and a log reduction calculation *56*
RESULTS 57
Generation and functional analysis of recombinant enhanced antiviral restrictors (REAVRs) *57*
Expression of a single copy of each REAVR in T-REx™ stable cell line systems and its effect on cell viability *63*
Antiviral effects of REAVRs on vaccinia virus *66*
Antiviral effects of REAVRs on dengue virus and Zika virus *71*
Expression of REAVR 7 inhibits SARS-CoV-2 replication *74*
Antiviral effects of REAVRs on vesicular stomatitis virus *77*
DISCUSION 81
REFERENCES 86

Chapter 3: Species Specificity of Primate Protein Kinase R Inhibition by Tanapox and Yaba Monkey Tumor Virus K3 Orthologs 94

ABSTRACT 94
INTRODUCTION 95
MATERIALS AND METHODS 99
Cell lines *99*
Plasmids *100*
Luciferase-based reporter assays *100*
Virus and infections *101*
PCR of viral genomic DNA *102*
Immunoblot analyses *103*
PKR phylogenetic tree *105*
RESULTS 106
Amino acid differences between Yatapoxvirus K3 orthologs *106*
Yatapoxvirus K3 orthologs inhibit primate PKR in a species-specific manner *107*
Differential PKR inhibition is governed by the C-terminus of yatapoxvirus K3 orthologs *110*
Chimeric viruses expressing Tanapox K3 or Yaba Monkey Tumor Virus K3 display cell type specific differences in plaque formation *111*
TPV K3 rescued chimeric virus replication more efficiently than YMTV K3 in primate-derived cell lines. *114*
Replication of chimeric viruses in T-REx PKR^{KO} stable cells expressing primate PKR. *116*
DISCUSSION 119
REFERENCES 125

List of Figures

Figure 1. 1. Double-stranded RNA (dsRNA) sensing by the innate immune system. 4
Figure 1. 2. Strategies by viruses to inhibit the PKR pathway. 6
Figure 1. 3. Strategies developed by viruses to evade the OAS/RNase L pathway. 17

Figure 2. 1. Optimization of GyrB-RNase L fusion proteins. 58
Figure 2. 2. Generation of REAVR constructs and functional analysis of REAVRs in transient transfection assays. 62
Figure 2. 3. Stable expression of single copy REAVRs in T-REx cells under doxycycline control. 65
Figure 2. 4. Antiviral effects of REAVRs against vaccinia virus. 67
Figure 2. 5. Antiviral effects of REAVRs on vaccinia virus in Flp-In T-REx 293 PKR^{KO} (T-REX PKR^{KO}). 69
Figure 2. 6. Antiviral effects of REAVRs against dengue virus and Zika virus. 72
Figure 2. 7. Antiviral effects of REAVR 7 against SARS-CoV-2. 76
Figure 2. 8. Antiviral effects of REAVRs against vesicular stomatitis virus strain VSV-12'GFP. 78
Figure 2. 9. eIF2α phosphorylation and rRNA degradation status after VSV-12'GFP infection. 79

Figure 3. 1. Multiple sequence alignment of VACV K3, TPV K3, and YMTV K3 orthologs. 106
Figure 3. 2. Differential sensitivities of tested PKRs to VACV K3, TPV K3, and YMTV K3 orthologs. 108
Figure 3. 3. Identification of region of TPV K3 and YMTV K3 orthologs that confer differential PKR inhibition. 111
Figure 3. 4. Generation of chimeric VC-R4 expressing yatapoxvirus K3 orthologs. 112
Figure 3. 5. Virus titer of chimeric vaccinia viruses in primate-derived cell lines. 115
Figure 3. 6. Generation of stable T-REx PKR^{KO} cells expressing primate PKR. 117
Figure 3. 7. Infection of stable T-REx PKRKO cells expressing primate PKR with chimeric viruses. 118

List of Tables

Table 1. 1. Viral RNA structures that potentially activate dsRNA innate immune sensors 2

Table 2. 1. Differential sensitivity of Syrian hamster and mouse PKR to viral antagonists. 60
Table 2. 2. Fold reduction in virus titers after induction of REAVR expression. 80

Table 3. 1. Accession numbers of genes used for phylogenetic analyses. 124

Chapter 1: Diverse strategies used by viruses to evade PKR and OAS/RNase L pathways

Dewi Megawati[1], Ryan C. Bruneau[1], Greg Brennan[1], Stefan Rothenburg [1]

1. Department of Medical Microbiology and Immunology, School of Medicine, University of California, Davis, California, USA

ABSTRACT

Protein kinase R (PKR) and 2',5'-oligoadenylate synthetase (OAS)/RNase L are potent antiviral proteins that act as both as sensors and effectors in response to viral infections. Both pathways are activated by double-stranded RNA produced during virus replication, yet they exert distinct antiviral activities. While PKR mainly restricts replication of viruses that depend on eIF2 for the synthesis of viral proteins, RNase L displays broad antiviral activity via host and viral RNA degradation. The critical role played by the PKR and OAS/RNase L pathways is emphasized by the many ways that viruses have evolved mechanisms to overcome the antiviral effects of these two pathways. In this review, we describe the mechanism of PKR and OAS/RNase L activation, how they exert their antiviral activities, and propose a new classification of diverse strategies evolved by viruses to antagonize PKR and OAS/RNase L pathways.

1. INTRODUCTION

An effective host immune response against viral infections depends on recognizing viral invasion by the innate immune system as the first line of defense. Sensing of viral infection by innate immunity is mediated through the recognition of pathogen-associated

molecular patterns (PAMPs) by host pattern recognition receptors (PRRs). One of the best-characterized PAMPs during viral infections is double-stranded RNA (dsRNA). Almost all viruses, including dsRNA viruses, both positive- and negative-stranded RNA viruses, and DNA viruses produce dsRNA during their lifecycle (1, 2). The origin of the dsRNA structures for RNA viruses could be the genome of dsRNA viruses, hybrids of RNA of opposite polarity generated during genome replication, and transcription or intramolecular secondary structures within ssRNA molecules (Table 1.1) (3). For DNA viruses, dsRNA can be derived from convergent bidirectional transcription, resulting in overlapping RNA formation (4). In addition, dsRNA sensors can also recognize long RNA with secondary structure or 5'ppp plus structured short ssRNA (3).

Table 1. 1. Viral RNA structures that potentially activate dsRNA innate immune sensors

Genome	Virus	Origin of dsRNA	References
dsDNA	Vaccinia virus Herpes simplex virus Adenovirus	Overlapping converging transcription	(1, 4-6)
dsDNA	HIV-1	TAR RNA possibly as dimer	(7)
dsRNA	Reovirus Rotavirus	dsRNA genome	(1, 8)
+ssRNA	Sindbis virus Dengue virus West Nile virus Japanese encephalitis virus Zika virus Hepatitis C Mouse hepatitis virus SARS-CoV, Encephalomyocarditis virus Polio virus Theiler murine virus	Replication intermediates or complementary based paired secondary structure elements	(1, 2, 9-11)
-ssRNA (segmented)	Influenza A virus	Panhandle structure of vRNA	(2)

-ssRNA (non-segmented)	Vesicular stomatitis virus	Replication intermediates or based paired secondary structure elements	(2, 11)

There are two categories of dsRNA innate immune sensors. The first category of dsRNA sensors comprises PRRs that, upon sensing dsRNA, upregulate the expression of antiviral effector proteins, chemokines, and cytokines (Figure 1.1) (12). The antiviral response by this first category of dsRNA innate immune sensors is dominated by type I IFN, and IFN stimulated genes (ISGs). This first category of dsRNA innate immune sensors comprises the family of RIG-I-like receptors (RLRs) and Toll-like receptor 3. The RLR family consists of the retinoic-inducible gene I (RIG-I), melanoma differentiation-associated gene 5 (MDA5), and laboratory of genetics and physiology 2 (LPG2). The RLRs helicase families are ubiquitously expressed in the cytoplasm and recognize distinct types of dsRNA (11). MDA5 recognizes long dsRNA >300bp independent of 5' triphosphate, while RIG-I preferentially bind to short dsRNA (13). Upon binding of dsRNA, MDA5 and RIG-I associate with mitochondrial antiviral signaling protein (MAVS) through its tandem caspase activation and recruitment domains (CARDs) (14). Activated MAVS phosphorylates the IκB kinase (IKK) complex, leading to the release of transcription factor NF-κB and IRF3/IRF7 into the nucleus to induce expression of pro-inflammatory cytokines and type I IFNs, respectively (Figure 1.1). Unlike MDA5 and RIG-I, LPG2 lacks tandem CARD domains, thus it is unable to interact with MAVS. LPG2 has been shown to recognize short dsRNA similarly to RIG-I and to modulate MAVS and RIG-I activation (15). Toll-like receptor 3 (TLR3) recognizes both short and long dsRNA in endosomes (12). Upon binding of dsRNA, TLR3 signals through myeloid differentiation primary response protein 88 (MYD88) and TIR domain-containing adaptor protein (TRIF) resulting

in pro-inflammatory cytokines and type I IFN induction (16). Type I IFNs bind to the IFN receptors (IFNAR1 and IFNAR2) present on the infected cells' surface and neighboring cells. Binding of type I IFNs to IFN receptors triggers a JAK-STAT signaling pathway, which leads to the expression of hundreds of IFN-stimulated genes (ISGs). ISGs further activate antiviral states in the infected cells and neighboring cells, as well as recruiting immune cells to the site of infection (17). Taken together, activation of these innate immune pathways orchestrates cellular antiviral states and commences host immune responses during viral infections.

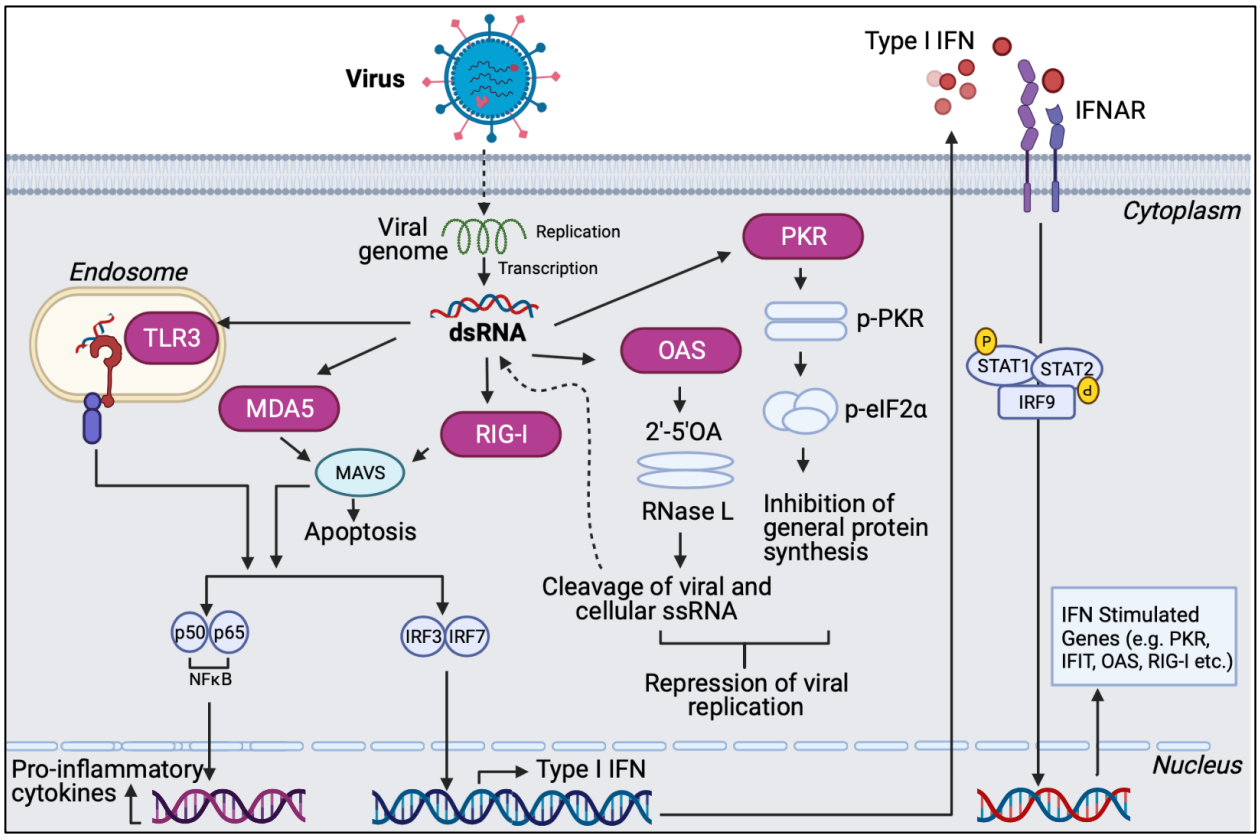

Figure 1. 1. Double-stranded RNA (dsRNA) sensing by the innate immune system.
Viral dsRNA is recognized as a pathogen associated molecular pattern (PAMP) by dsRNA innate immune sensing pathways in the cytosol and in endosomes. Viral dsRNA in the endosome is detected by TLR3. MDA5 and RIG-I detect dsRNA in the cytosol and signal via MAVS to induce type-I IFN and proinflammatory production and to promote apoptosis. These receptors signal via IRF3-IRF7 to induce type-I IFN production and via nuclear factor-κB (NF-κB) to induce proinflammatory cytokines and chemokines. OAS and PKR sense dsRNA in cytosol. Binding of dsRNA activates OAS to produce of 2'-5' oligoadenylates (2-5A), which promotes RNase L dimerization and activation. The OAS/RNase L pathway blocks viral infections through

degradation of viral and cellular single strand RNAs. In addition, RNase L activity produces cleaved RNAs that can amplify IFN signaling through activation of RIG-I. Activated PKR confers direct antiviral activity, by phosphorylating the alpha subunit of eukaryotic initiation factor (eIF2α) resulting in inhibition of general protein synthesis and thereby repress virus replication. Activation of these dsRNA immune sensing receptors further promote expression of type-I IFN which enhances an antiviral immune response through induction of IFN-stimulated genes. The graphic was created using Biorender.com.

The second category of dsRNA sensors comprises dsRNA-sensing pathways that act both as sensors and effectors in response to viral infections, for example protein kinase R (PKR) and oligoadenylate synthases/RNase L (OAS/RNase L) pathways. Upon dsRNA recognition, these two pathways directly inhibit viral replication by inhibiting general protein synthesis and cleavage of host and viral RNA (13). Notably, PKR and OAS/RNase L pathways have been reported to overlap with the RLR pathways. Specifically, activation of PKR has been implicated with NFκB signaling (18), and cleavage product of RNase L can form duplex RNA that are recognized by RIG-I and MDA5 (19). This review discusses the molecular basis and mechanism of action of PKR and OAS/RNase L pathways in-depth and provides updated strategies evolved by viruses to evade PKR and OAS/RNase L pathways.

2. DOUBLE STRANDED RNA-INDUCED PKR ACTIVATION

PKR is one of five eIF2α kinases found in vertebrates (the other four kinases are PERK, GCN2, HRI, PKZ) that regulate protein synthesis via eIF2α phosphorylation (20). PKR is constitutively expressed in many cell types and tissues at intermediate and is upregulated by Type-I IFN (21, 22) . Human PKR consists of 551 amino acids and contains of two double-stranded RNA binding domains (dsRBD1 and dsRBD2) in its N-terminus, a flexible linker that connects the dsRBDs with the kinase domain, and the kinase domain in its C-terminal domain (23). The catalytic domain of PKR comprises a smaller N-terminal lobe and a larger C-terminal lobe connected by a short hinge. PKR is

thought to exist in a monomeric latent form, which was reported to be supported by intramolecular inhibitory interaction between the kinase domain and dsRBD2 (Figure 1.2) (24).

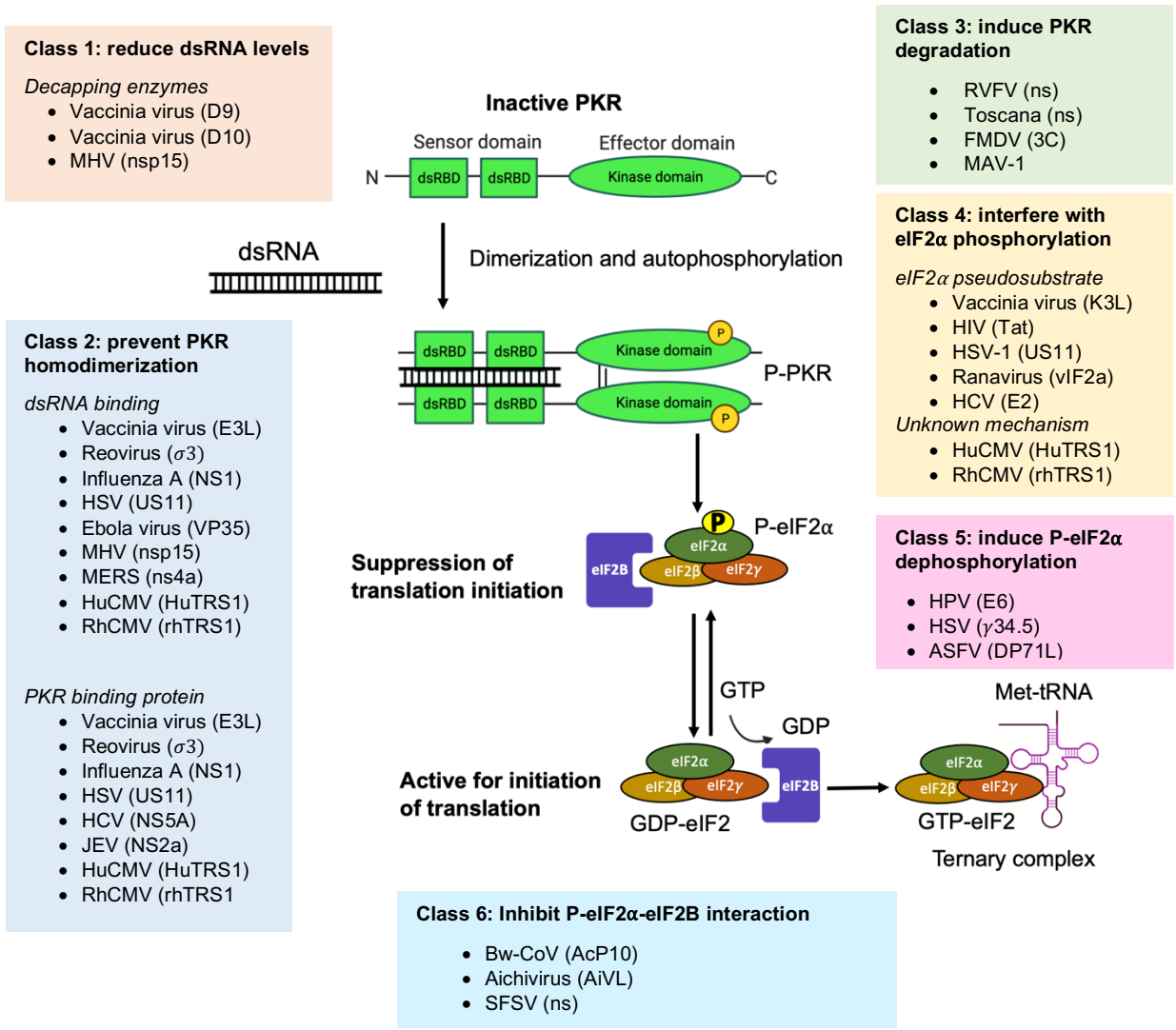

Figure 1. 2. Strategies by viruses to inhibit the PKR pathway.
PKR exists in monomeric latent form. Upon binding of dsRNA, PKR undergo dimerization and autophosphorylation. Activated PKR subsequently phosphorylates the eukaryotic translation initiation factor eIF2α. Phosphorylated eIF2α has high binding affinity to regulatory core of guanine nucleotide exchange factor, eIF2B, and prevents eIF2B from catalyzing the GTP-GDP exchange in eIF2. Low availability of GTP-eIF2 leads to inhibition of general protein synthesis including viral protein synthesis. Many viruses encode viral antagonists to evade PKR antiviral activity at each step of the PKR pathway by distinct mechanisms. We classified these viral antagonists into 6 classes based on their functions: reduce dsRNA levels, prevent PKR homodimerization, induce PKR degradation, interfere with eIF2α phosphorylation, induce P-eIF2α dephosphorylation, and inhibit P-eIF2α-eIF2B interaction.

PKR senses dsRNA in a sequence-independent manner and both dsRBDs are required for the high-affinity interaction with dsRNA (23, 25). The binding of dsRNA leads to PKR homodimerization and autophosphorylation (26) (Figure 1.2). PKR autophosphorylation occurs at multiple serine and threonine sites, including Ser242, Thr255, Thr258, Ser83, Thr88, Thr89, Thr90, Thr446, and Thr451 (26-28). Thr446 and Thr451 are consistently phosphorylated during PKR activation, with phosphorylation of Thr451 shown to be dependent on T446 phosphorylation (29). Further studies have shown that the catalytic-domain dimerization of PKR triggers Thr446 autophosphorylation and specific eIF2α recognition, emphasizing the importance of Thr446 as the major site of autophosphorylation (30) (31). The cellular substrate of the catalytic domain of PKR is Ser51 of eIF2α. Specific recognition of eIF2α is mediated primarily by a helix- αG located on the surface of the C-terminal lobe of the kinase domain (31).

PKR acts as an effector by decreasing global protein synthesis. Serine-threonine kinases tightly regulate phosphorylation of eIF2α in response to stress signals. During active translation, eIF2 binds GTP and Met-tRNAi to form the ternary complex (Figure 1.2). The ternary complex is then associated with the 40S ribosomal subunit and several eIF factors to form the 43S preinitiation complex (32). The 43-preinitiation complex recognizes specialized cap-binding complex at the 5' of the eukaryotic mRNAs, allowing the 43-preinitiation complex to scan the mRNA UTR for an AUG start codon. Various molecular events occur upon AUG recognition, starting with eIF2 hydrolysis of GTP to GDP with the help of the GTPase activating protein eIF5 and dissociation of EIF1, EIF1A, EIF2-GDP, EIF3, EIF5, and EIF5-B-GDP from the mRNA and 40s ribosomal subunit, followed by the joining of the 60S ribosomal subunit to the mRNA/40s complex and

elongation of the polypeptide chain (33). eIF2 remains bound to GDP in the presence of eIF5 acting as a GDP dissociation inhibitor (GDI) (34). To allow another round of initiation, eIF2B acts as a GDI displacement factor by replacing eIF5 and as a guanine exchange factor to exchange GDP for GTP on eIF2. Phosphorylation of eIF2α by PKR or other kinases stabilizes the binding of rate-limiting enzyme eIF2B to p-eIF2 and prevents the enzymatic activity of eIF2B from catalyzing GDP-GTP exchange (35). The accumulation of eIF2α-GDP limits the availability of the ternary complex, and therefore, causes a decrease in global protein synthesis (36). In addition to translational control, PKR has been reported to mediate apoptosis by regulating FADD and play a role in transcriptional control by interacting with stress-activated protein kinase family (p38, c-Jun N-terminal kinase) and IκB kinase (37).

3. STRATEGIES DEVELOPED BY VIRUSES TO INHIBIT PKR

PKR activation has deleterious effects on the replication of many viruses. For their survival, many viruses have developed strategies to overcome the antiviral effects of PKR. This review describes strategies developed by several families of viruses to evade the PKR pathway, including the expression of viral antagonists and activation of non-canonical cap-independent viral protein synthesis.

a. Expression of viral antagonists

A large number of viruses encode viral antagonists to circumvent PKR antiviral effects. With several new viral antagonists against PKR have been discovered, we classified these viral antagonists into 6 classes.

Class 1 antagonists: reduce dsRNA levels

VACV encodes two decapping enzymes (D9 and D10) that remove 5' caps on mRNAs. Uncapped mRNAs are susceptible to degradation by the host exonuclease Xrn1 (38). Thus, D9 and D10 decapping enzymes act coordinately with Xrn1 to prevent dsRNA accumulation and inhibit PKR and OAS/RNase L activation (39). BALB/c mice infected with a high dose of wild type VACV WR strain showed severe weight loss and succumbed on day 8 post-infection while no weight loss and death occurred in mice infected with a D9 and D10 double knock out virus, indicating strong attenuation (39). In addition, endonucleases (EndoU) encoded by mouse hepatitis virus (MHV) nsp15 have been shown to prevent dsRNA accumulation (40). Infection with EndoU deficient MHV virus significantly increased the cytosolic dsRNA and triggered PKR and OAS/RNase L pathways (40).

Class 2 antagonists: prevent PKR homodimerization by dsRNA binding and direct binding to PKR

Vaccinia virus (VACV) E3 is arguably one of the most studied dsRNA binding viral proteins. E3 contains a Z-DNA binding domain in the N-terminus and a dsRNA binding domain in the C-terminus (41, 42). Infection of E3 deficient vaccinia virus (VACVΔE3L) leads to PKR activation and eIF2α phosphorylation, and the virus fails to replicate in HeLa cells, indicating the dsRNA-binding domain of E3 is required for productive infection in HeLa cells (43). E3 is a multifunctional protein that has been suggested to directly interact with PKR leading to heterodimer formation, and therefore, inhibiting PKR activation (44). Similar to E3, reovirus σ3 (45), influenza A virus (IAV) NS1 (46), herpes simplex virus 1

(HSV-1) US11 (47), human cytomegalovirus (HuCMV) TRS1 (48-50) and rhesus cytomegalovirus (RhCMV) rhTRS1 (50) have been shown to function as multifunctional proteins that can bind dsRNA as well as bind to PKR to inhibit PKR activity. It is interesting to note that CMV HuTRS1 and rhesus CMV RhTR1 appear to have different binding properties and activities. HuTRS1 can bind inactive human PKR and prevent its autophosphorylation (50). HuTRS1 also can bind to phosphorylated human PKR and prevent eIF2α phosphorylation. In contrast, RhTRS1 cannot bind to inactive African green monkey PKR, but it can bind to phosphorylated African green monkey PKR and block eIF2α phosphorylation ((50), reviewed in (51).

Other viral antagonists have been shown to inhibit PKR by sequestering dsRNA, including Middle East Respiratory Coronavirus (MERS-CoV) ns4a (52) and Ebola virus VP35 (53). In addition, Japanese encephalitis virus (JEV) NS2A and hepatitis C virus (HCV) NS5A have been reported to interact with PKR directly and suppress eIF2α phosphorylation (54, 55).

Class 3 antagonists: induce PKR degradation

PKR degradation during virus infection was first described in HeLa cells infected with poliovirus. Both PKR and eIF2α are phosphorylated during poliovirus infection, yet the PKR level was significantly depleted (56). Further analysis has shown poliovirus-encoded proteases (2A and 3Cpro) are not responsible for the PKR degradation. Although the precise mechanism of PKR degradation remains elusive, the study has shown that the proteolysis of PKR requires divalent cations, RNA, and protein components (57). Two members of the bunyavirus family, Rift valley fever virus (RVFV) and Toscana virus NSs

can downregulate PKR with similar efficiency via proteasomal system (58-60). In contrast to poliovirus, foot and mouth disease virus (FMDV) 3Cpro has been shown to induce PKR degradation via lysosomal pathway (61). Interestingly, in mouse adenovirus 1 (MAV-1) infected cells, cellular proteasomes alone are responsible for PKR degradation as inhibiting proteasome resulted in reduced PKR depletion, whereas inhibiting cellular lysosomes had no effect (62), however the hypothetical viral protein behind this PKR degradation and it's mechanism of action is unknown.

Class 4 antagonists: interfere with eIF2α phosphorylation

Vaccinia virus encodes K3 that has been shown to act as pseudosubstrate of PKR (63). The S1 domain of K3, a homolog to eIF2α has been shown to interact with PKR and inhibit eIF2α phosphorylation (30, 31). K3L inhibits eIF2α phosphorylation without being phosphorylated itself (64). Orthologs of K3 protein are found in many genera of vertebrate poxviruses (Reviewed in Haller *et al.* (65) and Bratke *et al.* (66)). We and others have shown that inhibition of host PKR by K3 orthologs of several poxvirus families contribute to host-specificity (43, 67-71). Similar to VACV K3L, human CMV HuTRS1 and rhesus CMV RhTR1 also exhibit species specific PKR inhibition and prevent eIF2α phosphorylation. However, the mechanism of eIF2α phosphorylation inhibition by these two viral antagonists is currently unknown (50).

Ranaviruses encode viral (v) IF2α, which possess a S1 domain, which is homologous to eIF2α. vIF2a has been shown to act as pseudosubstrate of PKR in a manner comparable to VACV K3 (72). Both K3 and vIF2α are unable to block Thr446 phosphorylation and their binding to PKR is dependent on Thr446. Interestingly in a yeast

assay, vIF2α could effectively inhibit eIF2α phosphorylation by human and zebrafish PKR, whereas VACV K3 could only inhibit human PKR. Similar to K3 and vIF2α, HIV-1 trans-activating protein, Tat, has been shown to bind to PKR directly and act as a pseudosubstrate to eIF2α (73). However, in contrast to K3 and vIF2α, both the two-exon form (Tat-86) and the single exon form of Tat (Tat-72) are efficiently phosphorylated by PKR (74), leading to inhibition of cellular eIF2α phosphorylation and thereby allowing protein synthesis to resume (74). Like Tat, an in-vitro experiment showed that HSV-1 US11 inhibits eIF2α phosphorylation by providing an alternative substrate site for PKR (75). In the context of virus infection, the studies showed that the activated PKR phosphorylates 3 amino acids of the US11, which are located adjacent to the 30 amino acid PKR binding domain (76). Pseudosubstrate activity was also reported for the HCV E2 envelope protein. The E2 protein contains a short amino acid stretch that show similarity to the eIF2α phosphorylation site (4 amino acids are identical) and to residues 83 to 90 in human PKR (8 amino acids are identical). Interestingly, PKR phosphorylation is not required for HCV E2 binding, and E2 appears to be not phosphorylated by PKR (77).

Class 5 antagonists: induce dephosphorylation of p-eIF2α by recruiting the cellular phosphatase PP1

Under stress conditions, eukaryotic cells downregulate protein synthesis through eIF2α phosphorylation. To recover from stress, cellular GADD34 protein binds to the protein phosphatase 1 (PP1) that promotes dephosphorylation of p-eIF2α (78). In addition to GADD34, mammalian cells express CReP protein that also interacts with PP1 to

maintain pools of active eIF2α in unstressed cells (79). Both GADD34 and CReP use their C-terminus domain to recruit PP1 and bind to eIF2α to promote specific p-eIF2α dephosphorylation. Several viruses encode viral antagonists homologous to the C terminal regions of cellular GADD34 and CReP, which functions like GADD34 and CReP (80). This type of viral antagonist was first reported to be encoded by the HSV γ34.5 gene. In the absence of the C-terminus of γ34.5 protein, eIF2α remained phosphorylated and late viral protein synthesis was inhibited (81). Similarly, African swine fever virus (ASFV) DP71L protein recruits PP1 to reverse p-eIF2α in infected cells (82). Other families of viruses were shown to encode viral antagonists, which share homology with the C-terminus of GADD34, including the canarypox virus (CNPV), macropoid herpes virus (MaHV), and Amsacta moorei entomopoxvirus (AmEPV) (80). Other mechanisms to mediate eIF2α dephosphorylation include through physically associating with GADD34/PP1 holophosphatase complex as demonstrated by human papillomavirus (HPV) type18 E6 protein (83) and induction of GADD34 expression by the coronavirus infectious bronchitis virus (IBV) (84).

Class 6 antagonists: inhibit p-eIF2α and eIF2B interaction.

Beluga whale coronavirus (Bw-CoV) encodes the AcP10 protein that has been shown to rescue global mRNA translation in the presence of p-eIF2α through competitively binding to eIF2B. Essentially, direct binding of AcP10 to eIF2B causes eIF2B to preferentially bind eIF2 over p-eIF2α, thereby allowing the translation to proceed (85). Similarly, AiVL protein of Aichi picornavirus was shown to evade cap-dependent translation suppression in a similar manner as AcP10 (85). Interestingly, nonstructural

protein (NSs) of bunyavirus Sandfly Fever Sicilian Virus (SFSV) was found to interact with p-eIF2α-eIF2B complex and modify the catalytic structure of eIF2B, thereby restoring the nucleotide exchange activity of eIF2B (86). However, two recent publications suggest a slightly different mechanism of eIF2B inhibition by SFSV NSs. The studies have shown that the interaction of SFSV NSs with eIF2B blocks p-eIF2α binding, thus protecting eIF2B function to recycle eIF2α (87, 88).

b. Non-canonical cap-independent viral protein synthesis

It is also worth discussing that some viruses evade antiviral effects of PKR without expressing viral antagonists to PKR. They can switch from cap-dependent to cap-independent mRNA translation when eIF2α is phosphorylated by several mechanisms (89, 90). Infections of some members of *Togaviridae* (e.g. chikungunya, Sindbis, and Semliki Forest virus) induce PKR activation and trigger PKR-dependent phosphorylation of eIF2α (91-93). Phosphorylation of eIF2α during chikungunya infection appears to induce the widespread shutoff of host cell protein synthesis (92). Sindbis virus subgenomic 26s mRNA translation is resistant to phosphorylated eIF2α. Genetic and biochemical data suggest that a highly stable RNA hairpin loop located downstream of the AUG initiator codon is necessary to promote efficient translation. Essentially, the downstream hairpin loop stalls the 40S ribosome and allows non-canonical eIF2 to deliver the Met-tRNAi to the initiation complex of 26S subgenomic Sindbis mRNA (91). Unlike eIF2, non-canonical eIF2 does not require GTP to bind the Met-tRNAi; thereby, non-canonical eIF2α provides an alternative mechanism to carry out mRNA translation in the presence of phosphorylated eIF2α (91).

Internal Ribosomal Entry Site (IRES)-driven translation is another mechanism of eIF2 independence for protein synthesis initiation. IRESs are complex RNA structure located at 5' of mRNA or in the intergenic region of a polycistronic mRNA that can efficiently recruit 40s ribosomal subunit through a cap-independent mechanism (94). IRESs were originally discovered in uncapped picornavirus genomes, encephalomyocarditis virus (EMCV) and poliovirus (95, 96). These picornaviruses control their translation strictly through IRESs where the 43S ribosome is recruited by an eIF4G/eIF4A complex (95, 96). IRES of cricket paralysis virus can initiate mRNA translation in the absence of Met-tRNAi, eIF2 or GTP hydrolysis (97). However, IRES-driven translation is not exclusively used by uncapped viruses as the 5'UTR of capped DENV and ZIKV were shown to function as IRESs to facilitate mRNA translation when the canonical cap-dependent translation is inhibited (90). Other mechanisms have been proposed to modulate DENV translation when the canonical cap-dependent translation was inhibited, including binding of PABP to non-polyadenylated 3' UTR (98) and activation of the p38-Mnk1 signaling pathway (99).

4. DOUBLE STRANDED RNA-INDUCED OAS/RNASE L ACTIVATION

Like PKR, OAS/RNase L is an IFN-inducible antiviral system in vertebrate cells that is upregulated by IFN and activated in response to dsRNA produced during viral infections (100, 101). In the OAS/RNase L pathway, sensing of viral dsRNA by OAS leads to catalytic activation of OAS to convert ATP to secondary messenger 2-5A, short oligoadenylates with unconventional 2'-5' linkages (Figure 1.3) (102, 103). 2-5A is an unstable molecule that can be degraded by phosphatases and phosphodiesterase (103).

There are four OAS genes (OAS1, OAS2, OAS3, and OAS-like (OASL)) in humans encoded by OAS family genes. The first three OAS differ in their number of OAS domains, level of oligomerization, and type of synthesized 2-5A (104). Whereas OASL is catalytically inactive and does not synthesize 2-5A, however activation of OASL by dsRNA is required to enhance RIG-I signaling (105).

The 2-5A produced by OAS is a potent activator of RNase L (101). Human RNase L is a 741-amino-acid latent endoribonuclease ubiquitously expressed in the cytoplasm (101) and mitochondria (106). The structure of RNase L consists of 3 domains: a 9 ankyrin repeat (R1-R9) containing domain in its N-terminus, a catalytically inactive pseudokinase domain, and an endoribonuclease domain in its C-terminus (107). The crystal structures of human RNase L (108, 109) and porcine RNase L (110) further uncovered the function of the RNase L domains. The x-ray crystal structures of the RNase L showed direct binding of 2-5A to R2-R4 of the ankyrin repeats domain and leads to conformational change and dimerization of latent RNase L (108-110). The pseudokinase and RNase domains of RNase L are homologous with the serine/threonine-endoribonuclease IRE1, which drives the unfolded protein response at the ER membrane (107). Although the pseudokinase of RNase L has shown to have no kinase activity, the pseudokinase domain of RNase L is essential for 2-5A sensing, nucleotide (ADP/ATP) binding, dimerization, and cleavage functions of RNase L (109, 110). Active endoribonuclease RNase L cleaves ssRNA, both host and viral RNA, after UpN dinucleotide (111) as well as UpU and UpA dinucleotide recognition (112). However, later structural and biochemical studies support that RNase L cleaves ssRNA at the consensus sequence UN^N (N=A,U,G, or C; ^ is the cleavage site) (109, 113). In vitro assays and rRNA

cleavage assays indicated that a R462Q mutation impairs RNase L dimerization and R667A or H672A substitution inhibits the catalytic activity of RNase L (107). Further structural and biochemical analyses identified several mutations that could affect human RNase L activation, including R163A (ankyrin repeat domain), R412A and R427A (pseudokinase domain) and H672N (RNase domain) (109).

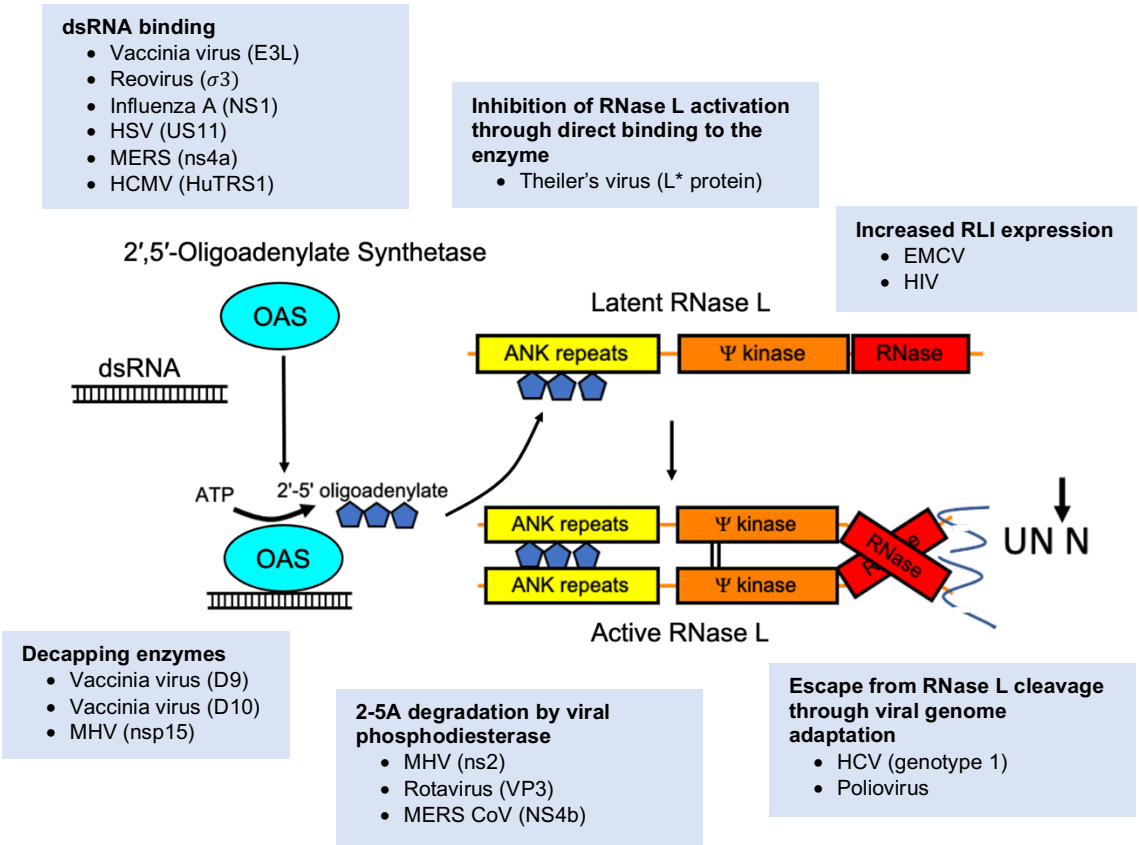

Figure 1. 3. Strategies developed by viruses to evade the OAS/RNase L pathway.
Viral dsRNA activates the catalytic site of OAS, which converts ATP into 2',5' oligoadenylates (2-5A). 2-5A then bind to ankyrin repeat domain of RNase L, which results in RNase L dimerization and activation. Active RNase L cleaves viral and cellular ssRNAs, directly inhibiting viral replication. Viruses developed various strategies to inhibit OAS/RNase L activation. Some viruses act upstream of the pathway by binding dsRNA and prevent OAS activation. Other mechanisms act to prevent RNase L activation including by expression of 2-5A phosphodiesterases that convert 2-5A into ATP and AMP, production of inactive or inhibitory 2-5A, expression of RLI/ABCE, and direct binding to the RNase L. Some viruses' genomes are inaccessible to RNase L because of their hairpin structures or reduced numbers of RNase L cleavage sites.

There are several proposed antiviral mechanisms of RNase L (reviewed in reference (104)). First, cleavage of the viral genome of ssRNA viruses due to the endonuclease activity of RNase L prevents viral genome replication (114). Second, inhibition of viral protein synthesis can occur through degradation of viral mRNA and host rRNA (115, 116) and inhibition of mRNA export (117). Upon binding of 2-5A to RNase L, RNase L interacts with eRF3, bringing RNase L to proximity to mRNA to act as endoribonuclease (118). In addition, formation of a RNase L-eRF3 complex has been shown to modulate translation termination by promoting ribosomal readthrough of the termination codon (119). The third method is by amplifying type I IFN production. Cleavage products of viral and cellular RNAs by RNase L can form duplex RNA, which amplify type I IFN productions through RIG-I, MDA5, and PKR activation (19, 120). Fourth, a cleavage product of RNase L activity, 2'3'-cyclic phosphorylated termini, activates the NLRP3 inflammasome to enhance IL-1β production (121). Fifth, in the absence of 2-5A, the monomeric latent form of RNase L interacts with Filamin A to modulate the actin cytoskeleton and inhibit virus entry independent of its usual enzymatic role (122). Sixth, RNase L activation cleaves Y-RNA and cytosolic tRNA, leading to arrest protein synthesis (113). Lastly, in the event of viral overload, RNase L can trigger a mitochondrial pathway of apoptosis to prevent viral dissemination (123).

5. STRATEGIES DEVELOPED BY VIRUSES TO EVADE THE OAS/RNASE L PATHWAY

Viruses have developed diverse strategies to evade the OAS/RNase L pathway (Figure 1.3). Some viruses inhibit the early stage of the OAS/RNase L pathway by

inhibiting OAS activation and promoting 2-5A degradation. Others inhibit OAS/RNase L pathway at a later stage by inhibiting RNase L dimerization and activation.

a. Reducing dsRNA availability for OAS activation

The presence of dsRNA activates the catalytic site of OAS to produce 2-5A from ATP. Several viruses encode viral antagonists to sequester dsRNA and thereby prevent OAS activation. Examples of proteins with this activity include vaccinia virus E3L (41), reovirus σ3 (124), influenza A virus NS1 (125), herpes simplex virus US11 (126), MERS-CoV NS4a (127), human cytomegalovirus (HuCMV) TRS1 (49) which are all covered in depth above.

VACV D9 and D10 decapping enzymes act coordinately with Xrn1 to prevent dsRNA accumulation and inhibit OAS/RNase L activation (39). MHV nsp15 encodes endonucleases (EndoU) that prevent dsRNA accumulation (40). Deletion EndoU in MHV leads to the increase of cytosolic dsRNA and activation of OAS/RNase L pathway as shown by increased rRNA degradation (40).

b. 2-5A degradation

The regulation of 2-5A degradation by phosphodiesterases and phosphatases is a key point of OAS/RNase L activation control (103). Some viruses have been shown to express phosphodiesterases that specifically cleave 2-5A, thus inhibiting RNase L activation. Unlike human phosphodiesterase that cleave 2-5A into ATP and 2 AMP, viral phosphodiesterases cleave trimeric 2-5A into mono- or deadenylates with 2’3’ cyclic phosphate termini (128). This phosphodiesterase activity was first described for mouse

hepatitis virus ns2 protein (129). In C57B6 mice, MHV ns2 is required for efficient viral replication in the liver and development of hepatitis, suggesting the importance of OAS/RNase L inhibition in establishing liver pathology (129). Other studies from the same group discovered the conserved expression of 2'5' phosphodiesterase by lineage A betacoronavirus (e.g. NS4b of MERS-CoV), toroviruses, and rotaviruses (e.g. rotavirus group A VP3) which are capable of antagonizing RNase L (128, 130, 131). Replacing ns2 of MHV with VP3 rotavirus can rescue the replication of recombinant MHV in macrophages and mouse liver, while MHV with an inactivated VP3 failed to replicate (132). Interestingly, both SARS-CoV and SARS-CoV-2 appear to lack phosphodiesterases (128, 133).

Promoting the synthesis of inactive 2-5A is another unique mechanism of OAS/RNase L evasion developed by viruses. A high concentration of 2-5A accumulation was observed during herpes simplex virus (HSV-1 and HSV-2), simian virus 40 (SV40) and vaccinia virus infections; nevertheless these 2-5A did not induce RNase L rRNA degradation through some unknown means (134-136).

c. Inhibiting RNase L dimerization and activation

RNase L inhibitor (RLI) represents the second control of RNase L besides 2-5A. RLI is a 68 kDa ATP binding cassette cellular protein also known as ABCE1 (137). RLI can form a heterodimer with RNase L, prevent 2-5A binding to RNase L, and therefore inhibit RNase L nuclease activity (137). An increase of RLI expression by the host cells was first observed in cells infected with encephalomyocarditis virus (EMCV) (137). The studies showed that expression of RLI in HeLa cells inhibits RNase L activity and partially

reverses the antiviral activity of IFN against EMCV (137). Similarly, overexpression of RLI in Hep-2 cells significantly decreased antiviral activity of RNase L against respiratory syncytial virus (RSV) (138). RLI expression was further shown in cells infected with HIV-1 (139). Besides interacting with RNase L, RLI appears to be critical for proper assembly of the HIV-1 capsid by interacting with the nucleocapsid domain of gag (140).

Theiler's murine encephalomyelitis virus (TMEV) expresses L* viral protein, which is required for chronic infection of the virus in the mouse central nervous system (141). Further analysis confirmed that L* protein directly binds to the ankyrin repeat domain of RNase L (142). Although L* does not target ankyrin repeat residues involved in 2-5A binding, binding of L* at R1-R2 site inhibits 2-5A binding to RNase L, thereby preventing RNase L homodimerization and activation (143). Using chimeric MHV lacking ns2 but expressing L* protein, the studies showed that L* protein expression rescued the virus replication in bone marrow-derived macrophages and the liver of infected mice, suggesting L* can functionally substitute for the phosphodiesterase ns2. Interestingly, RNase L inhibition by L* protein of TMEV is species-specific, where L* inhibited murine RNase L but not other species of RNase L, including human, equine, canine, porcine, bovine, guinea pig, or chicken RNase L (142).

d. Viral genome adaptation

Group C enteroviruses harbor a conserved RNA structure within their 3C protease gene, which is resistant to cleavage by RNase L and potently inhibits the antiviral endoribonuclease RNase L (144). The highly structured RNA associated with resistance to RNase L involved nucleotides 5742-5824 and nucleotides 5906-5967, at which the

complementary base pairs between sequences in the stem-loop 1 and 4 creates a pseudoknot or kissing interaction (145, 146). Further studies elucidated that the highly structured RNA of poliovirus can act as a competitive inhibitor of the endoribonuclease domain of RNase L (147). On the other hand, hepatitis C virus (HCV) from distinct genotypes have variably reduced UA and UU dinucleotides frequencies to evade RNase L cleavage activity (112). Deep sequencing methods revealed that RNase L predominantly cleaved poliovirus and HCV RNAs at UpN dinucleotides (UA and UU>UG) (148). Furthermore, the studies discover discrete regions in which poliovirus and HCV are susceptible to RNase L cleavage, whereas more structured RNA rendered the RNA resistant to RNase L cleavage (148).

e. Escape from RNase L cleavage through unknown mechanism

While the potent antiviral effects of RNase L are evident for most ssRNA viruses, vesicular stomatitis virus (VSV) is resistant to OAS/RNase L cleavage activity (149). Overexpression of OAS in murine NIH-3T3 cells impaired EMCV replication but did not affect VSV replication (150). Despite being highly sensitive to inhibition by IFN, VSV infection did not activate OAS, and no increase in 2-5A level was observed in infected cells (151). Similarly, no inhibition of the 2-5A binding activity of RNase L nor increased cellular RLI was observed during VSV infection (151). However, microinjection of 2-5A analogs in HeLa cells reduced VSV virus titer by 3-log (116). Interestingly, a recent study showed OAS1/RNase L exerted potent antiviral activity against +ssRNA viruses SARS-CoV-2 and EMCV, while three tested -ssRNA viruses (human respirovirus 3, RSV, and VSV) were unaffected by this pathway (152). Whether VSV and other -ssRNA viruses

produce a very small amount of dsRNA or mask dsRNA to reduce OAS activation, sequester 2-5A or express viral antagonists is largely unknown.

6. CONCLUDING REMARKS

In this review, we discussed PKR and OAS/RNase L pathways-mediated antiviral activities. PKR and OAS/RNase L pathways are potent antiviral proteins with overlapping yet distinct antiviral activities. We further presented strategies developed by diverse viruses to inhibit PKR and OAS/RNase L pathways. Some viruses appear to be resistant to these viral proteins by an unknown mechanism. Further investigation is required for elucidation of the mechanism behind virus resistance to PKR and OAS/RNase L pathways. In addition, some viruses' replications are independent of PKR activation, however sensitive to RNase L activity. The specific interaction between PKR and OAS/RNase L pathways and these viruses could be harnessed to establish effective strategies to prevent and control viral diseases

REFERENCES

1. Weber F, Wagner V, Rasmussen SB, Hartmann R, Paludan SR. Double-stranded RNA is produced by positive-strand RNA viruses and DNA viruses but not in detectable amounts by negative-strand RNA viruses. J Virol. 2006;80(10):5059-64. Epub 2006/04/28. doi: 10.1128/jvi.80.10.5059-5064.2006. PubMed PMID: 16641297; PMCID: PMC1472073.
2. Son KN, Liang Z, Lipton HL. Double-Stranded RNA Is Detected by Immunofluorescence Analysis in RNA and DNA Virus Infections, Including Those by Negative-Stranded RNA Viruses. J Virol. 2015;89(18):9383-92. Epub 2015/07/03. doi: 10.1128/jvi.01299-15. PubMed PMID: 26136565; PMCID: PMC4542381.
3. Dauber B, Wolff T. Activation of the Antiviral Kinase PKR and Viral Countermeasures. Viruses. 2009;1(3):523-44. Epub 2009/12/01. doi: 10.3390/v1030523. PubMed PMID: 21994559; PMCID: PMC3185532.
4. Colby C, Jurale C, Kates JR. Mechanism of synthesis of vaccinia virus double-stranded ribonucleic acid in vivo and in vitro. J Virol. 1971;7(1):71-6. Epub 1971/01/01. doi: 10.1128/jvi.7.1.71-76.1971. PubMed PMID: 5543434; PMCID: PMC356079.
5. Jacquemont B, Roizman B. RNA synthesis in cells infected with herpes simplex virus. X. Properties of viral symmetric transcripts and of double-stranded RNA prepared from them. J Virol. 1975;15(4):707-13. Epub 1975/04/01. doi: 10.1128/jvi.15.4.707-713.1975. PubMed PMID: 163916; PMCID: PMC354512.
6. Pettersson U, Philipson L. Synthesis of complementary RNA sequences during productive adenovirus infection. Proceedings of the National Academy of Sciences of the United States of America. 1974;71(12):4887-91. Epub 1974/12/01. doi: 10.1073/pnas.71.12.4887. PubMed PMID: 4612530; PMCID: PMC434004.
7. Heinicke LA, Wong CJ, Lary J, Nallagatla SR, Diegelman-Parente A, Zheng X, Cole JL, Bevilacqua PC. RNA dimerization promotes PKR dimerization and activation. J Mol Biol. 2009;390(2):319-38. Epub 2009/05/19. doi: 10.1016/j.jmb.2009.05.005. PubMed PMID: 19445956; PMCID: PMC2763119.
8. Richardson SJ, Willcox A, Hilton DA, Tauriainen S, Hyoty H, Bone AJ, Foulis AK, Morgan NG. Use of antisera directed against dsRNA to detect viral infections in formalin-fixed paraffin-embedded tissue. Journal of clinical virology : the official publication of the Pan American Society for Clinical Virology. 2010;49(3):180-5. Epub 2010/08/24. doi: 10.1016/j.jcv.2010.07.015. PubMed PMID: 20729142.
9. O'Brien CA, Hobson-Peters J, Yam AW, Colmant AM, McLean BJ, Prow NA, Watterson D, Hall-Mendelin S, Warrilow D, Ng ML, Khromykh AA, Hall RA. Viral RNA intermediates as targets for detection and discovery of novel and emerging mosquito-borne viruses. PLoS neglected tropical diseases. 2015;9(3):e0003629.

Epub 2015/03/24. doi: 10.1371/journal.pntd.0003629. PubMed PMID: 25799391; PMCID: PMC4370754.
10. Uchida L, Espada-Murao LA, Takamatsu Y, Okamoto K, Hayasaka D, Yu F, Nabeshima T, Buerano CC, Morita K. The dengue virus conceals double-stranded RNA in the intracellular membrane to escape from an interferon response. Sci Rep. 2014;4:7395. Epub 2014/12/11. doi: 10.1038/srep07395. PubMed PMID: 25491663; PMCID: PMC4261170.
11. Kato H, Takeuchi O, Mikamo-Satoh E, Hirai R, Kawai T, Matsushita K, Hiiragi A, Dermody TS, Fujita T, Akira S. Length-dependent recognition of double-stranded ribonucleic acids by retinoic acid-inducible gene-I and melanoma differentiation-associated gene 5. The Journal of experimental medicine. 2008;205(7):1601-10. Epub 2008/07/02. doi: 10.1084/jem.20080091. PubMed PMID: 18591409; PMCID: PMC2442638.
12. Bowie AG, Unterholzner L. Viral evasion and subversion of pattern-recognition receptor signalling. Nature reviews Immunology. 2008;8(12):911-22. Epub 2008/11/08. doi: 10.1038/nri2436. PubMed PMID: 18989317; PMCID: PMC7097711.
13. Schlee M, Hartmann G. Discriminating self from non-self in nucleic acid sensing. Nature reviews Immunology. 2016;16(9):566-80. Epub 2016/07/28. doi: 10.1038/nri.2016.78. PubMed PMID: 27455396; PMCID: PMC7097691
14. Hur S. Double-Stranded RNA Sensors and Modulators in Innate Immunity. Annu Rev Immunol. 2019;37:349-75. Epub 2019/01/24. doi: 10.1146/annurev-immunol-042718-041356. PubMed PMID: 30673536; PMCID: PMC7136661.
15. Uchikawa E, Lethier M, Malet H, Brunel J, Gerlier D, Cusack S. Structural Analysis of dsRNA Binding to Anti-viral Pattern Recognition Receptors LGP2 and MDA5. Molecular cell. 2016;62(4):586-602. Epub 2016/05/21. doi: 10.1016/j.molcel.2016.04.021. PubMed PMID: 27203181; PMCID: PMC4885022.
16. Vercammen E, Staal J, Beyaert R. Sensing of viral infection and activation of innate immunity by toll-like receptor 3. Clinical microbiology reviews. 2008;21(1):13-25. Epub 2008/01/19. doi: 10.1128/cmr.00022-07. PubMed PMID: 18202435; PMCID: PMC2223843.
17. Schneider WM, Chevillotte MD, Rice CM. Interferon-stimulated genes: a complex web of host defenses. Annu Rev Immunol. 2014;32:513-45. Epub 2014/02/22. doi: 10.1146/annurev-immunol-032713-120231. PubMed PMID: 24555472; PMCID: PMC4313732.
18. Yu H, Bruneau RC, Brennan G, Rothenburg S. Battle Royale: Innate Recognition of Poxviruses and Viral Immune Evasion. Biomedicines. 2021;9(7). Epub 2021/08/07. doi: 10.3390/biomedicines9070765. PubMed PMID: 34356829; PMCID: PMC8301327.

19. Malathi K, Dong B, Gale M, Jr., Silverman RH. Small self-RNA generated by RNase L amplifies antiviral innate immunity. Nature. 2007;448(7155):816-9. Epub 2007/07/27. doi: 10.1038/nature06042. PubMed PMID: 17653195; PMCID: PMC3638316.
20. Rothenburg S, Seo EJ, Gibbs JS, Dever TE, Dittmar K. Rapid evolution of protein kinase PKR alters sensitivity to viral inhibitors. Nat Struct Mol Biol. 2009;16(1):63-70. Epub 2008/12/02. doi: 10.1038/nsmb.1529. PubMed PMID: 19043413; PMCID: PMC3142916.
21. Kuhen KL, Samuel CE. Isolation of the interferon-inducible RNA-dependent protein kinase Pkr promoter and identification of a novel DNA element within the 5'-flanking region of human and mouse Pkr genes. Virology. 1997;227(1):119-30. Epub 1997/01/06. doi: 10.1006/viro.1996.8306. PubMed PMID: 9007065.
22. Das S, Ward SV, Tacke RS, Suske G, Samuel CE. Activation of the RNA-dependent protein kinase PKR promoter in the absence of interferon is dependent upon Sp proteins. The Journal of biological chemistry. 2006;281(6):3244-53. Epub 2005/12/13. doi: 10.1074/jbc.M510612200. PubMed PMID: 16339759.
23. Nanduri S, Carpick BW, Yang Y, Williams BR, Qin J. Structure of the double-stranded RNA-binding domain of the protein kinase PKR reveals the molecular basis of its dsRNA-mediated activation. Embo j. 1998;17(18):5458-65. Epub 1998/09/16. doi: 10.1093/emboj/17.18.5458. PubMed PMID: 9736623; PMCID: PMC1170871.
24. Li S, Peters GA, Ding K, Zhang X, Qin J, Sen GC. Molecular basis for PKR activation by PACT or dsRNA. Proceedings of the National Academy of Sciences of the United States of America. 2006;103(26):10005-10. Epub 2006/06/21. doi: 10.1073/pnas.0602317103. PubMed PMID: 16785445; PMCID: PMC1502496.
25. McKenna SA, Kim I, Liu CW, Puglisi JD. Uncoupling of RNA binding and PKR kinase activation by viral inhibitor RNAs. J Mol Biol. 2006;358(5):1270-85. Epub 2006/04/04. doi: 10.1016/j.jmb.2006.03.003. PubMed PMID: 16580685.
26. Romano PR, Garcia-Barrio MT, Zhang X, Wang Q, Taylor DR, Zhang F, Herring C, Mathews MB, Qin J, Hinnebusch AG. Autophosphorylation in the activation loop is required for full kinase activity in vivo of human and yeast eukaryotic initiation factor 2alpha kinases PKR and GCN2. Molecular and cellular biology. 1998;18(4):2282-97. Epub 1998/04/07. doi: 10.1128/mcb.18.4.2282. PubMed PMID: 9528799; PMCID: PMC121479.
27. Taylor DR, Lee SB, Romano PR, Marshak DR, Hinnebusch AG, Esteban M, Mathews MB. Autophosphorylation sites participate in the activation of the double-stranded-RNA-activated protein kinase PKR. Molecular and cellular biology. 1996;16(11):6295-302. Epub 1996/11/01. doi: 10.1128/mcb.16.11.6295. PubMed PMID: 8887659; PMCID: PMC231632.

28. Taylor DR, Tian B, Romano PR, Hinnebusch AG, Lai MM, Mathews MB. Hepatitis C virus envelope protein E2 does not inhibit PKR by simple competition with autophosphorylation sites in the RNA-binding domain. J Virol. 2001;75(3):1265-73. Epub 2001/01/11. doi: 10.1128/jvi.75.3.1265-1273.2001. PubMed PMID: 11152499; PMCID: PMC114032.
29. Zhang F, Romano PR, Nagamura-Inoue T, Tian B, Dever TE, Mathews MB, Ozato K, Hinnebusch AG. Binding of double-stranded RNA to protein kinase PKR is required for dimerization and promotes critical autophosphorylation events in the activation loop. The Journal of biological chemistry. 2001;276(27):24946-58. Epub 2001/05/05. doi: 10.1074/jbc.M102108200. PubMed PMID: 11337501.
30. Dey M, Cao C, Dar AC, Tamura T, Ozato K, Sicheri F, Dever TE. Mechanistic link between PKR dimerization, autophosphorylation, and eIF2alpha substrate recognition. Cell. 2005;122(6):901-13. Epub 2005/09/24. doi: 10.1016/j.cell.2005.06.041. PubMed PMID: 16179259.
31. Dar AC, Dever TE, Sicheri F. Higher-order substrate recognition of eIF2alpha by the RNA-dependent protein kinase PKR. Cell. 2005;122(6):887-900. Epub 2005/09/24. doi: 10.1016/j.cell.2005.06.044. PubMed PMID: 16179258.
32. Gebauer F, Hentze MW. Molecular mechanisms of translational control. Nature reviews Molecular cell biology. 2004;5(10):827-35. Epub 2004/10/02. doi: 10.1038/nrm1488. PubMed PMID: 15459663; PMCID: PMC7097087.
33. Sonenberg N, Hinnebusch AG. Regulation of translation initiation in eukaryotes: mechanisms and biological targets. Cell. 2009;136(4):731-45. Epub 2009/02/26. doi: 10.1016/j.cell.2009.01.042. PubMed PMID: 19239892; PMCID: PMC3610329.
34. Jennings MD, Pavitt GD. eIF5 has GDI activity necessary for translational control by eIF2 phosphorylation. Nature. 2010;465(7296):378-81. Epub 2010/05/21. doi: 10.1038/nature09003. PubMed PMID: 20485439; PMCID: PMC2875157.
35. Schoof M, Boone M, Wang L, Lawrence R, Frost A, Walter P. eIF2B conformation and assembly state regulate the integrated stress response. eLife. 2021;10. Epub 2021/03/11. doi: 10.7554/eLife.65703. PubMed PMID: 33688831; PMCID: PMC7990499.
36. Marintchev A, Ito T. eIF2B and the Integrated Stress Response: A Structural and Mechanistic View. Biochemistry. 2020;59(13):1299-308. Epub 2020/03/24. doi: 10.1021/acs.biochem.0c00132. PubMed PMID: 32200625; PMCID: PMC7189779.
37. Williams BR. Signal integration via PKR. Science's STKE : signal transduction knowledge environment. 2001;2001(89):re2. Epub 2001/12/26. doi: 10.1126/stke.2001.89.re2. PubMed PMID: 11752661.
38. Burgess HM, Mohr I. Cellular 5'-3' mRNA exonuclease Xrn1 controls double-stranded RNA accumulation and anti-viral responses. Cell Host Microbe. 2015;17(3):332-44. Epub 2015/03/15. doi: 10.1016/j.chom.2015.02.003. PubMed PMID: 25766294; PMCID: PMC4826345.

39. Liu SW, Katsafanas GC, Liu R, Wyatt LS, Moss B. Poxvirus decapping enzymes enhance virulence by preventing the accumulation of dsRNA and the induction of innate antiviral responses. Cell Host Microbe. 2015;17(3):320-31. Epub 2015/03/15. doi: 10.1016/j.chom.2015.02.002. PubMed PMID: 25766293; PMCID: PMC4359750.
40. Kindler E, Gil-Cruz C, Spanier J, Li Y, Wilhelm J, Rabouw HH, Züst R, Hwang M, V'Kovski P, Stalder H, Marti S, Habjan M, Cervantes-Barragan L, Elliot R, Karl N, Gaughan C, van Kuppeveld FJ, Silverman RH, Keller M, Ludewig B, Bergmann CC, Ziebuhr J, Weiss SR, Kalinke U, Thiel V. Early endonuclease-mediated evasion of RNA sensing ensures efficient coronavirus replication. PLoS Pathog. 2017;13(2):e1006195. Epub 2017/02/06. doi: 10.1371/journal.ppat.1006195. PubMed PMID: 28158275; PMCID: PMC5310923.
41. Chang HW, Jacobs BL. Identification of a conserved motif that is necessary for binding of the vaccinia virus E3L gene products to double-stranded RNA. Virology. 1993;194(2):537-47. Epub 1993/06/01. doi: 10.1006/viro.1993.1292. PubMed PMID: 8099244.
42. Kahmann JD, Wecking DA, Putter V, Lowenhaupt K, Kim YG, Schmieder P, Oschkinat H, Rich A, Schade M. The solution structure of the N-terminal domain of E3L shows a tyrosine conformation that may explain its reduced affinity to Z-DNA in vitro. Proceedings of the National Academy of Sciences of the United States of America. 2004;101(9):2712-7. Epub 2004/02/26. doi: 10.1073/pnas.0308612100. PubMed PMID: 14981270; PMCID: PMC365686.
43. Langland JO, Jacobs BL. The role of the PKR-inhibitory genes, E3L and K3L, in determining vaccinia virus host range. Virology. 2002;299(1):133-41. Epub 2002/08/09. doi: 10.1006/viro.2002.1479. PubMed PMID: 12167348.
44. Romano PR, Zhang F, Tan SL, Garcia-Barrio MT, Katze MG, Dever TE, Hinnebusch AG. Inhibition of double-stranded RNA-dependent protein kinase PKR by vaccinia virus E3: role of complex formation and the E3 N-terminal domain. Molecular and cellular biology. 1998;18(12):7304-16. Epub 1998/11/20. PubMed PMID: 9819417; PMCID: PMC109312.
45. Yue Z, Shatkin AJ. Double-stranded RNA-dependent protein kinase (PKR) is regulated by reovirus structural proteins. Virology. 1997;234(2):364-71. Epub 1997/08/04. doi: 10.1006/viro.1997.8664. PubMed PMID: 9268168.
46. Lu Y, Wambach M, Katze MG, Krug RM. Binding of the influenza virus NS1 protein to double-stranded RNA inhibits the activation of the protein kinase that phosphorylates the eIF-2 translation initiation factor. Virology. 1995;214(1):222-8. Epub 1995/12/01. doi: 10.1006/viro.1995.9937. PubMed PMID: 8525619.
47. Khoo D, Perez C, Mohr I. Characterization of RNA determinants recognized by the arginine- and proline-rich region of Us11, a herpes simplex virus type 1-encoded double-stranded RNA binding protein that prevents PKR activation. Journal of

virology. 2002;76(23):11971-81. doi: 10.1128/JVI.76.23.11971-11981.2002. PubMed PMID: 12414939.
48. Hakki M, Geballe AP. Double-stranded RNA binding by human cytomegalovirus pTRS1. J Virol. 2005;79(12):7311-8. Epub 2005/05/28. doi: 10.1128/jvi.79.12.7311-7318.2005. PubMed PMID: 15919885; PMCID: PMC1143672.
49. Marshall EE, Bierle CJ, Brune W, Geballe AP. Essential role for either TRS1 or IRS1 in human cytomegalovirus replication. J Virol. 2009;83(9):4112-20. Epub 2009/02/13. doi: 10.1128/jvi.02489-08. PubMed PMID: 19211736; PMCID: PMC2668495.
50. Child SJ, Brennan G, Braggin JE, Geballe AP. Species specificity of protein kinase r antagonism by cytomegalovirus TRS1 genes. J Virol. 2012;86(7):3880-9. Epub 2012/01/27. doi: 10.1128/jvi.06158-11. PubMed PMID: 22278235; PMCID: PMC3302489.
51. Rothenburg S, Brennan G. Species-Specific Host-Virus Interactions: Implications for Viral Host Range and Virulence. Trends in microbiology. 2020;28(1):46-56. Epub 2019/10/11. doi: 10.1016/j.tim.2019.08.007. PubMed PMID: 31597598; PMCID: PMC6925338.
52. Comar CE, Goldstein SA, Li Y, Yount B, Baric RS, Weiss SR. Antagonism of dsRNA-Induced Innate Immune Pathways by NS4a and NS4b Accessory Proteins during MERS Coronavirus Infection. mBio. 2019;10(2). Epub 2019/03/28. doi: 10.1128/mBio.00319-19. PubMed PMID: 30914508; PMCID: PMC6437052.
53. Leung DW, Prins KC, Borek DM, Farahbakhsh M, Tufariello JM, Ramanan P, Nix JC, Helgeson LA, Otwinowski Z, Honzatko RB, Basler CF, Amarasinghe GK. Structural basis for dsRNA recognition and interferon antagonism by Ebola VP35. Nat Struct Mol Biol. 2010;17(2):165-72. Epub 2010/01/19. doi: 10.1038/nsmb.1765. PubMed PMID: 20081868; PMCID: PMC2872155.
54. Tu YC, Yu CY, Liang JJ, Lin E, Liao CL, Lin YL. Blocking double-stranded RNA-activated protein kinase PKR by Japanese encephalitis virus nonstructural protein 2A. J Virol. 2012;86(19):10347-58. Epub 2012/07/13. doi: 10.1128/jvi.00525-12. PubMed PMID: 22787234; PMCID: PMC3457255.
55. Gale MJ, Jr., Korth MJ, Katze MG. Repression of the PKR protein kinase by the hepatitis C virus NS5A protein: a potential mechanism of interferon resistance. Clinical and diagnostic virology. 1998;10(2-3):157-62. Epub 1998/09/19. doi: 10.1016/s0928-0197(98)00034-8. PubMed PMID: 9741641.
56. Black TL, Safer B, Hovanessian A, Katze MG. The cellular 68,000-Mr protein kinase is highly autophosphorylated and activated yet significantly degraded during poliovirus infection: implications for translational regulation. J Virol. 1989;63(5):2244-51. Epub 1989/05/01. doi: 10.1128/jvi.63.5.2244-2251.1989. PubMed PMID: 2539516; PMCID: PMC250642.

57. Black TL, Barber GN, Katze MG. Degradation of the interferon-induced 68,000-M(r) protein kinase by poliovirus requires RNA. J Virol. 1993;67(2):791-800. Epub 1993/02/01. doi: 10.1128/jvi.67.2.791-800.1993. PubMed PMID: 7678306; PMCID: PMC237432.
58. Habjan M, Pichlmair A, Elliott RM, Overby AK, Glatter T, Gstaiger M, Superti-Furga G, Unger H, Weber F. NSs protein of rift valley fever virus induces the specific degradation of the double-stranded RNA-dependent protein kinase. J Virol. 2009;83(9):4365-75. Epub 2009/02/13. doi: 10.1128/jvi.02148-08. PubMed PMID: 19211744; PMCID: PMC2668506.
59. Ikegami T, Narayanan K, Won S, Kamitani W, Peters CJ, Makino S. Dual functions of Rift Valley fever virus NSs protein: inhibition of host mRNA transcription and post-transcriptional downregulation of protein kinase PKR. Annals of the New York Academy of Sciences. 2009;1171 Suppl 1(Suppl 1):E75-85. Epub 2009/09/16. doi: 10.1111/j.1749-6632.2009.05054.x. PubMed PMID: 19751406; PMCID: PMC3137120.
60. Kalveram B, Ikegami T. Toscana virus NSs protein promotes degradation of double-stranded RNA-dependent protein kinase. J Virol. 2013;87(7):3710-8. Epub 2013/01/18. doi: 10.1128/jvi.02506-12. PubMed PMID: 23325696; PMCID: PMC3624217.
61. Li C, Zhu Z, Du X, Cao W, Yang F, Zhang X, Feng H, Li D, Zhang K, Liu X, Zheng H. Foot-and-mouth disease virus induces lysosomal degradation of host protein kinase PKR by 3C proteinase to facilitate virus replication. Virology. 2017;509:222-31. Epub 2017/07/01. doi: 10.1016/j.virol.2017.06.023. PubMed PMID: 28662438; PMCID: PMC7126777.
62. Goodman DE, Pretto CD, Krepostman TA, Carnahan KE, Spindler KR. Enhanced Replication of Mouse Adenovirus Type 1 following Virus-Induced Degradation of Protein Kinase R (PKR). mBio. 2019;10(2). Epub 2019/04/25. doi: 10.1128/mBio.00668-19. PubMed PMID: 31015330; PMCID: PMC6479006.
63. Dar AC, Sicheri F. X-ray crystal structure and functional analysis of vaccinia virus K3L reveals molecular determinants for PKR subversion and substrate recognition. Molecular cell. 2002;10(2):295-305. Epub 2002/08/23. PubMed PMID: 12191475.
64. Davies MV, Elroy-Stein O, Jagus R, Moss B, Kaufman RJ. The vaccinia virus K3L gene product potentiates translation by inhibiting double-stranded-RNA-activated protein kinase and phosphorylation of the alpha subunit of eukaryotic initiation factor 2. J Virol. 1992;66(4):1943-50. Epub 1992/04/01. doi: 10.1128/jvi.66.4.1943-1950.1992. PubMed PMID: 1347793; PMCID: PMC288982.
65. Haller SL, Peng C, McFadden G, Rothenburg S. Poxviruses and the evolution of host range and virulence. Infect Genet Evol. 2014;21:15-40. Epub 2013/10/29. doi: 10.1016/j.meegid.2013.10.014. PubMed PMID: 24161410; PMCID: PMC3945082.

66. Bratke KA, McLysaght A, Rothenburg S. A survey of host range genes in poxvirus genomes. Infect Genet Evol. 2013;14:406-25. Epub 2012/12/27. doi: 10.1016/j.meegid.2012.12.002. PubMed PMID: 23268114; PMCID: PMC4080715.
67. Elde NC, Child SJ, Geballe AP, Malik HS. Protein kinase R reveals an evolutionary model for defeating viral mimicry. Nature. 2009;457(7228):485-9. Epub 2008/12/02. doi: 10.1038/nature07529. PubMed PMID: 19043403; PMCID: PMC2629804.
68. Peng C, Haller SL, Rahman MM, McFadden G, Rothenburg S. Myxoma virus M156 is a specific inhibitor of rabbit PKR but contains a loss-of-function mutation in Australian virus isolates. Proceedings of the National Academy of Sciences of the United States of America. 2016;113(14):3855-60. Epub 2016/02/24. doi: 10.1073/pnas.1515613113. PubMed PMID: 26903626; PMCID: PMC4833222.
69. Park C, Peng C, Brennan G, Rothenburg S. Species-specific inhibition of antiviral protein kinase R by capripoxviruses and vaccinia virus. Annals of the New York Academy of Sciences. 2019;1438(1):18-29. Epub 2019/01/16. doi: 10.1111/nyas.14000. PubMed PMID: 30644558.
70. Cao J, Varga J, Deschambault Y. Poxvirus encoded eIF2α homolog, K3 family proteins, is a key determinant of poxvirus host species specificity. Virology. 2020;541:101-12. Epub 2020/02/15. doi: 10.1016/j.virol.2019.12.008. PubMed PMID: 32056708.
71. Park C, Peng C, Rahman MJ, Haller SL, Tazi L, Brennan G, Rothenburg S. Orthopoxvirus K3 orthologs show virus- and host-specific inhibition of the antiviral protein kinase PKR. PLoS Pathog. 2021;17(1):e1009183. Epub 2021/01/15. doi: 10.1371/journal.ppat.1009183. PubMed PMID: 33444388; PMCID: PMC7840043.
72. Rothenburg S, Chinchar VG, Dever TE. Characterization of a ranavirus inhibitor of the antiviral protein kinase PKR. BMC Microbiol. 2011;11:56. Epub 2011/03/23. doi: 10.1186/1471-2180-11-56. PubMed PMID: 21418572; PMCID: PMC3068933.
73. McMillan NA, Chun RF, Siderovski DP, Galabru J, Toone WM, Samuel CE, Mak TW, Hovanessian AG, Jeang KT, Williams BR. HIV-1 Tat directly interacts with the interferon-induced, double-stranded RNA-dependent kinase, PKR. Virology. 1995;213(2):413-24. Epub 1995/11/10. doi: 10.1006/viro.1995.0014. PubMed PMID: 7491766.
74. Brand SR, Kobayashi R, Mathews MB. The Tat protein of human immunodeficiency virus type 1 is a substrate and inhibitor of the interferon-induced, virally activated protein kinase, PKR. The Journal of biological chemistry. 1997;272(13):8388-95. Epub 1997/03/28. doi: 10.1074/jbc.272.13.8388. PubMed PMID: 9079663.
75. Cassady KA, Gross M, Roizman B. The herpes simplex virus US11 protein effectively compensates for the gamma1(34.5) gene if present before activation of protein kinase R by precluding its phosphorylation and that of the alpha subunit of

eukaryotic translation initiation factor 2. J Virol. 1998;72(11):8620-6. Epub 1998/10/10. doi: 10.1128/jvi.72.11.8620-8626.1998. PubMed PMID: 9765401; PMCID: PMC110273.
76. Cassady KA, Gross M. The herpes simplex virus type 1 U(S)11 protein interacts with protein kinase R in infected cells and requires a 30-amino-acid sequence adjacent to a kinase substrate domain. J Virol. 2002;76(5):2029-35. Epub 2002/02/12. doi: 10.1128/jvi.76.5.2029-2035.2002. PubMed PMID: 11836380; PMCID: PMC135940.
77. Taylor DR, Shi ST, Romano PR, Barber GN, Lai MM. Inhibition of the interferon-inducible protein kinase PKR by HCV E2 protein. Science. 1999;285(5424):107-10. Epub 1999/07/03. doi: 10.1126/science.285.5424.107. PubMed PMID: 10390359.
78. Choy MS, Yusoff P, Lee IC, Newton JC, Goh CW, Page R, Shenolikar S, Peti W. Structural and Functional Analysis of the GADD34:PP1 eIF2α Phosphatase. Cell reports. 2015;11(12):1885-91. Epub 2015/06/23. doi: 10.1016/j.celrep.2015.05.043. PubMed PMID: 26095357; PMCID: PMC4489983.
79. Harding HP, Zhang Y, Scheuner D, Chen JJ, Kaufman RJ, Ron D. Ppp1r15 gene knockout reveals an essential role for translation initiation factor 2 alpha (eIF2alpha) dephosphorylation in mammalian development. Proceedings of the National Academy of Sciences of the United States of America. 2009;106(6):1832-7. Epub 2009/02/03. doi: 10.1073/pnas.0809632106. PubMed PMID: 19181853; PMCID: PMC2644123.
80. Rojas M, Vasconcelos G, Dever TE. An eIF2α-binding motif in protein phosphatase 1 subunit GADD34 and its viral orthologs is required to promote dephosphorylation of eIF2α. Proceedings of the National Academy of Sciences of the United States of America. 2015;112(27):E3466-75. Epub 2015/06/24. doi: 10.1073/pnas.1501557112. PubMed PMID: 26100893; PMCID: PMC4500263.
81. Chou J, Chen JJ, Gross M, Roizman B. Association of a M(r) 90,000 phosphoprotein with protein kinase PKR in cells exhibiting enhanced phosphorylation of translation initiation factor eIF-2 alpha and premature shutoff of protein synthesis after infection with gamma 134.5- mutants of herpes simplex virus 1. Proceedings of the National Academy of Sciences of the United States of America. 1995;92(23):10516-20. Epub 1995/11/07. doi: 10.1073/pnas.92.23.10516. PubMed PMID: 7479831; PMCID: PMC40642.
82. Rivera J, Abrams C, Hernáez B, Alcázar A, Escribano JM, Dixon L, Alonso C. The MyD116 African swine fever virus homologue interacts with the catalytic subunit of protein phosphatase 1 and activates its phosphatase activity. J Virol. 2007;81(6):2923-9. Epub 2007/01/12. doi: 10.1128/jvi.02077-06. PubMed PMID: 17215279; PMCID: PMC1865990.
83. Kazemi S, Papadopoulou S, Li S, Su Q, Wang S, Yoshimura A, Matlashewski G, Dever TE, Koromilas AE. Control of alpha subunit of eukaryotic translation initiation

factor 2 (eIF2 alpha) phosphorylation by the human papillomavirus type 18 E6 oncoprotein: implications for eIF2 alpha-dependent gene expression and cell death. Molecular and cellular biology. 2004;24(8):3415-29. Epub 2004/04/03. doi: 10.1128/mcb.24.8.3415-3429.2004. PubMed PMID: 15060162; PMCID: PMC381675.

84. Wang X, Liao Y, Yap PL, Png KJ, Tam JP, Liu DX. Inhibition of protein kinase R activation and upregulation of GADD34 expression play a synergistic role in facilitating coronavirus replication by maintaining de novo protein synthesis in virus-infected cells. J Virol. 2009;83(23):12462-72. Epub 2009/09/25. doi: 10.1128/jvi.01546-09. PubMed PMID: 19776135; PMCID: PMC2786722.
85. Rabouw HH, Visser LJ, Passchier TC, Langereis MA, Liu F, Giansanti P, van Vliet ALW, Dekker JG, van der Grein SG, Saucedo JG, Anand AA, Trellet ME, Bonvin A, Walter P, Heck AJR, de Groot RJ, van Kuppeveld FJM. Inhibition of the integrated stress response by viral proteins that block p-eIF2-eIF2B association. Nature microbiology. 2020;5(11):1361-73. Epub 2020/07/22. doi: 10.1038/s41564-020-0759-0. PubMed PMID: 32690955.
86. Wuerth JD, Habjan M, Kainulainen M, Berisha B, Bertheloot D, Superti-Furga G, Pichlmair A, Weber F. eIF2B as a Target for Viral Evasion of PKR-Mediated Translation Inhibition. mBio. 2020;11(4). Epub 2020/07/16. doi: 10.1128/mBio.00976-20. PubMed PMID: 32665273; PMCID: PMC7360930.
87. Schoof M, Wang L, Zachery Cogan J, Lawrence R, Boone M, Wuerth JD, Frost A, Walter P. Viral Evasion of the Integrated Stress Response Through Antagonistic eIF2-P Mimicry. bioRxiv. 2021:2021.06.07.447473. doi: 10.1101/2021.06.07.447473.
88. Kashiwagi K, Shichino Y, Osaki T, Sakamoto A, Nishimoto M, Takahashi M, Mito M, Weber F, Ikeuchi Y, Iwasaki S, Ito T. eIF2B-capturing viral protein NSs suppresses the integrated stress response. bioRxiv. 2021:2021.06.07.447466. doi: 10.1101/2021.06.07.447466.
89. Fernández-García L, Angulo J, Ramos H, Barrera A, Pino K, Vera-Otarola J, López-Lastra M. The internal ribosome entry site of the Dengue virus mRNA is active when cap-dependent translation initiation is inhibited. J Virol. 2020;95(5). Epub 2020/12/11. doi: 10.1128/jvi.01998-20. PubMed PMID: 33298544; PMCID: PMC8092825.
90. Song Y, Mugavero J, Stauft CB, Wimmer E. Dengue and Zika Virus 5' Untranslated Regions Harbor Internal Ribosomal Entry Site Functions. mBio. 2019;10(2). Epub 2019/04/11. doi: 10.1128/mBio.00459-19. PubMed PMID: 30967466; PMCID: PMC6456755.
91. Ventoso I, Sanz MA, Molina S, Berlanga JJ, Carrasco L, Esteban M. Translational resistance of late alphavirus mRNA to eIF2alpha phosphorylation: a strategy to overcome the antiviral effect of protein kinase PKR. Genes & development.

2006;20(1):87-100. Epub 2006/01/05. doi: 10.1101/gad.357006. PubMed PMID: 16391235; PMCID: PMC1356103.
92. White LK, Sali T, Alvarado D, Gatti E, Pierre P, Streblow D, Defilippis VR. Chikungunya virus induces IPS-1-dependent innate immune activation and protein kinase R-independent translational shutoff. J Virol. 2011;85(1):606-20. Epub 2010/10/22. doi: 10.1128/jvi.00767-10. PubMed PMID: 20962078; PMCID: PMC3014158.
93. Gorchakov R, Frolova E, Williams BR, Rice CM, Frolov I. PKR-dependent and -independent mechanisms are involved in translational shutoff during Sindbis virus infection. J Virol. 2004;78(16):8455-67. Epub 2004/07/29. doi: 10.1128/jvi.78.16.8455-8467.2004. PubMed PMID: 15280454; PMCID: PMC479073.
94. Martinez-Salas E, Francisco-Velilla R, Fernandez-Chamorro J, Embarek AM. Insights into Structural and Mechanistic Features of Viral IRES Elements. Front Microbiol. 2017;8:2629. Epub 2018/01/23. doi: 10.3389/fmicb.2017.02629. PubMed PMID: 29354113; PMCID: PMC5759354.
95. Jang SK, Kräusslich HG, Nicklin MJ, Duke GM, Palmenberg AC, Wimmer E. A segment of the 5' nontranslated region of encephalomyocarditis virus RNA directs internal entry of ribosomes during in vitro translation. J Virol. 1988;62(8):2636-43. Epub 1988/08/01. doi: 10.1128/jvi.62.8.2636-2643.1988. PubMed PMID: 2839690; PMCID: PMC253694.
96. Pelletier J, Sonenberg N. Internal initiation of translation of eukaryotic mRNA directed by a sequence derived from poliovirus RNA. Nature. 1988;334(6180):320-5. Epub 1988/07/28. doi: 10.1038/334320a0. PubMed PMID: 2839775.
97. Wilson JE, Pestova TV, Hellen CU, Sarnow P. Initiation of protein synthesis from the A site of the ribosome. Cell. 2000;102(4):511-20. Epub 2000/08/31. doi: 10.1016/s0092-8674(00)00055-6. PubMed PMID: 10966112.
98. Polacek C, Friebe P, Harris E. Poly(A)-binding protein binds to the non-polyadenylated 3' untranslated region of dengue virus and modulates translation efficiency. The Journal of general virology. 2009;90(Pt 3):687-92. Epub 2009/02/17. doi: 10.1099/vir.0.007021-0. PubMed PMID: 19218215.
99. Roth H, Magg V, Uch F, Mutz P, Klein P, Haneke K, Lohmann V, Bartenschlager R, Fackler OT, Locker N, Stoecklin G, Ruggieri A. Flavivirus Infection Uncouples Translation Suppression from Cellular Stress Responses. mBio. 2017;8(1). Epub 2017/01/12. doi: 10.1128/mBio.02150-16. PubMed PMID: 28074025; PMCID: PMC5225315.
100. Jacobsen H, Czarniecki CW, Krause D, Friedman RM, Silverman RH. Interferon-induced synthesis of 2-5A-dependent RNase in mouse JLS-V9R cells. Virology. 1983;125(2):496-501. Epub 1983/03/01. doi: 10.1016/0042-6822(83)90222-2. PubMed PMID: 6188272.

101. Zhou A, Hassel BA, Silverman RH. Expression cloning of 2-5A-dependent RNAase: a uniquely regulated mediator of interferon action. Cell. 1993;72(5):753-65. Epub 1993/03/12. doi: 10.1016/0092-8674(93)90403-d. PubMed PMID: 7680958.
102. Kerr IM, Brown RE. pppA2'p5'A2'p5'A: an inhibitor of protein synthesis synthesized with an enzyme fraction from interferon-treated cells. Proceedings of the National Academy of Sciences of the United States of America. 1978;75(1):256-60. Epub 1978/01/01. doi: 10.1073/pnas.75.1.256. PubMed PMID: 272640; PMCID: PMC411225.
103. Bisbal C, Silverman RH. Diverse functions of RNase L and implications in pathology. Biochimie. 2007;89(6-7):789-98. Epub 2007/04/03. doi: 10.1016/j.biochi.2007.02.006. PubMed PMID: 17400356; PMCID: PMC2706398.
104. Silverman RH. Viral encounters with 2',5'-oligoadenylate synthetase and RNase L during the interferon antiviral response. J Virol. 2007;81(23):12720-9. Epub 2007/09/07. doi: 10.1128/jvi.01471-07. PubMed PMID: 17804500; PMCID: PMC2169107.
105. Ibsen MS, Gad HH, Andersen LL, Hornung V, Julkunen I, Sarkar SN, Hartmann R. Structural and functional analysis reveals that human OASL binds dsRNA to enhance RIG-I signaling. Nucleic Acids Res. 2015;43(10):5236-48. Epub 2015/05/01. doi: 10.1093/nar/gkv389. PubMed PMID: 25925578; PMCID: PMC4446440.
106. Le Roy F, Silhol M, Salehzada T, Bisbal C. Regulation of mitochondrial mRNA stability by RNase L is translation-dependent and controls IFNalpha-induced apoptosis. Cell death and differentiation. 2007;14(8):1406-13. Epub 2007/04/14. doi: 10.1038/sj.cdd.4402130. PubMed PMID: 17431428.
107. Dong B, Niwa M, Walter P, Silverman RH. Basis for regulated RNA cleavage by functional analysis of RNase L and Ire1p. RNA (New York, NY). 2001;7(3):361-73. Epub 2001/05/03. doi: 10.1017/s1355838201002230. PubMed PMID: 11333017; PMCID: PMC1370093.
108. Tanaka N, Nakanishi M, Kusakabe Y, Goto Y, Kitade Y, Nakamura KT. Structural basis for recognition of 2',5'-linked oligoadenylates by human ribonuclease L. Embo j. 2004;23(20):3929-38. Epub 2004/09/24. doi: 10.1038/sj.emboj.7600420. PubMed PMID: 15385955; PMCID: PMC524351.
109. Han Y, Donovan J, Rath S, Whitney G, Chitrakar A, Korennykh A. Structure of human RNase L reveals the basis for regulated RNA decay in the IFN response. Science. 2014;343(6176):1244-8. Epub 2014/03/01. doi: 10.1126/science.1249845. PubMed PMID: 24578532; PMCID: PMC4731867.
110. Huang H, Zeqiraj E, Dong B, Jha BK, Duffy NM, Orlicky S, Thevakumaran N, Talukdar M, Pillon MC, Ceccarelli DF, Wan LC, Juang YC, Mao DY, Gaughan C, Brinton MA, Perelygin AA, Kourinov I, Guarne A, Silverman RH, Sicheri F. Dimeric

structure of pseudokinase RNase L bound to 2-5A reveals a basis for interferon-induced antiviral activity. Molecular cell. 2014;53(2):221-34. Epub 2014/01/28. doi: 10.1016/j.molcel.2013.12.025. PubMed PMID: 24462203; PMCID: PMC3974923.
111. Wreschner DH, McCauley JW, Skehel JJ, Kerr IM. Interferon action--sequence specificity of the ppp(A2'p)nA-dependent ribonuclease. Nature. 1981;289(5796):414-7. Epub 1981/01/29. doi: 10.1038/289414a0. PubMed PMID: 6162102.
112. Washenberger CL, Han JQ, Kechris KJ, Jha BK, Silverman RH, Barton DJ. Hepatitis C virus RNA: dinucleotide frequencies and cleavage by RNase L. Virus Res. 2007;130(1-2):85-95. Epub 2007/07/03. doi: 10.1016/j.virusres.2007.05.020. PubMed PMID: 17604869; PMCID: PMC2186174.
113. Donovan J, Rath S, Kolet-Mandrikov D, Korennykh A. Rapid RNase L-driven arrest of protein synthesis in the dsRNA response without degradation of translation machinery. RNA (New York, NY). 2017;23(11):1660-71. Epub 2017/08/16. doi: 10.1261/rna.062000.117. PubMed PMID: 28808124; PMCID: PMC5648034.
114. Li XL, Blackford JA, Hassel BA. RNase L mediates the antiviral effect of interferon through a selective reduction in viral RNA during encephalomyocarditis virus infection. J Virol. 1998;72(4):2752-9. Epub 1998/04/03. doi: 10.1128/jvi.72.4.2752-2759.1998. PubMed PMID: 9525594; PMCID: PMC109719.
115. Silverman RH, Skehel JJ, James TC, Wreschner DH, Kerr IM. rRNA cleavage as an index of ppp(A2'p)nA activity in interferon-treated encephalomyocarditis virus-infected cells. J Virol. 1983;46(3):1051-5. Epub 1983/06/01. doi: 10.1128/jvi.46.3.1051-1055.1983. PubMed PMID: 6190010; PMCID: PMC256583.
116. Hovanessian AG, Wood JN. Anticellular and antiviral effects of pppA(2'p5'A)n. Virology. 1980;101(1):81-90. Epub 1980/02/01. doi: 10.1016/0042-6822(80)90485-7. PubMed PMID: 6243832.
117. Burke JM, Gilchrist AR, Sawyer SL, Parker R. RNase L limits host and viral protein synthesis via inhibition of mRNA export. Science advances. 2021;7(23). Epub 2021/06/06. doi: 10.1126/sciadv.abh2479. PubMed PMID: 34088676; PMCID: PMC8177694.
118. Le Roy F, Laskowska A, Silhol M, Salehzada T, Bisbal C. Characterization of RNABP, an RNA binding protein that associates with RNase L. Journal of interferon & cytokine research : the official journal of the International Society for Interferon and Cytokine Research. 2000;20(7):635-44. Epub 2000/08/05. doi: 10.1089/107999000414817. PubMed PMID: 10926206.
119. Le Roy F, Salehzada T, Bisbal C, Dougherty JP, Peltz SW. A newly discovered function for RNase L in regulating translation termination. Nat Struct Mol Biol. 2005;12(6):505-12. Epub 2005/05/24. doi: 10.1038/nsmb944. PubMed PMID: 15908960.

120. Manivannan P, Siddiqui MA, Malathi K. RNase L Amplifies Interferon Signaling by Inducing Protein Kinase R-Mediated Antiviral Stress Granules. J Virol. 2020;94(13). Epub 2020/04/17. doi: 10.1128/jvi.00205-20. PubMed PMID: 32295917; PMCID: PMC7307175.
121. Chakrabarti A, Banerjee S, Franchi L, Loo YM, Gale M, Jr., Núñez G, Silverman RH. RNase L activates the NLRP3 inflammasome during viral infections. Cell Host Microbe. 2015;17(4):466-77. Epub 2015/03/31. doi: 10.1016/j.chom.2015.02.010. PubMed PMID: 25816776; PMCID: PMC4393362.
122. Malathi K, Siddiqui MA, Dayal S, Naji M, Ezelle HJ, Zeng C, Zhou A, Hassel BA. RNase L interacts with Filamin A to regulate actin dynamics and barrier function for viral entry. mBio. 2014;5(6):e02012. Epub 2014/10/30. doi: 10.1128/mBio.02012-14. PubMed PMID: 25352621; PMCID: PMC4217177.
123. Rusch L, Zhou A, Silverman RH. Caspase-dependent apoptosis by 2',5'-oligoadenylate activation of RNase L is enhanced by IFN-beta. Journal of interferon & cytokine research : the official journal of the International Society for Interferon and Cytokine Research. 2000;20(12):1091-100. Epub 2001/01/11. doi: 10.1089/107999000750053762. PubMed PMID: 11152576.
124. Huismans H, Joklik WK. Reovirus-coded polypeptides in infected cells: isolation of two native monomeric polypeptides with affinity for single-stranded and double-stranded RNA, respectively. Virology. 1976;70(2):411-24. Epub 1976/04/01. doi: 10.1016/0042-6822(76)90282-8. PubMed PMID: 1266045.
125. Min JY, Krug RM. The primary function of RNA binding by the influenza A virus NS1 protein in infected cells: Inhibiting the 2'-5' oligo (A) synthetase/RNase L pathway. Proceedings of the National Academy of Sciences of the United States of America. 2006;103(18):7100-5. Epub 2006/04/22. doi: 10.1073/pnas.0602184103. PubMed PMID: 16627618; PMCID: PMC1459024.
126. Sànchez R, Mohr I. Inhibition of cellular 2'-5' oligoadenylate synthetase by the herpes simplex virus type 1 Us11 protein. J Virol. 2007;81(7):3455-64. Epub 2007/01/19. doi: 10.1128/jvi.02520-06. PubMed PMID: 17229694; PMCID: PMC1866071.
127. Rabouw HH, Langereis MA, Knaap RC, Dalebout TJ, Canton J, Sola I, Enjuanes L, Bredenbeek PJ, Kikkert M, de Groot RJ, van Kuppeveld FJ. Middle East Respiratory Coronavirus Accessory Protein 4a Inhibits PKR-Mediated Antiviral Stress Responses. PLoS Pathog. 2016;12(10):e1005982. Epub 2016/10/27. doi: 10.1371/journal.ppat.1005982. PubMed PMID: 27783669; PMCID: PMC5081173.
128. Asthana A, Gaughan C, Dong B, Weiss SR, Silverman RH. Specificity and Mechanism of Coronavirus, Rotavirus, and Mammalian Two-Histidine Phosphoesterases That Antagonize Antiviral Innate Immunity. mBio. 2021;12(4):e0178121. Epub 2021/08/11. doi: 10.1128/mBio.01781-21. PubMed PMID: 34372695; PMCID: PMC8406329.

129. Zhao L, Jha BK, Wu A, Elliott R, Ziebuhr J, Gorbalenya AE, Silverman RH, Weiss SR. Antagonism of the interferon-induced OAS-RNase L pathway by murine coronavirus ns2 protein is required for virus replication and liver pathology. Cell Host Microbe. 2012;11(6):607-16. Epub 2012/06/19. doi: 10.1016/j.chom.2012.04.011. PubMed PMID: 22704621; PMCID: PMC3377938.
130. Goldstein SA, Thornbrough JM, Zhang R, Jha BK, Li Y, Elliott R, Quiroz-Figueroa K, Chen AI, Silverman RH, Weiss SR. Lineage A Betacoronavirus NS2 Proteins and the Homologous Torovirus Berne pp1a Carboxy-Terminal Domain Are Phosphodiesterases That Antagonize Activation of RNase L. J Virol. 2017;91(5). Epub 2016/12/23. doi: 10.1128/jvi.02201-16. PubMed PMID: 28003490; PMCID: PMC5309944.
131. Thornbrough JM, Jha BK, Yount B, Goldstein SA, Li Y, Elliott R, Sims AC, Baric RS, Silverman RH, Weiss SR. Middle East Respiratory Syndrome Coronavirus NS4b Protein Inhibits Host RNase L Activation. mBio. 2016;7(2):e00258. Epub 2016/03/31. doi: 10.1128/mBio.00258-16. PubMed PMID: 27025250; PMCID: PMC4817253.
132. Zhang R, Jha BK, Ogden KM, Dong B, Zhao L, Elliott R, Patton JT, Silverman RH, Weiss SR. Homologous 2',5'-phosphodiesterases from disparate RNA viruses antagonize antiviral innate immunity. Proceedings of the National Academy of Sciences of the United States of America. 2013;110(32):13114-9. Epub 2013/07/24. doi: 10.1073/pnas.1306917110. PubMed PMID: 23878220; PMCID: PMC3740845.
133. V'Kovski P, Kratzel A, Steiner S, Stalder H, Thiel V. Coronavirus biology and replication: implications for SARS-CoV-2. Nature reviews Microbiology. 2021;19(3):155-70. Epub 2020/10/30. doi: 10.1038/s41579-020-00468-6. PubMed PMID: 33116300; PMCID: PMC7592455.
134. Cayley PJ, Davies JA, McCullagh KG, Kerr IM. Activation of the ppp(A2'p)nA system in interferon-treated, herpes simplex virus-infected cells and evidence for novel inhibitors of the ppp(A2'p)nA-dependent RNase. European journal of biochemistry. 1984;143(1):165-74. Epub 1984/08/15. PubMed PMID: 6088228.
135. Hersh CL, Brown RE, Roberts WK, Swyryd EA, Kerr IM, Stark GR. Simian virus 40-infected, interferon-treated cells contain 2',5'-oligoadenylates which do not activate cleavage of RNA. The Journal of biological chemistry. 1984;259(3):1731-7. Epub 1984/02/10. PubMed PMID: 6319408.
136. Rice AP, Kerr SM, Roberts WK, Brown RE, Kerr IM. Novel 2',5'-oligoadenylates synthesized in interferon-treated, vaccinia virus-infected cells. J Virol. 1985;56(3):1041-4. Epub 1985/12/01. PubMed PMID: 2415713; PMCID: PMC252683.
137. Bisbal C, Martinand C, Silhol M, Lebleu B, Salehzada T. Cloning and characterization of a RNAse L inhibitor. A new component of the interferon-

regulated 2-5A pathway. The Journal of biological chemistry. 1995;270(22):13308-17. Epub 1995/06/02. doi: 10.1074/jbc.270.22.13308. PubMed PMID: 7539425.
138. Behera AK, Kumar M, Lockey RF, Mohapatra SS. 2'-5' Oligoadenylate synthetase plays a critical role in interferon-gamma inhibition of respiratory syncytial virus infection of human epithelial cells. The Journal of biological chemistry. 2002;277(28):25601-8. Epub 2002/05/01. doi: 10.1074/jbc.M200211200. PubMed PMID: 11980899.
139. Martinand C, Montavon C, Salehzada T, Silhol M, Lebleu B, Bisbal C. RNase L inhibitor is induced during human immunodeficiency virus type 1 infection and down regulates the 2-5A/RNase L pathway in human T cells. J Virol. 1999;73(1):290-6. Epub 1998/12/16. doi: 10.1128/jvi.73.1.290-296.1999. PubMed PMID: 9847332; PMCID: PMC103833.
140. Lingappa JR, Dooher JE, Newman MA, Kiser PK, Klein KC. Basic residues in the nucleocapsid domain of Gag are required for interaction of HIV-1 gag with ABCE1 (HP68), a cellular protein important for HIV-1 capsid assembly. The Journal of biological chemistry. 2006;281(7):3773-84. Epub 2005/11/09. doi: 10.1074/jbc.M507255200. PubMed PMID: 16275648.
141. van Eyll O, Michiels T. Influence of the Theiler's virus L* protein on macrophage infection, viral persistence, and neurovirulence. J Virol. 2000;74(19):9071-7. Epub 2000/09/12. doi: 10.1128/jvi.74.19.9071-9077.2000. PubMed PMID: 10982352; PMCID: PMC102104.
142. Sorgeloos F, Jha BK, Silverman RH, Michiels T. Evasion of antiviral innate immunity by Theiler's virus L* protein through direct inhibition of RNase L. PLoS Pathog. 2013;9(6):e1003474. Epub 2013/07/05. doi: 10.1371/journal.ppat.1003474. PubMed PMID: 23825954; PMCID: PMC3694852.
143. Drappier M, Jha BK, Stone S, Elliott R, Zhang R, Vertommen D, Weiss SR, Silverman RH, Michiels T. A novel mechanism of RNase L inhibition: Theiler's virus L* protein prevents 2-5A from binding to RNase L. PLoS Pathog. 2018;14(4):e1006989. Epub 2018/04/14. doi: 10.1371/journal.ppat.1006989. PubMed PMID: 29652922; PMCID: PMC5927464.
144. Han JQ, Townsend HL, Jha BK, Paranjape JM, Silverman RH, Barton DJ. A phylogenetically conserved RNA structure in the poliovirus open reading frame inhibits the antiviral endoribonuclease RNase L. J Virol. 2007;81(11):5561-72. Epub 2007/03/09. doi: 10.1128/jvi.01857-06. PubMed PMID: 17344297; PMCID: PMC1900262.
145. Townsend HL, Jha BK, Silverman RH, Barton DJ. A putative loop E motif and an H-H kissing loop interaction are conserved and functional features in a group C enterovirus RNA that inhibits ribonuclease L. RNA biology. 2008;5(4):263-72. Epub 2008/12/18. doi: 10.4161/rna.7165. PubMed PMID: 19088502; PMCID: PMC2953469.

146. Keel AY, Jha BK, Kieft JS. Structural architecture of an RNA that competitively inhibits RNase L. RNA (New York, NY). 2012;18(1):88-99. Epub 2011/11/25. doi: 10.1261/rna.030007.111. PubMed PMID: 22114318; PMCID: PMC3261747.
147. Townsend HL, Jha BK, Han JQ, Maluf NK, Silverman RH, Barton DJ. A viral RNA competitively inhibits the antiviral endoribonuclease domain of RNase L. RNA (New York, NY). 2008;14(6):1026-36. Epub 2008/04/23. doi: 10.1261/rna.958908. PubMed PMID: 18426919; PMCID: PMC2390801.
148. Cooper DA, Jha BK, Silverman RH, Hesselberth JR, Barton DJ. Ribonuclease L and metal-ion-independent endoribonuclease cleavage sites in host and viral RNAs. Nucleic Acids Res. 2014;42(8):5202-16. Epub 2014/02/07. doi: 10.1093/nar/gku118. PubMed PMID: 24500209; PMCID: PMC4005677.
149. Hassel BA, Zhou A, Sotomayor C, Maran A, Silverman RH. A dominant negative mutant of 2-5A-dependent RNase suppresses antiproliferative and antiviral effects of interferon. Embo j. 1993;12(8):3297-304. Epub 1993/08/01. PubMed PMID: 7688298; PMCID: PMC413597.
150. Coccia EM, Romeo G, Nissim A, Marziali G, Albertini R, Affabris E, Battistini A, Fiorucci G, Orsatti R, Rossi GB, et al. A full-length murine 2-5A synthetase cDNA transfected in NIH-3T3 cells impairs EMCV but not VSV replication. Virology. 1990;179(1):228-33. Epub 1990/11/01. doi: 10.1016/0042-6822(90)90292-y. PubMed PMID: 2171206.
151. Martinand C, Salehzada T, Silhol M, Lebleu B, Bisbal C. RNase L inhibitor (RLI) antisense constructions block partially the down regulation of the 2-5A/RNase L pathway in encephalomyocarditis-virus-(EMCV)-infected cells. European journal of biochemistry. 1998;254(2):248-55. Epub 1998/07/11. doi: 10.1046/j.1432-1327.1998.2540248.x. PubMed PMID: 9660177.
152. Wickenhagen A, Sugrue E, Lytras S, Kuchi S, Noerenberg M, Turnbull ML, Loney C, Herder V, Allan J, Jarmson I, Cameron-Ruiz N, Varjak M, Pinto RM, Lee JY, Iselin L, Palmalux N, Stewart DG, Swingler S, Greenwood EJD, Crozier TWM, Gu Q, Davies EL, Clohisey S, Wang B, Trindade Maranhão Costa F, Freire Santana M, de Lima Ferreira LC, Murphy L, Fawkes A, Meynert A, Grimes G, Da Silva Filho JL, Marti M, Hughes J, Stanton RJ, Wang ECY, Ho A, Davis I, Jarrett RF, Castello A, Robertson DL, Semple MG, Openshaw PJM, Palmarini M, Lehner PJ, Baillie JK, Rihn SJ, Wilson SJ. A prenylated dsRNA sensor protects against severe COVID-19. Science. 2021;374(6567):eabj3624. Epub 2021/09/29. doi: 10.1126/science.abj3624. PubMed PMID: 34581622.

Chapter 2: Broad Spectrum Antiviral Activity of Recombinant Enhanced Antiviral Restrictors (REAVRs)

Dewi Megawati[1], Chen Peng[2], Ana M Stoian[1], Shefali Banerjee[1], Greg Brennan[1], Stefan Rothenburg [1]

1. Department of Medical Microbiology and Immunology, School of Medicine, University of California, Davis, California, USA
2. College of Veterinary Medicine, China Agricultural University, Beijing, China

ABSTRACT

Most virus families produce double-stranded (ds) RNA during their lifecycles, which can be sensed by multiple dsRNA-dependent innate immune sensors, including two potent host restriction factors protein kinase R (PKR) and 2',5'-oligoadenylate synthetase (OAS)/RNase L. PKR mainly restricts replication of viruses that are dependent on eIF2, and RNase L inhibits viral replication via degradation of host and viral RNAs. However, while PKR is directly activated by dsRNA and thus serves as sensor and effector, RNase L activation depends on OAS to both bind dsRNA and synthesize 2'-5' oligoadenylate (2-5A). We hypothesized that engineering proteins to combine the dsRNA sensor domain of PKR with the effector domain of RNase L would bypass the need for OAS activation, making them less susceptible to inhibition by viral molecules, and preserve their potent antiviral activity. To test this, we generated **R**ecombinant **E**nhanced **A**nti**v**iral **R**estrictors (REAVRs) by combining dsRNA-binding domains of PKR from different species with the effector domain of human RNase L. We show that REAVRs led to RNA degradation and decreased the activity of a luciferase reporter, suggesting the REAVRs are functionally

active. To investigate whether REAVRs could restrict viral replication, we generated T-REx 293 cells containing a single REAVR copy under the control of a doxycycline-inducible promoter. Some REAVRs exerted potent antiviral activities against five tested viruses: vaccinia virus, dengue virus, Zika virus, SARS-CoV-2, and vesicular stomatitis virus. Importantly, these REAVRs were also effective against viruses that are resistant to PKR activation, for example, SARS CoV-2 and flaviviruses. This study provides proof-of-concept that REAVRs are active *in vitro* and exhibit broad spectrum antiviral effects on various families of viruses.

SIGNIFICANCE

Cells of higher vertebrates possess a unique set of innate immune proteins that offer one of the first lines of defense against viral infections. In turn, viruses have evolved a plethora of mechanisms to evade the host antiviral response to ensure their survival and propagation. Here, we harness the specific interaction between the innate immune system and viruses to make cells more resistant to a broad range of viruses. We demonstrate that REAVRs have unique and broadly acting antiviral activities and simultaneously act as virus sensors and antiviral effectors. Importantly, REAVRs exert potent antiviral activities against multiple RNA and DNA viruses, including those not traditionally inhibited by PKR. We envision that REAVRs can be used to generate transgenic organisms with increased viral resistance and represent promising candidates as therapeutics for viral infections.

INTRODUCTION

The world has been through major pandemics and epidemics caused by virus infections such as smallpox, 1918 influenza, SARS-CoV, MERS-CoV and currently the ongoing SARS-CoV-2 pandemic (1). As SARS-CoV-2 spreads globally, tropical and subtropical countries are also battling the additional challenge of vector-borne diseases that have been endemic for decades (2). Infectious diseases continue to present significant challenges because viruses acquire the ability to overcome host immune responses and to spread efficiently. The innate immune system acts as one of the first lines of defense against virus infection. Substantial research has focused on the interactions between viruses and innate immune system, and it is now possible to use this knowledge to establish strategies to prevent and control viral diseases.

An effective host immune response against viral infections depends on the recognition of signatures of viral infections by the innate immune system (3). During viral infections, one of the best characterized pathogens-associated molecular patterns (PAMPs) is double-stranded RNA (dsRNA). Almost all virus families produce dsRNA during their lifecycles (4, 5). Viral dsRNA can be sensed by multiple dsRNA-dependent innate immune sensors, including two potent host restriction factors PKR and OAS/RNase L (6, 7). PKR and OAS/RNase L are interferon-stimulated genes; however, they differ at the basal expression level and responsiveness to type I IFNs (8). PKR is constitutively expressed as an inactive form at significant levels in most cell types, but it is up-regulated about 2- to 5-fold upon interferon stimulation (9, 10). OAS and RNase L are constitutively expressed at low levels and are considerably induced by virus infection or interferon stimulation (8, 11). Importantly, PKR and OAS/RNase L pathways act as

both sensor as well as effector molecules that can directly sense and repress viral replication (3).

PKR exists in a monomeric latent form in the absence of dsRNA (12). In mammals, PKR contains two N-terminal dsRNA binding domains (dsRBD) and a C-terminal kinase domain, which are connected by a linker region. The binding of dsRNA to the sensor domain of PKR leads to PKR dimerization and autophosphorylation (13, 14). Activated PKR phosphorylates Ser51 of the α subunit of the eukaryotic translation initiation factor eIF2, a GTP binding protein that delivers the initiator Met-tRNA (Met-tRNAi) to the small ribosomal subunit in the first step of translation initiation (15). Phosphorylated eIF2α has a high binding affinity to the guanine nucleotide exchange factor eIF2B, thus preventing eIF2B from catalyzing the GDP-GTP exchange to recharge eIF2α (16). The accumulation of eIF2α-GDP limits the availability of the eIF2α-GTP-Met-tRNAi ternary complex and leads to the inhibition of cap-dependent mRNA translation (17). Consequently, PKR cannot restrict viruses that initiate mRNA translation independent of eIF2α (18-21). For example, some arboviruses have been shown to harbor internal ribosome entry sites (IRES) that allow viral protein synthesis when the canonical cap-dependent translation is inhibited (22).

Activation of the OAS/RNase L pathway is initiated by binding dsRNA to latent OAS, which activates its catalytic site to synthesize 2'-5' oligoadenylate (2-5A) from ATP (11). 2-5A subsequently binds to the ankyrin repeat domain of monomeric RNase L, leading to RNase L dimerization and activation (6). In addition to the N-terminal ankyrin repeats domain, RNase L contains a pseudokinase domain which contributes to RNase L

dimerization, and a C-terminal endoribonuclease domain that cleaves target single-stranded (ss)RNA (23, 24). Enzymatically active RNase L cleaves both host and viral ssRNA at the consensus sequences UN^N, UU^N and UA^N (25, 26). Cleavage products of RNase L are further degraded by cellular exonucleases resulting in inhibition of mRNA translation, stalling the host cell machinery required for viral replication and eliminating ssRNA viral genomes (27). Interestingly, many viruses antagonize this pathway by targeting either OAS or 2-5A, instead of direct interactions with RNase domain of RNase L (28, 29).

The importance of the antiviral effects of PKR and OAS/RNase L is emphasized by the fact that many viruses have evolved strategies to evade PKR and OAS/RNase L activation by encoding viral antagonists (7, 28). One approach to controlling viral replication is through engineering more resistant host proteins. The generation of viral resistant MxA antiviral protein by combinatorial mutagenesis has been shown to improve the antiviral activity of MxA against Thogotovirus (30). The Malik group further generated an APOBEC3C “super restrictor” by creating a synthetic tandem domain which was shown to be more resistant to the viral antagonist Vif and increased its antiviral activity against HIV by about 4-fold (31).

Here we report the construction of **R**ecombinant **E**nhanced **A**ntiviral **R**estrictors (REAVRs) by combining the sensor domain of PKR with the effector domain of RNase L. We chose PKR and RNase L because PKR and RNase L share commonalities in that they exist in a monomeric inactive form and their dimerization and activation require N-terminal ligand binding. Additionally, the kinase domain in PKR and pseudokinase domain of RNase L both play important roles in dimerization and activation (14, 23, 24). We

therefore reasoned that engineering these proteins by combining the sensor domain of PKR with the effector domain of RNase L would generate a dsRNA-responsive fusion protein with enhanced antiviral activity. This fusion would make RNase L directly activatable by dsRNA, bypassing the highly targeted OAS/2-5A portion of this pathway.

In this study, we generated multiple REAVRs by combining the dsRNA-binding domains of PKR from either Syrian hamster or mouse PKR at the N-terminus to act as a dsRNA sensor and dimerization domain with the effector domain of human RNase L at the C-terminus. We selected PKR orthologs from either Syrian hamster or mouse because they share only 64% amino acid identity and show differential sensitivity to viral antagonists ((32), unpublished data). We demonstrated that these REAVRs were expressed and functionally active. Some REAVRs showed antiviral effects on dsDNA vaccinia virus *(*VACV*, Poxviridae)*, +ssRNA dengue virus (DENV, *Flaviviridae*), +ssRNA Zika virus (ZIKV, *Flaviviridae*), +ssRNA SARS-CoV-2 (*Coronaviridae*) and -ssRNA vesicular stomatitis virus (VSV, *Rhabdoviridae*). Taken together, we provide proof-of-concept that REAVRs were active and some REAVRs showed potent antiviral activities on multiple families of viruses.

MATERIALS AND METHODS

Cell lines

HeLa PKR knock out cells (HeLa PKR^{KO}) kindly provided by Dr. Adam Geballe (33), HeLa PKR knock down cells (HeLa PKR^{KD}) kindly provided by Dr. Charles Samuel, RK13 cells (rabbit) expressing E3L and K3L (designated RK13+E3L+K3L) were first described by Rahman et al. (34), Vero cells (ATCC® CCL-81) were kindly provided by Dr. Priya Shah, and Vero E6 cells was purchased from ATCC (ATCC® CRL-1586). Cells were grown in GlutaMax™ Dulbecco's Modified Eagle's Medium (DMEM, Life Technologies) supplemented with 5% or 10% fetal bovine serum (FBS, Lonza) and 100 IU/ml penicillin/streptomycin (Gibco). HeLa-PKR^{KD} cells were maintained in media additionally supplemented with 1 µg/ml puromycin (Sigma). RK13+E3L+K3L cell culture medium contained 500 µg/ml geneticin and 300 µg/ml zeocin (Life Technologies). Tetracycline-regulated expression human embryonic kidney 293 wild-type cell lines (Flp-In™ T-REx™ 293, Invitrogen) and of Flp-In™ T-REx™ 293 PKR^{KO} (Rothenburg lab, unpublished) were grown in 10% FBS DMEM culture medium containing zeocin (10µg/ml) and blasticidin S (15 µg/ml, Gibco). To generate stable cells, T-REx WT cells were co-transfected with Flp recombinase expression vector pOG44 (Invitrogen) and pcDNA5/FRT/TO (Invitrogen) encoding a single copy of REAVR 3, 4, 5, 7, 8, and 9. T-REx PKR^{KO} cells were co-transfected with pOG44 and pcDNA5/FRT/TO encoding either a single copy of the REAVR or human PKR. Transfection was done with Lipofectamine® 2000: plasmid ratio (3:1). The surviving cells were selected with hygromycin (50 µg/ml) and blasticidin (15 µg/ml) for 10-15 days. TREx-293 stable cells were maintained in a culture medium containing 200 µg/ml of hygromycin (Invitrogen) and 15 µg/ml of blasticidin S (Gibco).

Generation of T-REx WT^{ACE2} and T-REx REAVR7^{ACE2} cells was done by plasmid transfection. The pcDNA3.1+/C-(K)-DYK plasmid was linearized with PvuI enzyme and transfected into the indicated cells with Lipofectamine® 2000: plasmid ratio (3:1). The T-REx WT^{ACE2} cells were selected with geneticin 800µg/ml and T-REx REAVR7^{ACE2} were selected with geneticin 800µg/ml and hygromycin 50µg/ml for 10-15 days. Monoclonal cells expressing ACE2 were screened by western blot. ACE2 expression from the monoclonal cells was confirmed by flow cytometry.

Plasmids

Syrian hamster PKR (*Mesocricetus auratus* GenBank NP_001268874.1), and mouse PKR (*Mus musculus*, Genbank NP_035293.1) were cloned by the Rothenburg lab. Hybrid GyrB-human PKR (*E. coli* GyrB Genbank AXZ71263.1; *Homo sapiens* Genbank NP_001129123.1) was kindly provided by Dr. Thomas Dever (35), hybrids GyrB-human RNase L (Genbank NP_066956), a single copy of each REAVR, vaccinia E3L, vaccinia K3L genes were subcloned into the pSG5 mammalian expression vector (Stratagene) for luciferase-based reporter assays. pGL3 luciferase reporter vector was purchased from Promega. Human RNase L was subcloned into the pSG5 for RNA integrity assay. Cloning was done either using classical restriction enzyme digestion or Gibson assembly techniques. Human PKR and a single copy of each REAVR were cloned into pCDNA5/FRT/TO mammalian expression vector to generate T-REx stable cells. Flp recombinase expression vector (pOG44) was obtained from Invitrogen. The pcDNA3.1+/C-(K)-DYK plasmid encoding the cDNA of human ACE2 (NM_021804.2) was purchased from GenScript. All DNA sequences were validated by Sanger sequencing.

Luciferase-based reporter assays

Luciferase-based assays were performed to determine which domain of RNase L is critical for the generation of REAVRs. Briefly, 5 x 10^4 HeLa PKR^{KD} cells per well were seeded in 24 well plates overnight. The next day the cells were co-transfected with 50 ng of pGL3 firefly luciferase expression vector (Promega) with 950ng of the indicated plasmids. Transfection was done using GenJet (Signagen) with DNA to GenJet ratio of 1:2 as described by the manufacturer's protocol. The transfected cells were treated with either DMSO, 10ng/ml or 50ng/ml coumermycin. Cells were lysed with mammalian lysis buffer (GE Healthcare) at 24 hours post-coumermycin induction. Luciferase activity was measured using a GloMax luminometer (Promega) by adding luciferin (Promega) reagent to the cell lysates as manufacturer's recommendations. Data were presented as relative luciferase activity in which all data were normalized to pSG5 empty vector. Experiments were conducted in triplicate for each of the three independent experiments. The same protocol was used to determine whether REAVRs are functionally active in the luciferase assay (except that the cells were not treated with coumermycin).

To test the sensitivity of REAVRs to vaccinia virus E3L and K3L, we transfected HeLa PKR^{KO} cells with 200ng of the pSG5 vector control, 200ng of indicated PKR expression vector, 200ng of indicated REAVRs expression vector, 400ng of each viral antagonist expression vector, and 50ng of pGL3 firefly luciferase expression vector (Promega). Luciferase activity was measured as described above. Data were normalized to pSG5 empty vector.

Virus and infections

Vaccinia virus strain Copenhagen (VC-2) and vP872 were kindly provided by Dr. Bertram Jacobs (36). Dengue serotype-2 (strain 16681) was kindly provided by Dr. Priya Shah and VSV-12'GFP was provided by Dr. Qizhi Gong, SARS-CoV-2mNG was provided by Dr. Pei-Yong Shi, and Zika virus strain PRVABC59 was provided by Dr. Lark Coffey.

Vaccinia virus

About 8 x 10^5 indicated cells were seeded in 12-well plates and the next day, the cells were treated with 0.5µg doxycycline or left untreated for 6 hours prior to virus infections. The cells were infected with vP872 and VC-2 at an MOI of 0.1. After 48 hours, cells and supernatants were collected and subjected to three rounds of freeze at -80°C and thawing at 37°C. The cell lysates were sonicated for 15s twice with 50% amplitude (Qsonica Q500). Viruses were tittered by infecting RK13+E3L+K3L cells plated in 12-well plates with 10-fold serial dilutions of viral lysates in reduced-serum DMEM media. The cells were then incubated at 37°C and 5% CO_2 for 1 hour. Following this incubation, we added overlay DMEM media consisting of 1% methylcellulose (Millipore 17851-1KG), 5% FBS and 100U penicillin/streptomycin. The plaques were visualized with 1% crystal violet (Sigma cat # C0775) in 25% methanol (v/v H2O) solution at 48 hours post infections.

Dengue virus serotype 2 strain 16681 and Zika virus strain PRVABC59

About 1.5 x 10^6 indicated cells were seeded in 6-well plates and the next day, the cells were treated with 0.5µg doxycycline or left untreated for 6 hours prior to virus infections. DENV infections were done with an MOI of 0.1 and ZIKV infections were done with an MOI of 1. Viruses were added to the cells for absorption for 2 hours at 37°C. The

supernatant was harvested at indicated time points and stored at -80°C for infectious virus titration. For titration, about $8x10^5$ Vero CCL-81 cells were plated in 6-well plates. The next day the media were removed, and the cells were infected with 10-fold serial dilutions of virus supernatant in reduced-serum DMEM media. The cells were then incubated at 37°C and 5% CO_2 for 2 hours. Following this incubation, we added an overlay of DMEM media consisting of 0.8% methylcellulose (for DENV) or 1% methylcellulose (for ZIKV) and 1% FBS. The cells were fixed with 4% formaldehyde for 20 min and were visualized with 1% crystal violet (Sigma cat # C0775) in 25% methanol (v/v H2O) solution on day 5 for ZIKV and day 6 for DENV.

VSV-12'GFP

About 1.5×10^6 indicated cells were seeded in 6-well plates and the next day, the cells were treated with 0.5µg doxycycline or left untreated for 6 hours prior to virus infections. Indicated cells were infected with VSV-12'GFP at MOI of 0.01 and pictures were taken 24 hours post infection with EVOS FL Auto 2 using the FITC filter to visualize EGFP. The supernatant was collected afterward and stored at -80°C for infectious virus titration. For titration, about $4x10^5$ Vero CCL-E6 cells were plated in 6-well plates. The next day the media were removed, and the cells were infected with 10-fold serial dilutions of virus supernatant in reduced-serum DMEM media. The cells were then incubated at 37°C and 5% CO_2 for 1 hour. Following this incubation, overlay DMEM media consisting of 1% methylcellulose (Millipore 17851-1KG) and 5% FBS were added to the wells, and the cells were incubated for 4 days. The cells were fixed with 4% formaldehyde for 20 min and were visualized with 1% crystal violet (Sigma cat # C0775) in 25% methanol (v/v H2O) solution.

SARS-CoV-2mNG

About 5 x 10^5 indicated cells were seeded in 12-well plates. On day 2 post-seeding, the cells were treated with 0.5µg doxycycline or left untreated for 6 hours prior to virus infections. SARS-CoV-2mNG infections and titrations were performed in a biosafety level 3 (BSL-3) laboratory using appropriate and approved personal protective equipment and protocols. Indicated cells were infected with SARS-CoV-2mNG at an MOI of 1 and allowed for absorption for 1 hour at 37°C 5% CO_2. Pictures were taken on day 2 post infections to visualize green fluorescence by using a Primovert iLED microscope. The supernatant was collected afterward and stored at -80°C for infectious virus titration. For titration, about 2.5x10^5 Vero CCL-E6 cells were plated in 6-well plates. The next day the media were removed, and the cells were infected with 10-fold serial dilutions. The cells were then incubated at 37°C and 5% CO_2 for 1 hour. Following this incubation, an overlay of DMEM media consisting of 1% methylcellulose (Millipore 17851-1KG) and 10% FBS were added to the wells and the cells were incubated for 4 days. The cells were fixed with 4% formaldehyde for 20 min and were visualized with 1% crystal violet (Sigma cat # C0775) in 25% methanol (v/v H2O) solution.

Immunoblot analyses

Western blot was done to determine the level of REAVRs expression under tetracycline induction. Indicated cells were seeded in 6-well plates overnight. The cells were either treated with doxycycline 0.5µg/ml or left untreated. Cells were washed once with ice-cold PBS and lysates harvested at 24-hours post-induction with 1% SDS buffer. Cell lysates were sonicated for 10s twice at 50% amplitude, centrifuged for 5 minutes at 13,000 rpm. About 10µg of protein from supernatant mixed with 2x Laemmli sample

buffer. The sample mixtures were heated at 95°C, then separated on 12% SDS polyacrylamide gels and transferred to polyvinyl difluoride (PVDF, GE Healthcare) membranes. Blots were blocked with SuperBlock™blocking buffer (Thermofisher Scientific, Cat #37515) or 5% BSA for 1 hour at room temperature and probed with primary antibodies (table below) diluted in the same blocking buffer. Primary antibodies were incubated overnight at 4°C. After washing, the blots were probed with secondary antibodies for 1 hour at room temperature. The blots were washed three times for 10 minutes and proteins were detected with Amersham™ ECL™ (GE Healthcare cat #28980926) or SuperSignal West Femto (Thermoscientific Cat #34096). Images were taken using the iBright Imaging System (Invitrogen). Blots were sequentially probed with antibodies and in between treatments stripped using mild stripping buffer.

Western blots were conducted to investigate whether the level of protein expression might contribute to the level of RNA degradation. Briefly, A549 PKR and RNase L double knockout cells were seeded in 6-well plates. The next day, the cells were transfected with 2.5 µg of empty vector as negative control, RNase L-encoding plasmid as positive control, or REAVRS-encoding plasmids. Transfection was done as Lipofectamine LTX manufacturer's instruction (plasmid: lipofectamine LTX ratio = 1:3). Cell lysates were harvested at 24-hours post transfection and western blot was done as described above.

Further Western blots were carried out to determine whether REAVR 5 and 9, which have full-length PKR, work through eIF2α phosphorylation. T-REx PKR^{KO} served as negative control, T-REx PKR^{KO}-human PKR served as positive control. About 1.8×10^6 cells were seeded in six-well plates. The next day, 0.5µg doxycycline was added to the cells. After 24 hours, each cell line was infected with either VC-R4 (VACV△E3L△K3L) or

vP872 (VACV△K3L) at an MOI of 3. After an hour, media were replaced with complete media containing 0.5μg/ml doxycycline. Cell lysates were harvested at 6 hours post infection, and western blot was done as described above.

Primary antibody	Antibody species	Blocking buffer	Dilution	Catalog number
RNase L-E9	mouse	Thermofisher SuperBlocking buffer	1:500	Santa Cruz, sc-74405
phospho-eIF2α	rabbit	5% BSA	1:1,000	Cell signaling, #9721
total eIF2α	rabbit	5% BSA	1:1,000	Santa Cruz, sc11386
Phospho-PKR E-120	rabbit	5% BSA	1:1,000	Abcam, ab32036
PKR A12	mouse	5% milk	1:1,000	Santa Cruz, sc393038
Beta actin	mouse	Thermofisher SuperBlocking buffer	1:2,000	Sigma, A1978
Secondary antibody				
goat anti-rabbit IgG	goat,HRP-linked	1% milk TBST	1:10,000	Invitrogen, A16023
goat anti-mouse IgG	goat, HRP-linked	1% milk TBST	1:10,000	Invitrogen, A16110

Flow Cytometry

Flow cytometry analysis was performed to detect human ACE2 receptors in T-REx WT and T-REx WT REAVR 7 cells stably expressing human ACE2. Briefly, cells were incubated with primary antibody to human ACE2 polyclonal goat IgG (R&D Cat #AF933) at a concentration of 0.25 μg/10^6 cells for 30 min at room temperature. After washing, the cells were incubated with secondary antibody F(ab')2 donkey anti-goat IgG (H+L) cross adsorbed PE (Thermofisher scientific Cat #PI31860) at a concentration of 1:200 for 30

min at room temperature. Cells were analyzed by flow cytometry (CytoFLEX, Beckman Coulter).

RNA degradation assay

RNA degradation assay was performed to assess RNA cleavage activities of REAVRs. Briefly, A549 PKR and RNase L double knockout cells were seeded in 6-well plates. The next day, the cells were transfected with 2.5 µg of empty vector as a negative control, RNase L-encoding plasmid as the positive control, or each indicated REAVR-encoding plasmid. Transfection was done according to Lipofectamine LTX manufacturer's instruction (plasmid: lipofectamine LTX ratio = 1:3). At 24-hours after transfection, the cells were infected with either the vaccinia virus lacking E3L and K3L at an MOI of 5, DENV2 at an MOI of 3, or VSV-12'GFP at an MOI of 1. RNAs were isolated using TRI Reagent (Millipore Sigma, T9424) at 24 hours post infection. RNA isolation and DNA digestion were done according to Zymo Research RNA Extraction's instruction. About 1µl (about 150ng/µl) of RNAs were run in RNA 6000 Nano Kit (Agilent Cat #: 5067-1961511) and RNA cleavage activity was determined using 2100 Bioanalyzer.

Cell viability test

To assess the cell viability upon REAVR expression, we seeded T-REx PKR^{KO} and T-REx WT expressing REAVR cells in 96-well plates (white opaque culture plate, Corning Cat# 07-200-628) at 8×10^4 cells/well. The next day, the cells were treated with 0.5µg/ml doxycycline or left untreated. At 6 hours post doxycycline treatment, the T-REx PKR^{KO} cells were infected with VC-2 at an MOI of 0.1 as a positive control. Cell viability was assessed by measuring the ATP content using the Viral ToxGlo™ assay (Promega

Cat#G8941) at 48 hours by reading luminescence with GloMax Discover (Promega). Relative light units relative to medium only were plotted in GraphPad Prism.

Statistical analysis and fold-change and a log reduction calculation

Statistical analysis and graph plotting were performed using GraphPad Prism 8 (GraphPad Software, USA). We used two-way ANOVA with Sidak's multiple comparisons test for analysis of cell viability RLU. Statistically significant differences between groups were marked with *$P < 0.05$; **$P < 0.005$; ***$P < 0.001$; and ****$P < 0.0001$.

Fold-change virus titer was determined by calculating the ratio between virus titer in doxycycline-treated and untreated cells. The difference between virus titer in doxycycline-treated and untreated samples was then expressed as a log reduction. Formulas are presented below for fold-change calculations, log reduction calculations, and percent reduction calculations.

Fold-change = $\frac{\mathrm{A}}{\mathrm{B}}$

Log reduction = $\log10\left(\frac{\mathrm{A}}{\mathrm{B}}\right)$ or $\log10(\mathrm{A})\text{-}\log10(\mathrm{B})$

Percent reduction = $\frac{(\mathrm{A}\text{-}\mathrm{B})\mathrm{X}100}{\mathrm{A}}$

Where,

A is the number of virus titer in doxycycline untreated cells

B is the number of virus titer in doxycycline-treated cells.

RESULTS

Generation and functional analysis of recombinant enhanced antiviral restrictors (REAVRs)

It was previously demonstrated that fusion of coumermycin-inducible dimerization domain of *Escherichia coli (E. coli)* DNA gyrase subunit B (GyrB) with the kinase domain of human PKR resulted in activation of the PKR kinase domain under control of coumermycin (35, 37). We took advantage of this system to determine which domains of RNase L are critical for the generation of active fusion proteins. We generated three hybrid constructs of GyrB-RNase L consisting of the first 221 amino acids of *E. coli* GyrB fused to different lengths of the human RNase L effector domain: GyrB-RNase L short (containing residues 588-741), GyrB-RNase L medium (starting from the β1 region of pseudokinase residues 375-741), and GyrB-RNase L long (starting from the αA region of pseudokinase domain residues 333-741) **(Figure 2.1A).** As controls, we used constructs to express fusion proteins consisting of the GyrB dimerization domain fused to either the wild-type or inactivated (K296H) human PKR kinase domain (residues 258-551) which were previously shown to confer coumermycin dimerization-dependent eIF2α kinase activity in a mammalian cell line (35, 37). We transfected cells with indicated plasmids and added two different coumermycin concentrations to promote GyrB dimerization and measured the amount of light produced by transfected cells upon the addition of luciferin. In this assay, luciferase activity is inversely correlated with PKR activity. We found both 10ng/ml and 50ng/ml of coumermycin led to a reduction of luciferase activity for the GyrB-PKR construct, whereas the addition of coumermycin had no effects on luciferase activity for the kinase-inactivated construct **(Figure 2.1B).** Among the three GyrB-RNase L

hybrids, only GyrB-RNase L medium resulted in a marked reduction of luciferase activity comparable to that of human PKR, suggesting that RNase L medium is the optimal length of RNase L effector domain for retaining RNase L activity.

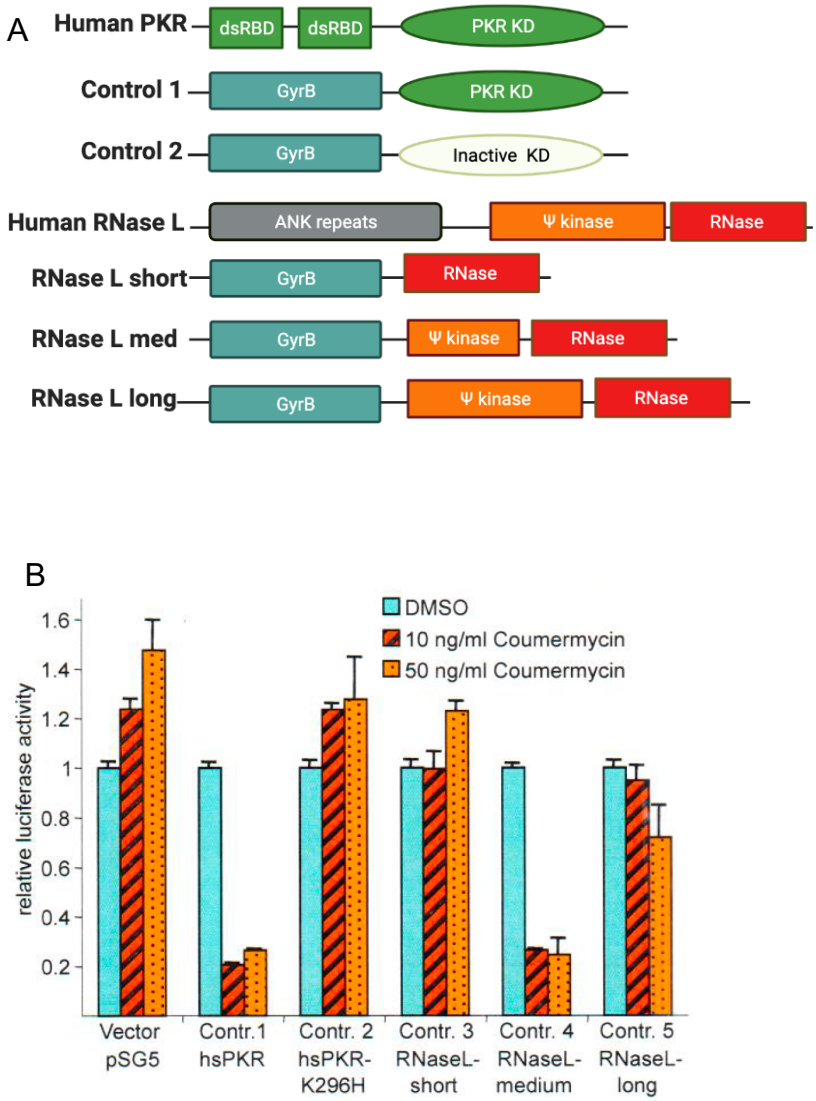

Figure 2. 1. Optimization of GyrB-RNase L fusion proteins.
(A). The schematic domain organization of PKR, RNase L, and GyrB-RNase L hybrid constructs. To determine which domain of RNase L is critical, we combined the coumermycin-inducible dimerization domain of E. coli GyrB with pseudokinase and RNase domain of human RNase L. As a control, we used GyrB- human PKR proteins (wild type PKR and kinase-inactivated PKR mutant (K296H)). We generated three hybrid constructs: GyrB-RNase L short (starting from RNase domain), GyrB-RNase L medium (starting from β1 region of pseudokinase), and GyrB-RNase L long (starting from the αA region of pseudokinase domain). (B). Inhibition of luciferase activity by fusion constructs. We analyzed the effects of the constructs on a reporter assay in HeLa PKR knock-down cells by treating the cells with 10ng/ml or 50ng/ml coumermycin.

We generated multiple REAVRs by combining the sensor domain of PKR with the medium-length effector domain of human RNase L. First, we fused the dsRNA sensing domains of Syrian hamster PKR with the effector domain of human RNase L. We chose Syrian hamster PKR as the sensor domain because our previous data showed that Syrian hamster PKR is resistant to some viral antagonists that can inhibit PKR activation including vaccinia virus (VACV) E3L, herpes simplex virus 1 (HSV-1) US11, and reovirus σ3 (Unpublished data, Table 2.1). As we demonstrated with GyrB constructs, the linker region connecting the PKR dsRBDs and the RNase L effector domain might influence the activity of fusion proteins. Therefore, we generated six structural variants of REAVRs. Specifically, we included both dsRBDs with no linker region (REAVR 1, residues 1-158), a portion of the linker region (REAVR 2 residues 1-183; REAVR 3 residues 1-206), the entire linker region (REAVR 4 residues 1-243), the entire Syrian hamster PKR sequence (REAVR 5 residues 1-527), and kinase-inactivated Syrian hamster PKR K272R (REAVR 6) **(Figure 2. 2A)**. In addition, we designed REAVRs 7-9 that contain parts mouse PKR as sensors, which structures correspond to REAVRs 3-5 **(Figure 2.2A)**. We chose mouse PKR because our previous unpublished data showed that mouse PKR was susceptible to E3L, US11, and σ3, whereas Syrian hamster PKR was resistant to these antagonists (Table 2.1). We first compared the effects of REAVRs on protein expression in a luciferase-based reporter system, which we previously established for measuring PKR activity (38, 39). In this assay, plasmids encoding PKR and a luciferase reporter were co-transfected into PKR-deficient HeLa cells. In this assay, luciferase activity is inversely correlated with PKR activity. PKR and REAVRs are likely activated by dsRNA that is

formed by overlapping transcripts generated from plasmids (40). We found all REAVRs as well as Syrian hamster and mouse PKR substantially reduced luciferase expression, indicating that they are functional **(Figure 2.2B).** REAVR 6, which contains a kinase-inactivating mutation in PKR showed the lowest activity, but still reduced luciferase expression ~3-fold.

Table 2. 1. Differential sensitivity of Syrian hamster and mouse PKR to viral antagonists.

PKR	VACV K3	VACV E3	HSV1 US11	Reovirus σ3
Syrian Hamster	sensitive	resistant	resistant	resistant
Mouse	sensitive	sensitive	sensitive	sensitive

VACV=Vaccinia virus; HSV1= Herpes simplex virus 1

Ribosomal RNA (rRNA) degradation is a hallmark of RNase L endonuclease activity (6). Therefore, to determine whether REAVRs exhibit endonuclease activity, we transiently transfected A549$^{RNase\ L-/-/PKR-/-}$ cells with either pSG5 (empty vector), or expression vectors encoding either RNase L or the indicated REAVRs. We assessed rRNA degradation products at 6 and 24 after infection with vaccinia virus (VACV) VC-R4, which lacks PKR antagonists K3L and E3L**.** We observed RNA cleavage products in cells expressing RNase L and REAVRs as early as 6 hours post infection **(Figure 2.2C)**. The RNA degradation was more pronounced at 24 hours post infection, while empty vector-transfected cells did not show rRNA degradation products. RNA cleavage products were detected in all cells expressing REAVRs, to a lesser extend in REAVR 5, which contains entire sequence of Syrian hamster PKR. Interestingly, REAVR 6 consisting of full-length inactivated Syrian hamster PKR and human RNase L showed rRNA cleavage products, suggesting that the RNase L effector domain in this construct is active. Altogether, this

rRNA degradation assay indicates the RNase L effector domain of REAVRs is functionally active.

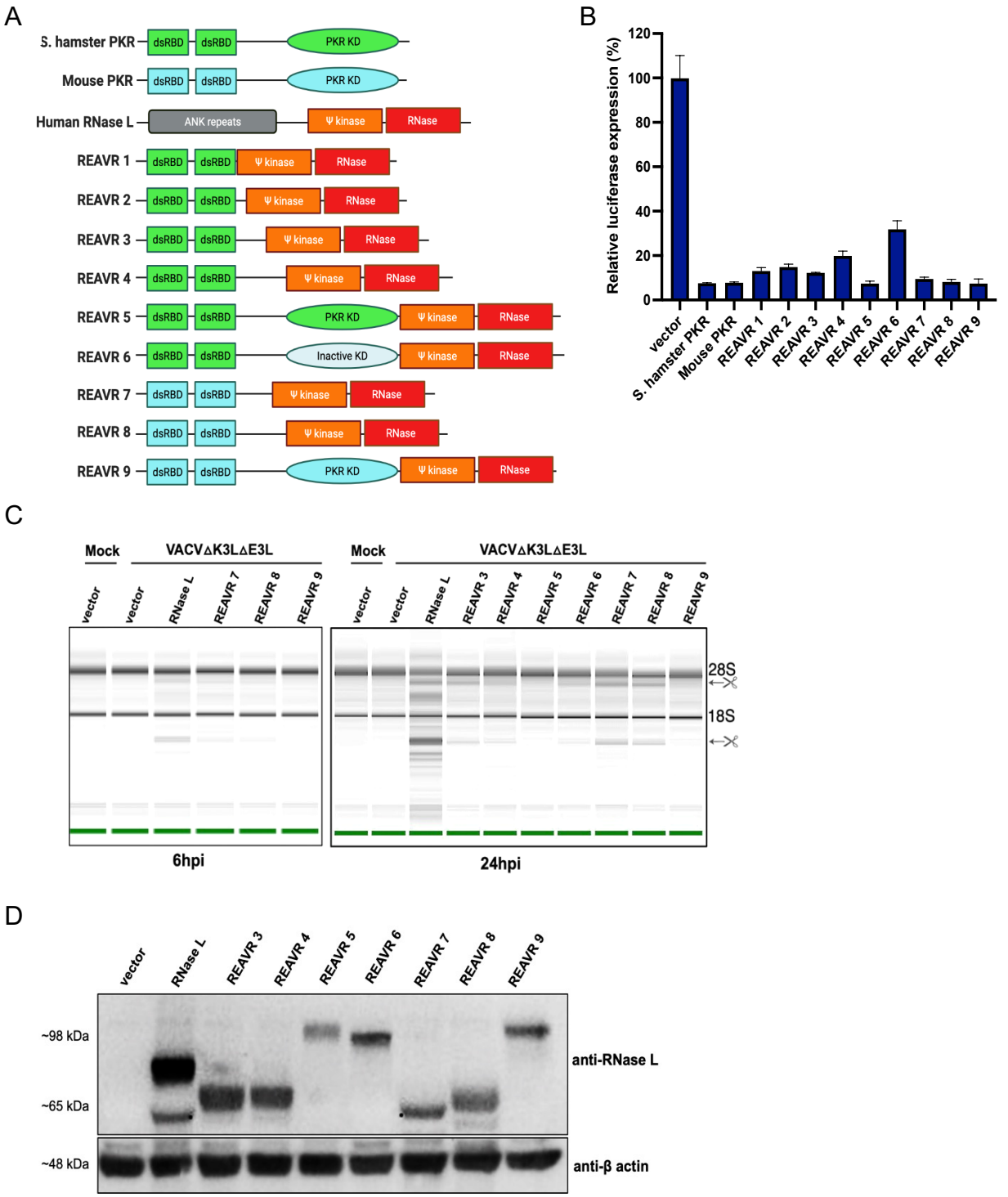

Figure 2. 2. Generation of REAVR constructs and functional analysis of REAVRs in transient transfection assays.

(A). Schematic domain organization of Syrian hamster PKR, mouse PKR, human RNase L, and REAVR constructs. REAVR 1-6 are composed of different parts of Syrian hamster PKR and the human RNase L effector domain. REAVR 7-9 are composed of parts of mouse PKR and the human RNase L effector domain. (dsRB = double-stranded RNA binding domain; PKR KD = PKR kinase domain; ANK = ankyrin repeat domain; Ψ kinase = pseudokinase domain). (B). Inhibition of luciferase expression by REAVRs. Human HeLa-PKR knock-down cells were co-transfected with firefly luciferase pGL3 and either pSG5 empty vector, Syrian hamster PKR, mouse PKR or the indicated REAVRs. Luciferase activities were measured 48 hours after transfection. (C). RNA cleavage activity of REAVRs in A549$^{RNase\ L-/-\ /PKR-/-}$ cells. The cells were transiently transfected with either pSG5 empty vector, expression vector for RNase L, or the indicated REAVRs. The next day, the cells were infected with VACV⊿K3L⊿E3L at an MOI of 5. RNA integrity was assessed at 6 hours or 24 hours after infection using a 2100 Bioanalyzer. (D). REAVR expression in A549$^{RNase\ L-/-\ /PKR-/-}$ cells. The same amount of the indicated plasmids were transfected into the A549$^{RNase\ L-/-\ /PKR-/-}$ cells. Protein lysates were collected at 48 hours after transfection and subjected to Western blot analysis to detect RNase L and REAVRs expressions using RNase L-specific antibodies.

To further investigate whether the level of protein expression might contribute to the degree of rRNA degradation, A549$^{RNase\ L-/-/PKR-/-}$ cells were transfected with the same amount of plasmid, and we performed Western blots analyses. These blots did not detect endogenous RNase L expression in the pSG5 transfected cells **(Figure 2.2D).** RNase L was expressed at higher level than REAVRs, which might explain why the cells expressing RNase L had the highest RNA degradation activity. Interestingly, despite a lower level of expression in cells transfected with either REAVR 7 and 8, the RNA cleavage assay showed a slightly higher degree of RNA degradation than for REAVR 3 and 4. In addition, we observed that REAVR 6, which contains an inactive PKR, migrated faster on the gel than that of REAVR 5 containing wild-type Syrian hamster PKR. The slower mobility of wild-type PKR compared to inactive PKR is most likely due to autophosphorylation of the wild-type protein (41). Overall, these transfection-based luciferase reporters and RNA-integrity assays show that these REAVRs decreased luciferase expression and led to RNA degradation, suggesting REAVRs are functionally active.

Expression of a single copy of each REAVR in T-REx™ stable cell line systems and its effect on cell viability

In order to determine whether REAVRs have antiviral effects in mammalian cells, we generated Flp-In™ T-REx™ (T-REx) cells stably expressing a single copy of each REAVR under the control of a doxycycline-inducible promoter. The T-REx system consists of a stably expressed tetracycline repressor (TetR) gene from *E. coli*, a promoter with two tetracycline repressor binding sites and a single gene-of-interest Flp Recombination Target (FRT) integration site. Integration of the gene-of-interest into the FRT site is mediated by Flp recombinase from *Saccharomyces cerevisiae* (42). In this Tet-On system, the TetR repressor constitutively inhibits expression of the gene-of-interest unless tetracycline or doxycycline is present to bind the TetR repressor **(Figure 2.3A).** Thus, REAVR expression in the T-REx cell system is controlled by the presence of tetracycline or doxycycline in the media. Western blot analyses showed that there is little if any leaky expression in the absence of doxycycline. All REAVRs were expressed at 24 hours post doxycycline induction with relatively weaker expression of REAVRs 5 and 9 **(Figure 2.3B).**

To determine the effects of REAVRs on cell viability, we used the Viral ToxGlo™ assay (Promega) to determine the number of viable cells in culture. The assay quantifies ATP, as a proxy for the presence of metabolically active cells. The luminescence readout is proportional to the number of viable cells in culture. T-REx PKR^{KO} infected with vaccinia virus (VACV) Copenhagen strain (VC-2) served as positive control and T-REx WT cells

A

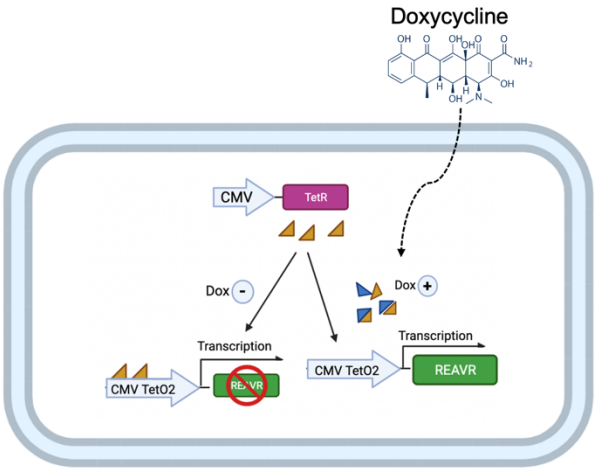
Doxycycline
CMV
TetR
Dox -
Dox +
Transcription
Transcription
CMV TetO2
REAVR
CMV TetO2
REAVR

B

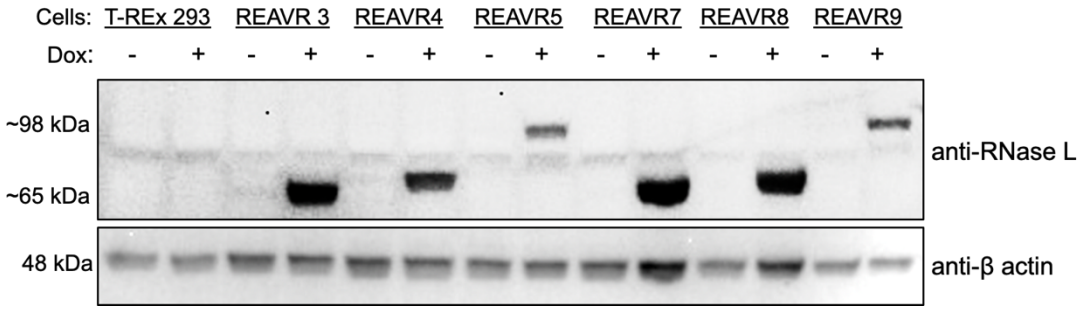
Cells: T-REx 293 REAVR 3 REAVR4 REAVR5 REAVR7 REAVR8 REAVR9
Dox: - + - + - + - + - + - + - +
~98 kDa
~65 kDa
anti-RNase L
48 kDa
anti-β actin

C

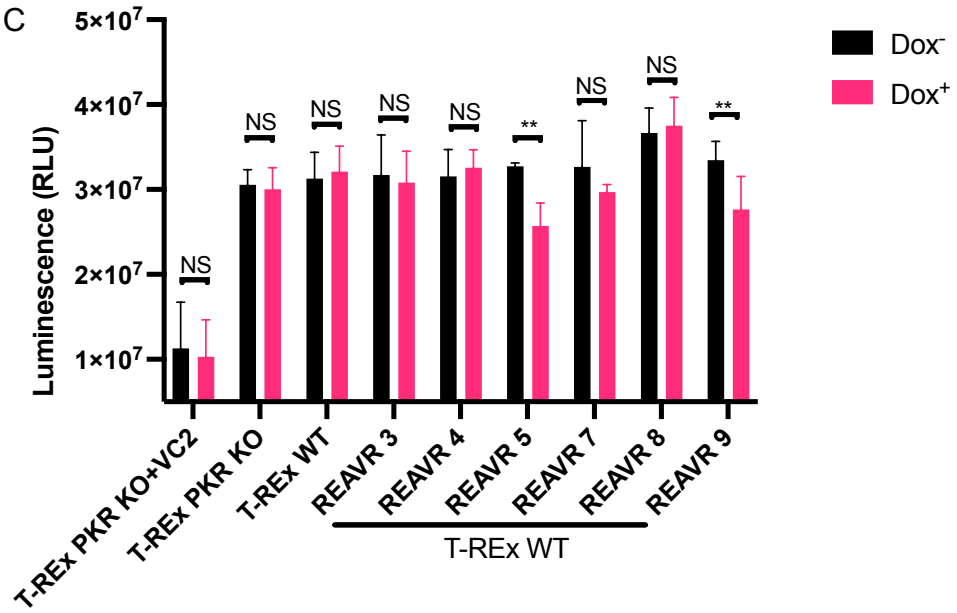
Luminescence (RLU)
5×10^7
4×10^7
3×10^7
2×10^7
1×10^7
NS
NS
NS
NS
NS
**
NS
NS
**
Dox-
Dox+
T-REx PKR KO+VC2
T-REx PKR KO
T-REx WT
REAVR 3
REAVR 4
REAVR 5
REAVR 7
REAVR 8
REAVR 9
T-REx WT

Figure 2. 3. Stable expression of single copy REAVRs in T-REx cells under doxycycline control. *(A). Schematic figure of REAVR expression under control of a doxycycline-inducible promoter. (B). Expression of REAVRs after doxycycline induction. The parental T-REx WT and T-REx WT stably expressing REAVRs were treated with 0.5µg/ml doxycycline or left untreated. At 24 hours post-treatment, cell lysates were harvested, and proteins were subjected to a Western blot analysis. REAVRs expression was detected using anti-human RNase L. Anti β-actin was used as a control (β-actin 48kDa, REAVR3 64.88 kDa, REAVR4 71.52 kDa, REAVR5 98.56kDa, REAVR7 65kDa, REAVR8 68.04 kDa and REAVR9 100.9kDa). (C). Effect of REAVRs expression on the cell viability. The indicated cell lines were treated with 0.5 ug/ml doxycycline for 48 hours. T-REx PKR^{KO} cells were infected with VC2 (MOI of 0.1) as a positive control. Cell viability was assessed with ToxGlo Assay (Promega TM393). Luminescent signals are proportional to viable cell numbers. Standard deviations were determined from four independent replicates. RLU values were normalized to media only. Data were analyzed by two-way ANOVA followed by Sidak's multiple comparisons test. Significant value showed as asterisk (NS=p>0.05, *p<0.05, **p<0.01 ***p<0.001, ****P<0.0001).*

with and without doxycycline treatment served as a negative control. As expected, relative light unit (RLU) doxycycline-treated and untreated parental T-REx WT cells was not significantly different, suggesting no significant effects of doxycycline treatment on cell viability. In contrast, we observed low RLU in T-REx PKR^{KO} cells infected with VACV at 48 hours post infection **(Figure 2.3C).** Similar to the parental T-REx WT, the RLU values between doxycycline and non-doxycycline treated cells were not significantly different in REAVR 3, 4, 7, and 8 expressing cells. These data suggest that expression of REAVR 3, 4, 7 and 8 did not cause cytotoxicity at 0.5µg/ml doxycycline induction for 48 hours. Notably, although not significant, the RLU value of REAVR 7 expressing cells was slightly lower than in untreated cells, indicating REAVR 7 might slightly affect cell health. In contrast, the RLU values of doxycycline-treated T-REx WT REAVR 5 and 9 cells were significantly lower than the untreated cells, suggesting that expression of REAVR 5 and 9 might negatively affect cell viability. Overall, the cell viability test confirmed that the integrated REAVRs had no adverse effects on cells without doxycycline, while control cells infected with VACV had substantially reduced viability **(Figure 2.3C)**. Furthermore,

REAVRs did not significantly reduce cell viability even 48 hours after doxycycline induction, with exception of REAVR 5 and 9, which both contain full PKR protein.

Antiviral effects of REAVRs on vaccinia virus

We performed luciferase-based assays to test the sensitivity of REAVRs to the VACV innate immune antagonists E3L and K3L. Human HeLa PKR^{KO} cells were transfected with expression vectors for individual REAVRs, vaccinia virus viral antagonists E3L or K3L, and firefly luciferase. As a control, cells were also transfected without viral antagonists to determine fully active REAVR luciferase inhibition. Syrian hamster PKR and mouse PKR served as positive controls. At 48 hours after transfection

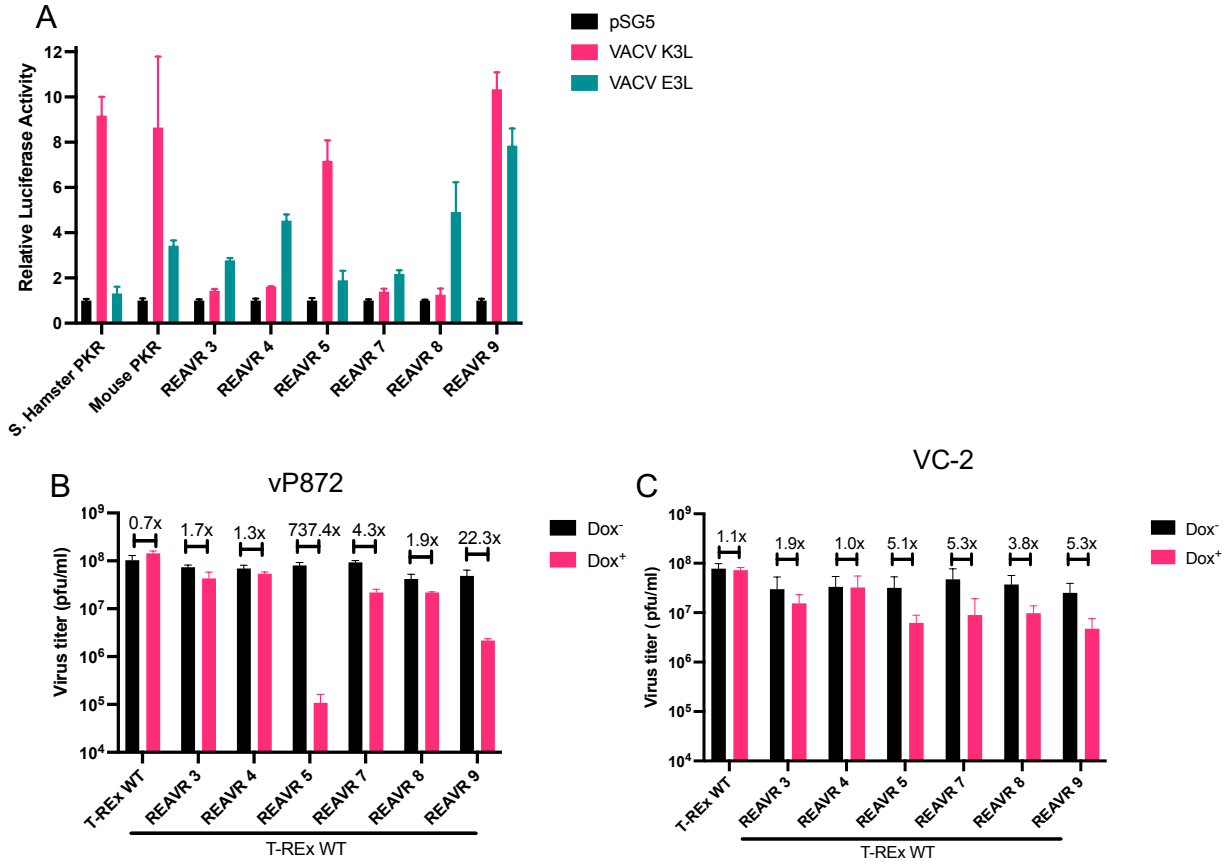

Figure 2. 4. Antiviral effects of REAVRs against vaccinia virus.
(A). Differential sensitivity of REAVRs to viral antagonists. Human HeLa-PKR^{ko} cells were transfected with expression vectors for vaccinia virus viral antagonists E3L or K3L, and pGL3 firefly luciferase, and the indicated REAVRs. As baseline, HeLa-PKR^{ko} were transfected with the indicated REAVRs, pSG5, and pGL3 firefly luciferase without viral antagonists. Syrian hamster PKR and mouse PKR served as positive controls. Luciferase activity was measured 48 hours after transfection. Luciferase light units were normalized to PKR or REAVR-only transfected cells to obtain relative luciferase activity. Standard deviations of three independent transfections are shown. Data are representative of two biological replicates. (B) T-REx WT and T-REx WT cells expressing REAVRs were infected with vP872 and VC-2 strain Copenhagen (C) at an MOI of 0.1. Cell lysates were collected at 48 hours post infection and virus titers were determined by plaque assay on RK13+K3L+E3L cells. The virus titer is presented in log10 pfu/ml. Fold-change of the virus titer relative to untreated doxycycline are indicated. Data presented as mean and standard deviations were determined from three independent infections.

our results showed differential sensitivity of the REAVRs to these viral antagonists **(Figure 2.4A)**. REAVRs 3 and 4, consisting of Syrian hamster PKR sensor domain and human RNase L effector domain, were sensitive to E3L but resistant to K3L. REAVR 5, which consists of full-length Syrian hamster PKR and human RNase L was sensitive to K3L and largely resistant to E3L, resembling the Syrian hamster PKR sensitivity profile. Similarly, REAVR 9, which consists of full-length mouse PKR and human RNase L effector domain also resembled sensitivity profile of mouse PKR. Interestingly, REAVR 7, was largely resistant to E3L while REAVR 8 was sensitive. Since K3L targets the kinase domain of PKR, the lack of inhibition of REAVRs devoid of the PKR kinase domain was predicted, whereas the relative resistance of REAVR 7 to E3L was surprising and indicates that the linker region of PKR is involved in the inhibition by E3L.

We further tested the ability of REAVRs to restrict a variant vaccinia virus that lacks the K3L gene but expresses the E3L gene (vP872), and wild-type vaccinia virus that is expressing both K3L and E3L genes. First, we infected parental T-REx WT and T-REx WT cells stably expressing REAVRs with vP872. We observed no difference in the virus titer of doxycycline-treated and untreated parental T-REx WT. REAVR 3 and 4 appear to

have minimal or no effect on vP872 **(Figure 2.4B).** In contrast, REAVR 5 expression diminished virus titer by about 700-fold compared to REAVR 5 untreated cells. To a lesser extent, REAVR 9 diminished virus titer by about 20-fold compared to REAVR 9 untreated cells. REAVRS 7 showed minimal effect on vP872 with 4.3-fold reduction of virus titer. This result indicated that the PKR kinase activity was more important in inhibiting vP872 than the RNase activity. This finding was not surprising for REAVR 5 that contains active Syrian hamster PKR kinase domain as Syrian hamster PKR was known to be resistant to VACV E3L (Rothenburg lab, unpublished data). However, this is unique for REAVR 9 as it consists of mouse PKR, which was known to be sensitive to VACV E3L (43).

To further test the effect of vaccinia E3L and K3L on virus replication in REAVR expressing cells, we infected these cells with wild-type VACV strain Copenhagen (VC-2). We observed no difference in the virus titer of doxycycline-treated and untreated parental T-REx WT and REAVR 4 expressing cell lines **(Figure 2.4C).** REAVR 5 expression only slightly reduced the VC-2 virus titer by about 5-fold, suggesting that VACV K3L dramatically rescued virus replication. There was also about 5-fold reduction of VC-2 virus titer in doxycycline-treated REAVR 7, 8, and 9 stable cell lines compared to doxycycline untreated cells.

Our lab and others have shown that human PKR was sensitive to VACV E3L but resistant to VACV K3L (32, 43, 44). To avoid confounding effects with PKR, we used a PKR-deficient T-REx cell line in which we knocked out the PKR by CRISPR-Cas9 (Rothenburg lab, unpublished) and then generated stably transfected cells with REAVRs 3, 5, 7, 8 and 9. We conducted time-dependent doxycycline induction to see REAVRs

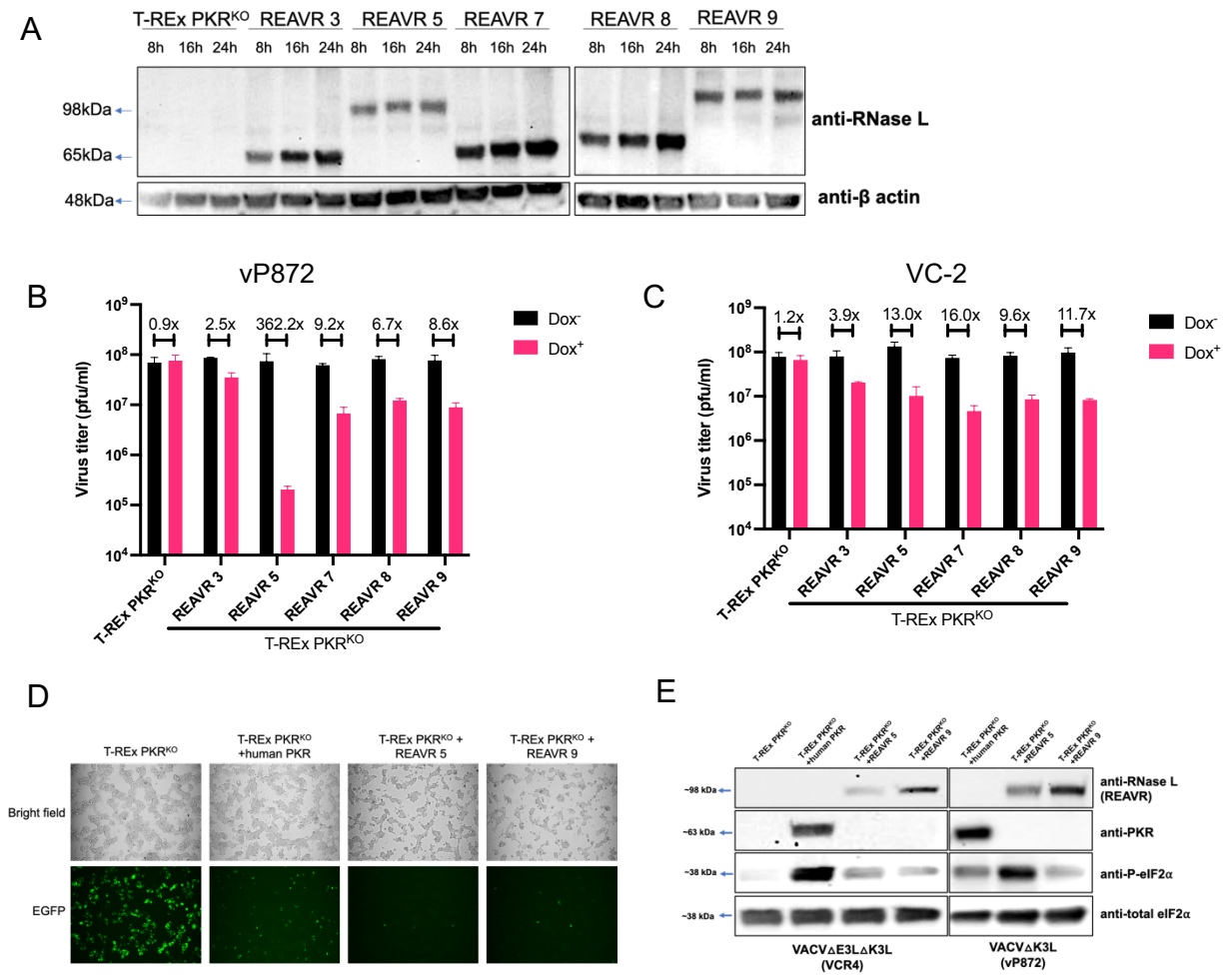

Figure 2. 5. Antiviral effects of REAVRs on vaccinia virus in Flp-In T-REx 293 PKR^{KO} (T-REX PKR^{KO}).

(A). Time-dependent REAVRs expression. T-REx PKR^{KO} and T-REx PKR^{KO} stably transfected with REAVRs were grown to a confluence of 80-90% and treated with 0.5µg/ml doxycycline. At 8-,16-, and 24-hours post-treatment, cell lysates were harvested and 10µg of protein was subjected to a Western blot analysis. Membranes were probed with primary antibodies against RNase L and beta-actin. T-REx PKR^{KO} and T-REx PKR^{KO} cells expressing REAVRs were infected with vP872 (B) and VC-2 strain Copenhagen at an MOI of 0.1 (C). Cell lysates were collected at 48 hours post infection and virus titers were determined by plaque assay on RK13+K3L+E3L cells. The virus titer is presented in log_{10} pfu/ml. Fold-change of the virus titer relative to untreated doxycycline is indicated. Data presented as mean and standard deviations were determined from three independent infections. (D, E). Phosphorylation of eIF2α by REAVR 5 and 9. T-REx PKR^{KO} served as negative control, T-REx WT and T-REx PKR^{KO}-human PKR served as positive control. All cells were treated with 0.5µg of doxycycline prior to VCR4 or vP872 virus infection at an MOI of 3. Pictures were taken at 6 hours post infection. Cell lysates were harvested shortly after taking pictures and the proteins were subjected to a Western blot analysis. The membranes were probed with primary antibodies against phospho-eIF2α, total eIF2α, PKR and RNase L.

expression at 8, 16, and 24 hours. Immunoblot analysis showed that all REAVRs were expressed at 8 hours post-induction and the expression increased over time **(Figure 2.5A)**. We infected both parental T-REx PKR^{KO} and T-REx PKR^{KO} cells stably expressing

REAVRs with either vP872 or VC-2 **(Figure 2.5B, C).** Although the general trend of virus inhibition obtained from this infection assay was similar to that of T-REx WT cells, there was a notably stronger reduction of viral titer between doxycycline-treated and untreated cells for most REAVR-expressing cells, suggesting endogenous PKR might interfere with the antiviral activity of REAVRs.

Because of the notable antiviral effects of REAVRs 5 and 9 on vaccinia virus, we next asked whether REAVR 5 and REAVR 9 phosphorylate eIF2α. We used T-REx PKR^{KO} as a negative control, and T-REx PKR^{KO} stably expressing human PKR served as positive control. All cells were treated with 0.5μg of doxycycline at 24 hours before infected with the VACV E3L and K3L double-knockout strain VC-R4 (VC-R4) or vP872 at an MOI of 3. Use of VC-R4, which expresses EGFP under control of the natural E3L promoter, allowed us to monitor virus replication using fluorescence microscopy. We observed a robust EGFP signal in T-REx PKR^{KO} cells and considerably lower EGFP signal in T-REx PKR^{KO} expressing human PKR, as expected. Remarkably less EGFP was observed in REAVR 5 and 9 expressing cells at 6 hours post infection relative to T-REx PKR^{KO} and T-REx PKR^{KO}-human PKR **(Figure 2.5D)**. Cells were photographed, and then lysates were harvested for western blot analysis using an antibody specific for eIF2α phosphorylation at S51. Only little eIF2α phosphorylation was observed in the absence of PKR **(Figure 2.5E).** Human PKR induced a high level of eIF2α phosphorylation in VCR4 infected cells. Although eIF2α phosphorylation levels in both REAVR 5 and 9 expressing cells infected with VCR4 were lower than in human PKR-expressing cells, the levels of eIF2α phosphorylation in REAVR 5 and 9 cells were comparable. Upon infection with vP872, the eIF2α phosphorylation level was lower in human PKR-expressing cells

infected with vP872 than VCR4 infected cells, which can be explained by the sensitivity of human PKR to E3L. In contrast, eIF2α phosphorylation levels where higher in REAVR 5-expressing cells, which correlates with the high inhibition of virus replication **(Figure 2.5B),** and can be explained by the resistance of Syrian hamster PKR to E3L. eIF2α phosphorylation levels in in REAVR 9-expressing cells, was more similar to that found in human PKR-expressing cells.

Antiviral effects of REAVRs on dengue virus and Zika virus

Some arboviruses strongly activate PKR but are not sensitive to eIF2α phosphorylation while being sensitive to RNase L activation, including dengue virus, chikungunya virus and West Nile virus (45-47). As REAVRs contain the human RNase L effector domain, we predicted that REAVRs would show antiviral effects against viruses sensitive to RNase L activity. In this study, we assessed the antiviral effects of REAVRs against two members of flaviviruses, dengue virus serotype 2 strain 16681 (DENV2) and Zika virus (ZIKV) strain PRVABC59, which are both +ssRNA viruses.

First, we assessed replication of DENV2 by infecting REAVR-expressing T-REx cells and determined the virus titers at 48 hours post infection. There was no substantial difference in the DENV2 titer of doxycycline-treated and untreated parental T-REx WT **(Figure 2.6A).** REAVR 4 and 9 showed a minimal to moderate antiviral effects on the DENV2 with a 2-to 8-fold reduction in viral titers, respectively. Induction of REAVRs 3 and 5 showed stronger effects on DENV2 with about 31 and 25- fold reduction in virus titer, respectively. REAVRs 7 and 8 diminished virus titer by 2,485 and 295-fold compared to

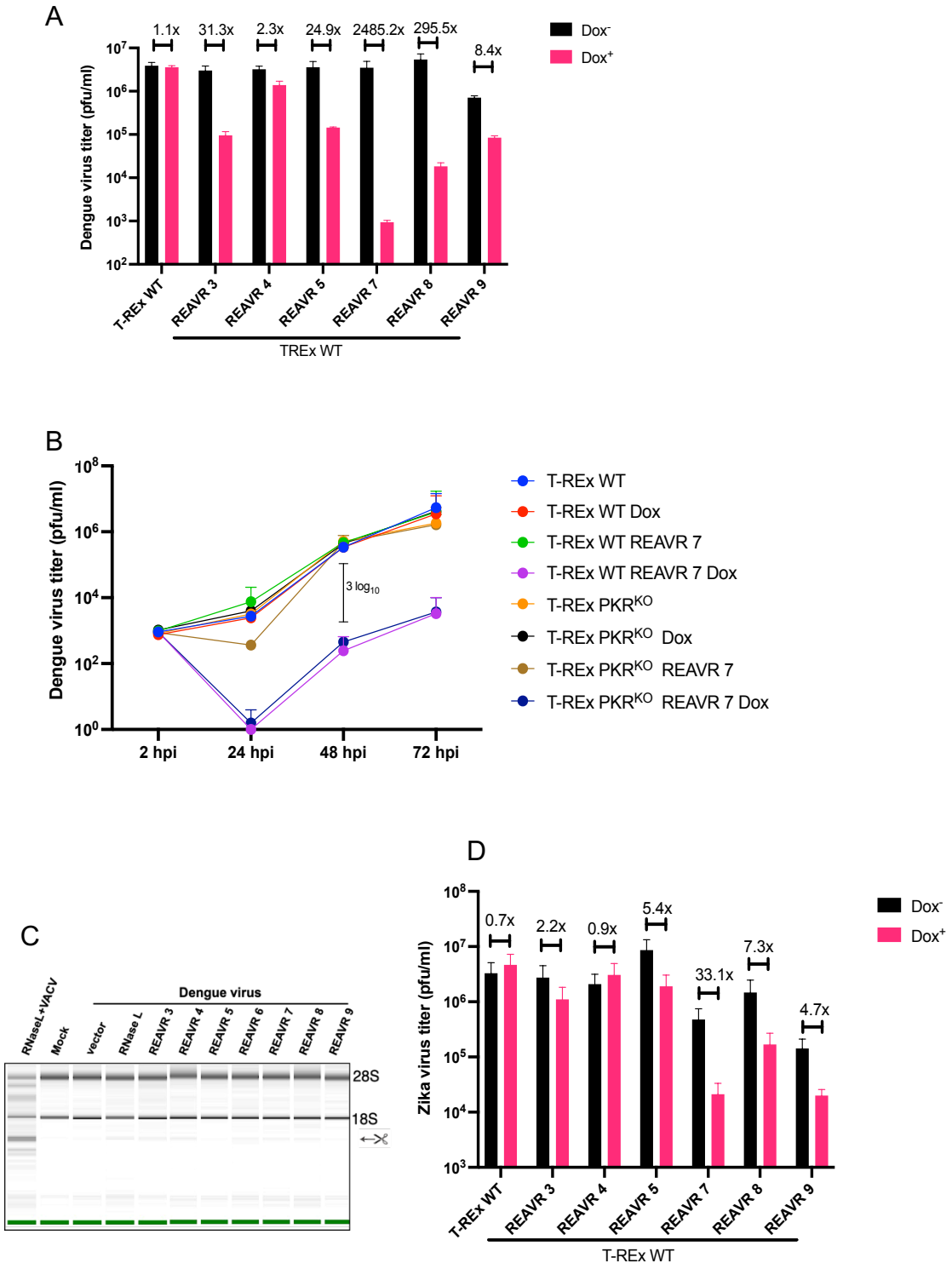

Figure 2. 6. Antiviral effects of REAVRs against dengue virus and Zika virus.
(A). Parental T-REx WT and T-REx WT cells expressing REAVRs were infected with dengue serotype 2 strain 16681 at an MOI of 0.1. Supernatant was collected at 48 hours post infection and the virus titers were determined by plaque assay on Vero CCL-81 cells. The virus titer is presented in log10 pfu/ml. Data presented as mean and standard deviations were determined from three independent infections. Fold-

change of the virus titer relative to doxycycline untreated is indicated. (B). Time course of dengue virus replication in REAVR 7 expressing cells. Parental T-REx WT and T-REx WT expressing REAVR 7 as well as T-REx PKR^{KO} and T-REx PKR^{KO} expressing REAVR7 were infected with dengue serotype 2 at an MOI of 0.1. The supernatant was collected at indicated time points. The virus titer from four replicate experiments were presented with error bars indicating standard deviations. (C). A549$^{RNase\ L-/-\ /PKR-/-}$ cells were transiently transfected with either pSG5 empty vector, expression vector for RNase L, or the indicated REAVRs. The next day, the cells were infected with dengue serotype 2 strain 16681 at an MOI of 3. RNA integrity was assessed at 24 hours after infection using a 2100 Bioanalyzer. D. Parental T-REx WT and T-REx WT cells expressing REAVRs were infected with Zika virus strain PRVABC59 at an MOI of 1. Supernatants were collected at 72 hours after infection and virus titers were performed similarly to dengue plaque assay.

doxycycline untreated cells, respectively. Distinct antiviral effects of REAVR 7 and 8 suggests the linker region between the PKR and RNase L domains influence the antiviral activity of REAVRs. To test if endogenous PKR influences the the effect of REAVR 7 on the viral replication, we infected T-REx WT, T-REx PKR^{KO}, T-REx WT-REAVR7 and T-REx KO-REAVR7 with DENV2 at MOI of 0.1 in the presence and absence of doxycycline. We monitored infectious particle production over time by measuring viral titers from supernatants **(Figure 2.6B).** Viral titers were similar across cell lines at 2 hours post infection. Both T-REx PKR^{KO}-REAVR7 and T-REx WT-REAVR7 doxycycline treated-cells showed about 1,000 less virus titer compared to doxycycline untreated cells, at 24-, 48-, and 72-hours post infection. There was no substantial difference between virus titers in T-REx PKR^{KO} and T-REx WT cells. This finding further supports that DENV replication is independent of PKR (48) and that REAVR 7 activity was not influenced by endogenous PKR.

Next, we assessed RNase L activity of REAVRs after dengue virus infection by monitoring rRNA degradation products using 2100 Bioanalyzer to test whether the reduction of virus titers correlated with rRNA degradation. Because T-REx cells have endogenous RNase L, we used A549$^{RNase\ L-/-/PKR-/-}$ cells to test rRNA cleavage activities, as described above for VACV. We transiently transfected A549$^{RNase\ L-/-/PKR-/-}$ cells with the

indicated plasmids. About 24 hours after transfections, the cells were mock-infected or infected with dengue serotype 2 at an MOI of 3. RNA degradation was assessed at 24 hours post infection **(Figure 2.6C).** Surprisingly, the rRNA degradation products were not as prominent as when the cells were infected with VACV. However, there were noticeable rRNA cleavage products in all cells expressing REAVRs, except for REAVRs 5 and 9. Of note, cleavage products in REAVR 7 and 8 transfected cells were not more prominent than in REAVR 3 and 4 transfected cells, indicating a lack of correlation between rRNA cleavage and antiviral activities.

A current study has shown that RNase L has a pro-viral effect on Zika virus replication (49). Because some REAVRs showed strong antiviral effects against DENV, we also assessed whether REAVRs exhibit antiviral effects against ZIKV. We observed there was minimal or no effect of REAVR 3 and 4 against ZIKV. REAVR 5, 7, 8, and 9 showed a moderate antiviral effect on ZIKV replication. REAVR 7 mediated the strongest antiviral effect on ZIKV replication (33-fold reduction). None of the REAVRs had pro-viral effects on ZIKV and there was a similar trend of virus inhibition as for DENV2, although the antiviral effects were lower than observed for DENV2.

Expression of REAVR 7 inhibits SARS-CoV-2 replication

SARS-CoV-2 is arguably one of the most intensely studied viruses since causing a pandemic in 2020. Previously, SARS-CoV-2 was shown to promote PKR and RNase L activation in a lung cancer cell lines A549 (50). Because SARS-CoV-2 and DENV2 are both +ssRNA viruses, and due to the strong antiviral effect of REAVR 7 on DENV2 and ZIKV, we were interested in assessing the ability of REAVR 7 on inhibiting SARS-CoV-2

replication. To facilitate SARS-CoV-2 infection, we generated T-REx WT and T-REx REAVR 7 cells stably expressing the human ACE2 receptor. We then used selected monoclonal cell lines for all the experiments, T-REx WT^{ACE2} C9 and T-REx REAVR7^{ACE2} C1. ACE2 expression in both cell lines was robustly detected by flow cytometry using antibodies against human ACE2, which showed about 89.46% cells expressing ACE2 in T-REx WT^{ACE2} C9 and about 93.17% cells expressing ACE2 in T-REx REAVR7^{ACE2} C1 **(Figure 2.7A).** In contrast, there was no ACE2 expression in untransfected cells. We also validated the level of ACE2 expression using Western blot analysis **(Figure 2.7B),** which showed ACE2 expression in all cell lines. In addition, Western blot analysis confirmed REAVR7 expression when the T-REx REAVR7^{ACE2} C1 cells were treated with doxycycline. An infection assay with SARS-CoV-2 mNG at an MOI of 1 showed SARS-CoV2 mNG replicated robustly in both doxycycline-treated and control T-REx WT^{ACE2} C9 cells **(Figure 2.7C)**. In contrast, SARS-CoV-2 only replicated robustly in T-REx REAVR7^{ACE2} C1 control cells but not in doxycycline-treated cells. Consistent with the green florescence signal, there was an about 431-fold (2.7-log) reduction in virus titer in TREx REAVR7^{ACE2} C1 doxycycline-treated cells compared to the control T-REx REAVR7^{ACE2} C1 cells **(Figure 2.7D)**. This finding suggests REAVR 7 is a potent antiviral protein against SARS-CoV-2.

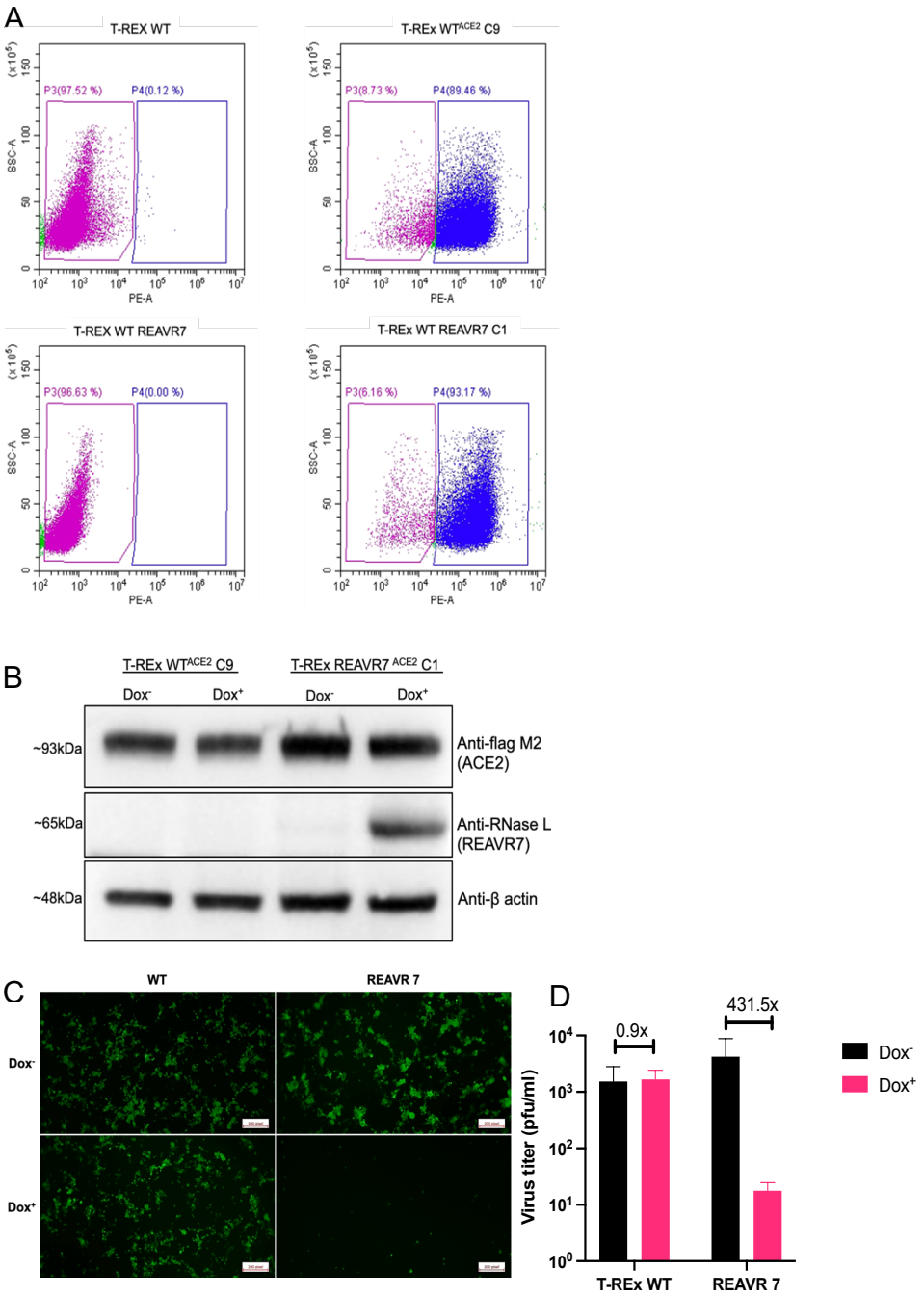

Figure 2. 7. Antiviral effects of REAVR 7 against SARS-CoV-2.
To facilitate SARS-CoV-2 infection, we generated monoclonal cells T-REx WT C9 and T-REx REAVR7 C1 stably expressing ACE2. ACE2 expression was confirmed by flow cytometry (A) and Western blot analysis (B). (C). Parental T-REx WT and T-REx WT cells expressing REAVRs were infected with SARS-CoV-2 mNG at an MOI of 1. Pictures were taken at 48 hours post infection. (D). Supernatants were collected, and the virus titers were determined by plaque assay on Vero E6 cells. The virus titer is presented in log10 pfu/ml. Data presented as mean and standard deviations were determined from three independent infections. Fold-change of the virus titer relative to doxycycline untreated is indicated in the figure.

Antiviral effects of REAVRs on vesicular stomatitis virus

The strong antiviral effect of some REAVRs on the tested +ssRNA viruses raises the question of whether REAVRs would also restrict -ssRNA viruses. To further test the antiviral effects of REAVRs on an -ssRNA virus, we infected T-REx PKR^{KO}, the parental T-REx WT and T-REx WT expressing REAVRs with VSV-12'GFP at an MOI of 0.01. VSV-12'GFP is an attenuated vesicular stomatitis virus derived from the Indiana serotype (51). VSV-12'GFP replicated robustly in T-REx PKR^{KO} and T-REx WT cells with almost all cells were infected at 24 hours after infection as seen by a strong GFP signal **(Figure 2.8A).** Among the REAVRs, only REAVRs that contain full-length PKR restricted VSV-12'GFP replication. Interestingly, REAVR 9 that contains mouse PKR had a more substantial effect, resulting in a 201-fold reduction, while in REAVR 5 that contains Syrian hamster PKR caused a 10-fold reduction compared to doxycycline untreated cells **(Figure 2.8B).** Notably, REAVR 7, which had a strong effect on dengue virus, Zika virus and SARS-CoV2 mNG appeared to have minimal effect on VSV-12'GFP, indicating that VSV replication is independent of RNase L activation.

Next, we determined whether the inhibition of VSV-12'GFP replication correlated with eIF2α phosphorylation. We infected the indicated cells with VSV-12'GFP MOI of 0.1 **(Figure 2.9A)**. All cells were treated with 0.5μg of doxycycline for 6 hours before VSV-12'GFP infections. We observed strong GFP signals in T-REx PKR^{KO}, T-REx WT and T-REx PKR^{KO} expressing human PKR after infection with VSV-12'GFP, whereas considerably less GFP signal was observed in REAVR 5 and 9 expressing cells at 14 hours post infection**.** In addition, Western blotting results showed only high levels of eIF2α

phosphorylation in REAVR 5 and 9 expressing cells, with a stronger signal in the former. **(Figure 2.9B)**.

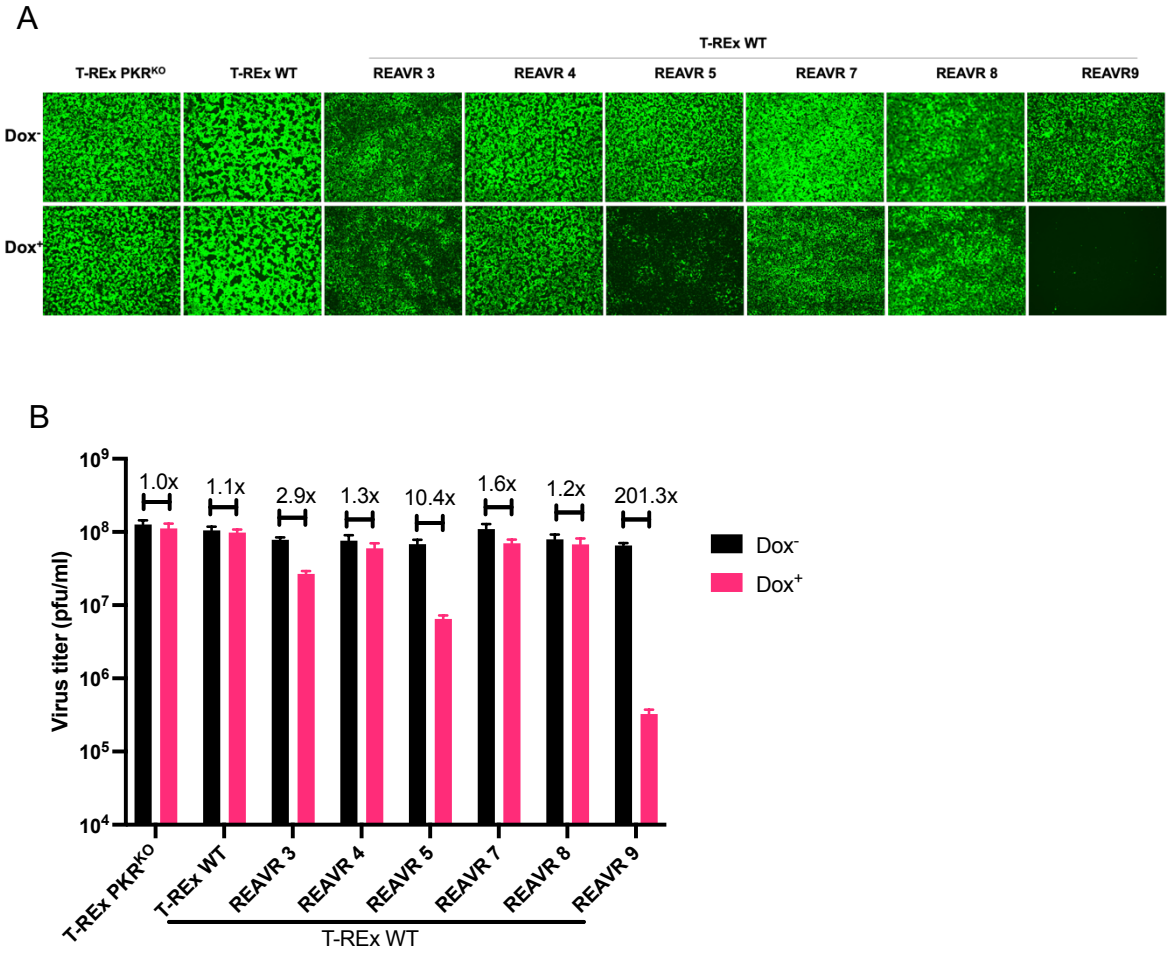

Figure 2. 8. Antiviral effects of REAVRs against vesicular stomatitis virus strain VSV-12'GFP. *(A). T-REx PKR^{KO}, T-REx WT and stably T-REx WT cells expressing REAVRs were infected with VSV12'GFP at an MOI of 0.01. Pictures were taken at 24 hours post infection. (B). Supernatants were collected after pictures were taken and virus titers were determined by plaque assay on Vero E6 cells. The virus titer is presented as log_{10} pfu/ml. Standard deviations were determined from three independent infections. Fold-change of the virus titer relative to doxycycline untreated cells is indicated.*

Unlike the T-REx WT expressing REAVR 5 that showed a higher GFP signal than REAVR 9 expressing cells, there was a comparable GFP signal in T-REx PKR^{KO} expressing REAVR 5 and 9. We also assessed RNase L activity of REAVRs by monitoring rRNA degradation products using 2100 Bioanalyzer. We transiently transfected A549 RNase L and PKR double knockout cells with either pSG5 empty vector, RNase L

encoding plasmid, or the indicated REAVR encoding plasmids. About 24 hours after transfections, the cells were mock-infected or infected with VSV-12'GFP MOI of 1. RNA degradation was assessed at 24hours post infection **(Figure 2.9C).** No rRNA cleavage products were observed in cells transfected with RNase L or REAVRs. This result is consistent with a previous finding that showed that VSV infection in A549 cells failed to generate detectable levels of RNase L-mediated rRNA cleavage, indicating minimal or no antiviral effect of RNase L (47).

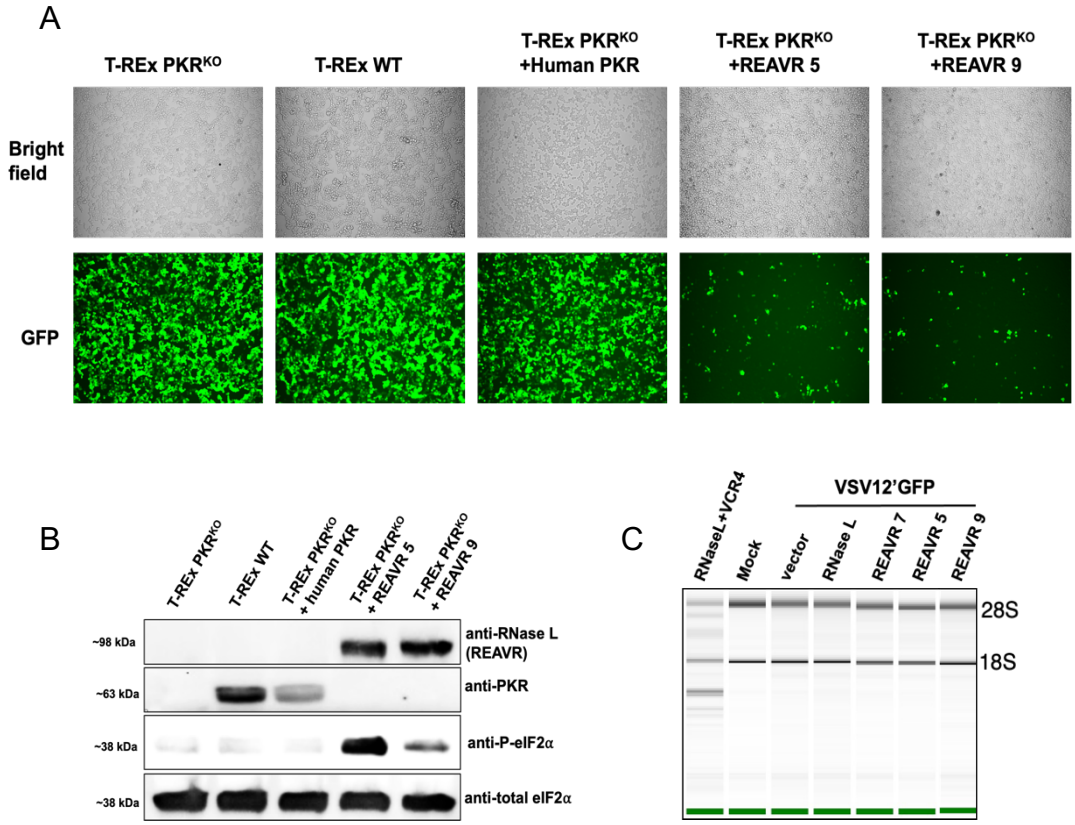

Figure 2. 9. eIF2α phosphorylation and rRNA degradation status after VSV-12'GFP infection. *(A). Indicated cells were grown to a confluence of 80% and were treated 0.5μg/ml doxycycline for about 6 hours. The cells were then infected with VSV12'GFP at an MOI of 0.1. GFP expressions were monitored at 14 hours after infection. (B). Cell lysates were harvested at 14 hours after infection and the proteins were subjected to a Western blot analysis. The membrane was probed with primary antibodies against phospho-eIF2α, total eIF2α, PKR and RNase L. (C). A549$^{RNase\ L-/-\ /PKR-/-}$ cells were transiently transfected with either pSG5 empty vector, expression vector for RNase L, or the indicated REAVRs. The next day, the cells were infected with VSV-12'GFP at an MOI of 1. RNA integrity was assessed at 24 hours post infection using a 2100 Bioanalyzer.*

Table 2. 2. Fold reduction in virus titers after induction of REAVR expression.

Cell lines	Fold-change virus titer (relative to Dox$^-$)					
	Vaccinia (VC-2)	Vaccinia (Vp872)	VSV-12' GFP	Dengue	Zika	SARS-CoV-2 mNG
T-REx	1.2	0.9	1.1	1.1	0.7	0.9
REAVR 3	3.9	2.5	2.9	31	2.2	n.d.
REAVR 4	n.d.	n.d	1.3	2.3	0.9	n.d.
REAVR 5	13	362	10	25	5.4	n.d.
REAVR 7	16	9.2	1.6	2,485	33.1	431
REAVR 8	9.6	6.7	1.2	296	7.3	n.d.
REAVR 9	11.7	8.6	201	8.4	4.7	n.d.

Colors indicate levels of virus restriction. Yellow: >5-10 fold; Orange:>10-100; Red:>100-1,000 fold; Dark red: >1,000 fold; n.d. = not determine

DISCUSION

PKR and OAS/RNase L exert potent antiviral effects on various viruses. We generated REAVRs by harnessing the extensive knowledge about sensor and effector domains of PKR and RNase L. We demonstrated that REAVRs containing the dsRNA binding domain of the virus sensor PKR with the effector domain of RNase L were expressed and functionally active. All REAVRs showed some RNA cleavage in A549$^{PKR-/-RNase\ L-/-}$ cells infected with VACV, confirming that the RNase domain of REAVRs was activated. Interestingly, despite being expressed at a higher level than REAVR 7 and 8 **(Figure 2.2)**, REAVR 3 and 4 showed lower levels of rRNA degradation. Whether REAVR 7 and 8 imposed higher affinity for dsRNA or possessed a more productive conformation of the ribonuclease domain remains to be explored. Furthermore, REAVR 5 and 9 that contain kinase and RNase effector domains showed rRNA degradation and eIF2α phosphorylation (Figure 2.4E, 2.9C), suggesting both kinase and RNase effector domains were active during virus infections. Overall, we demonstrated that REAVRs are active and act as both sensors and effectors molecules in cultured mammalian cells.

All tested viruses replicated in T-REx cells under non-inducing conditions, indicating that these viruses can overcome the antiviral effects of the endogenous human PKR and OAS/RNase L pathways. Although all REAVRs strongly decreased luciferase expression, different REAVRs exhibited different antiviral potency against viruses, as shown by fold change in virus titer of doxycycline-treated and untreated cells in Table 2.2. REAVR 3 showed antiviral effects only on DENV2, and REAVR 4 had no effects on all tested viruses. REAVR 5 exhibited the strongest inhibition on VACV vP872 and moderate effects on DENV2, VSV-12'GFP, and VACV VC-2. Inhibition of VACV vP872 and VACV VC-2 by REAVR 5 correlated with our results from the luciferase-based reporter assay **(Figure 2.4A)** and was consistent with other studies

demonstrating that Syrian hamster PKR was sensitive to K3L, which directly targets the PKR kinase domain, but was resistant to E3L ((32) and Rothenburg lab unpublished). In contrast, REAVR 9, which contains full length mouse PKR showed lower antiviral activity on VACV vP872, likely due to the sensitivity of moue PKR to E3L. Altogether our data suggest that the species of origin for the different REAVR domains influence the antiviral spectra of REAVRs.

REAVR 7 mediated the strongest antiviral effects on DENV2, ZIKV, and VACV VC-2. Interestingly, REAVR 8, which has a longer linker region than REAVR 7, showed lower antiviral activity, suggesting that the linker region between the PKR and RNase L domains influences REAVR efficiency. DENV2 was the most sensitive to REAVR 7-mediated antiviral activity, with titers reduced by more than 1,000-fold **(Figure 2.6A)** in agreement with prior studies that showed canonical RNase L activity decreased the amount of detectable DENV genomes as well as DENV infectious particle production (45, 52). REAVR 7 also mediated the most potent antiviral effect on ZIKV replication (33-fold reduction) **(Figure 2.6A)**. RNase L was previously reported to decrease ZIKV genomes however having positive effects on ZIKV replication (49, 52), which might explain the weaker overall effects of REAVRs on ZIKV replication. Both REAVR 7 and 8, which have only the RNase effector domain, showed antiviral effects on VACV VC-2, further supporting multiple studies that have demonstrated antiviral activity of RNase L on poxviruses (53-55).

Our data showed REAVR 7 robustly reduced SARS-CoV-2 mNG replication**,** which is in agreement to findings that show that SARS-CoV-2 is sensitive to RNase L (56). PKR and RNase L activation was evident in A549 and Calu-3 cells infected SARS-CoV-2 (50). Despite the high level of p-eIF2α observed in SARS-CoV-2 infected cells, there was no

significant difference between virus titers in PKR^{KO} and WT A549^{ACE2} cells (50). Meanwhile, virus titer in RNase L^{KO} cells was about 4-fold higher than WT A549^{ACE2} cells, indicating a weak antiviral effect of RNase L against SARS-CoV-2 (50). In addition, ISG expression screening revealed OAS1 potently inhibited SARS-CoV-2 by activating RNase L (56). As we currently understand, delayed IFN response is one of the significant contributors to severe COVID-19 (57). Excessive inhibition of IFN production during SARS-CoV-2 infection might prevent robust expression of ISGs, including OAS1/RNase L, which has been shown to play a significant role in generating an antiviral state during SARS-CoV-2 infection (56). The ability of REAVR 7 to induce a protective effect against SARS-CoV-2 makes it an attractive target for continued study as a SARS-CoV-2 mRNA-based therapy independent of IFN signaling.

REAVR 7 showed minimal or no effect on VSV, supporting previous data showing VSV resistance to RNase L (58-60). We also did not observe VSV induced rRNA degradation in A549 cell lines consistent with the previous report (47). VSV resistance to OAS/RNase L pathway and REAVR 7 might be due to dsRNA intermediates located within different subcellular compartments or driven by VSV-specific evasion/antagonism strategies (56). Further investigation is required to elucidate the mechanism behind VSV resistance to the OAS/RNase L pathway. Furthermore, VSV replication was most strongly inhibited by either REAVR 5 or REAVR 9 **(Figure 2.8, Table 2.2)**. Interestingly, REAVR 9 containing mouse PKR mediated a remarkably higher VSV-12'GFP virus titer reduction (200-fold) than did REAVR 5 that contains Syrian hamster PKR **(Figure 2. 8B)**. A previous report showed VSV replicated more efficiently in Syrian hamster BHK and HeLa cell lines than in mouse L-929 cells (61). In addition, PKR^{KO} mice were highly susceptible and

succumbed to a very low dose of VSV infection, further supporting PKR as an important contributor of IFN-mediated resistance to VSV infection in mice (62). Notably, human PKR appeared to be dispensable for VSV-12'GFP replication **(Figure 2.8, 2.9)**. This result is unexpected since some studies showed the significant role of PKR as the component of IFN-mediated resistance to VSV infection (62, 63). Thus, with the evidence from previous reports and our data, it is tempting to hypothesize that there might be species-specific PKR inhibition by VSV.

DENV2 replicated to comparable levels in T-REx WT and T-REx PKR^{KO} cells, supporting the findings that DENV translation can occur independently of PKR activation (64-66). Several mechanisms have been described to facilitate DENV RNA translation when the canonical cap-dependent translation was inhibited, including binding of PABP to the non-polyadenylated 3' UTR (64), the function of 5'UTR as an internal ribosomal entry site (IRES) (22) and activation of the p38-Mnk1 signaling pathway (66). Overall, our data suggest REAVR 7-mediated potent antiviral activities, including against viruses that are not traditionally inhibited by PKR (e.g. DENV, ZIKV and SARS-CoV-2). However, there was no correlation between the virus titer and rRNA cleavage pattern upon DENV infection **(Figure 2.6C)**. It might be possible that viral RNA cleavage may occur even while the majority of rRNA is visibly intact during DENV infection (49, 67). Further investigation is required to elucidate the mechanism of REAVRs inhibition of virus replication.

Different REAVRs have different antiviral potency and some REAVRs possess broad-spectrum antiviral effects against several groups of viruses that have a substantial

public health burden. REAVR 5 showed the strongest effect on vP872, while REAVR 9 showed the strongest effect on VSV-12'GFP (about 99% reduction in virus titer). REAVR 7 showed the most potent effect on DENV2, SARS-CoV2 mNG, ZIKV, and VACV VC-2 (about 95-99.9% reduction in virus titer), but it appeared to have no effect or minimal effect on VSV-12'GFP. REAVR 8 also exhibited a strong antiviral effect on DENV2 with about 99% reduction in virus titer. Future investigation is warranted to test the antiviral effect of REAVRs on other viruses and generate a second generation of REAVRs that increase the breadth and potency of REAVR-mediated antiviral activities. In an effort to mitigate transmission of the arboviruses, REAVR 7 and 8 showed antiviral effects on DENV and ZIKV could be used as a candidate of effector genes to block arbovirus infection in *Aedes aegypti*. Lastly, with the rapid development of mRNA-based vaccines and therapeutics against infectious diseases (68), REAVR-mediated antiviral activities might have implications for mRNA-based drug discovery and development in the future.

REFERENCES

1. Morens DM, Daszak P, Markel H, Taubenberger JK. Pandemic COVID-19 Joins History's Pandemic Legion. mBio. 2020;11(3). Epub 2020/05/31. doi: 10.1128/mBio.00812-20. PubMed PMID: 32471830; PMCID: PMC7267883.
2. Rückert C, Weger-Lucarelli J, Garcia-Luna SM, Young MC, Byas AD, Murrieta RA, Fauver JR, Ebel GD. Impact of simultaneous exposure to arboviruses on infection and transmission by Aedes aegypti mosquitoes. Nat Commun. 2017;8:15412. Epub 2017/05/20. doi: 10.1038/ncomms15412. PubMed PMID: 28524874; PMCID: PMC5454532.
3. Schlee M, Hartmann G. Discriminating self from non-self in nucleic acid sensing. Nature reviews Immunology. 2016;16(9):566-80. Epub 2016/07/28. doi: 10.1038/nri.2016.78. PubMed PMID: 27455396; PMCID: PMC7097691
4. Weber F, Wagner V, Rasmussen SB, Hartmann R, Paludan SR. Double-Stranded RNA Is Produced by Positive-Strand RNA Viruses and DNA Viruses but Not in Detectable Amounts by Negative-Strand RNA Viruses. Journal of Virology. 2006;80(10):5059. doi: 10.1128/JVI.80.10.5059-5064.2006.
5. Son K-N, Liang Z, Lipton HL. Double-Stranded RNA Is Detected by Immunofluorescence Analysis in RNA and DNA Virus Infections, Including Those by Negative-Stranded RNA Viruses. Journal of Virology. 2015;89(18):9383. doi: 10.1128/JVI.01299-15.
6. Silverman RH. Viral encounters with 2',5'-oligoadenylate synthetase and RNase L during the interferon antiviral response. J Virol. 2007;81(23):12720-9. Epub 2007/09/07. doi: 10.1128/jvi.01471-07. PubMed PMID: 17804500; PMCID: PMC2169107.
7. Langland JO, Cameron JM, Heck MC, Jancovich JK, Jacobs BL. Inhibition of PKR by RNA and DNA viruses. Virus Research. 2006;119(1):100-10. doi: https://doi.org/10.1016/j.virusres.2005.10.014.
8. Sadler AJ, Williams BR. Interferon-inducible antiviral effectors. Nature reviews Immunology. 2008;8(7):559-68. Epub 2008/06/26. doi: 10.1038/nri2314. PubMed PMID: 18575461; PMCID: PMC2522268.
9. Kuhen KL, Samuel CE. Isolation of the interferon-inducible RNA-dependent protein kinase Pkr promoter and identification of a novel DNA element within the 5'-flanking region of human and mouse Pkr genes. Virology. 1997;227(1):119-30. Epub 1997/01/06. doi: 10.1006/viro.1996.8306. PubMed PMID: 9007065.
10. Das S, Ward SV, Tacke RS, Suske G, Samuel CE. Activation of the RNA-dependent protein kinase PKR promoter in the absence of interferon is dependent upon Sp proteins. The Journal of biological chemistry. 2006;281(6):3244-53. Epub 2005/12/13. doi: 10.1074/jbc.M510612200. PubMed PMID: 16339759.

11. Zhou A, Hassel BA, Silverman RH. Expression cloning of 2-5A-dependent RNAase: a uniquely regulated mediator of interferon action. Cell. 1993;72(5):753-65. Epub 1993/03/12. doi: 10.1016/0092-8674(93)90403-d. PubMed PMID: 7680958.
12. Nanduri S, Carpick BW, Yang Y, Williams BR, Qin J. Structure of the double-stranded RNA-binding domain of the protein kinase PKR reveals the molecular basis of its dsRNA-mediated activation. The EMBO journal. 1998;17(18):5458-65. doi: 10.1093/emboj/17.18.5458. PubMed PMID: 9736623.
13. Wu S, Kaufman RJ. A model for the double-stranded RNA (dsRNA)-dependent dimerization and activation of the dsRNA-activated protein kinase PKR. The Journal of biological chemistry. 1997;272(2):1291-6. Epub 1997/01/10. doi: 10.1074/jbc.272.2.1291. PubMed PMID: 8995434.
14. Dey M, Cao C, Dar AC, Tamura T, Ozato K, Sicheri F, Dever TE. Mechanistic link between PKR dimerization, autophosphorylation, and eIF2alpha substrate recognition. Cell. 2005;122(6):901-13. Epub 2005/09/24. doi: 10.1016/j.cell.2005.06.041. PubMed PMID: 16179259.
15. Sonenberg N, Hinnebusch AG. Regulation of translation initiation in eukaryotes: mechanisms and biological targets. Cell. 2009;136(4):731-45. Epub 2009/02/26. doi: 10.1016/j.cell.2009.01.042. PubMed PMID: 19239892; PMCID: PMC3610329.
16. Adomavicius T, Guaita M, Zhou Y, Jennings MD, Latif Z, Roseman AM, Pavitt GD. The structural basis of translational control by eIF2 phosphorylation. Nat Commun. 2019;10(1):2136. Epub 2019/05/16. doi: 10.1038/s41467-019-10167-3. PubMed PMID: 31086188; PMCID: PMC6513899.
17. Marintchev A, Ito T. eIF2B and the Integrated Stress Response: A Structural and Mechanistic View. Biochemistry. 2020;59(13):1299-308. Epub 2020/03/24. doi: 10.1021/acs.biochem.0c00132. PubMed PMID: 32200625; PMCID: PMC7189779.
18. Fernández-García L, Angulo J, Ramos H, Barrera A, Pino K, Vera-Otarola J, López-Lastra M. The internal ribosome entry site of the Dengue virus mRNA is active when cap-dependent translation initiation is inhibited. J Virol. 2020;95(5). Epub 2020/12/11. doi: 10.1128/jvi.01998-20. PubMed PMID: 33298544; PMCID: PMC8092825.
19. Ventoso I, Sanz MA, Molina S, Berlanga JJ, Carrasco L, Esteban M. Translational resistance of late alphavirus mRNA to eIF2alpha phosphorylation: a strategy to overcome the antiviral effect of protein kinase PKR. Genes & development. 2006;20(1):87-100. Epub 2006/01/05. doi: 10.1101/gad.357006. PubMed PMID: 16391235; PMCID: PMC1356103.
20. White LK, Sali T, Alvarado D, Gatti E, Pierre P, Streblow D, DeFilippis VR. Chikungunya Virus Induces IPS-1-Dependent Innate Immune Activation and Protein Kinase R-Independent Translational Shutoff. Journal of Virology. 2011;85(1):606. doi: 10.1128/JVI.00767-10.

21. Gorchakov R, Frolova E, Williams BR, Rice CM, Frolov I. PKR-dependent and -independent mechanisms are involved in translational shutoff during Sindbis virus infection. J Virol. 2004;78(16):8455-67. Epub 2004/07/29. doi: 10.1128/jvi.78.16.8455-8467.2004. PubMed PMID: 15280454; PMCID: PMC479073.
22. Song Y, Mugavero J, Stauft CB, Wimmer E. Dengue and Zika Virus 5' Untranslated Regions Harbor Internal Ribosomal Entry Site Functions. mBio. 2019;10(2). Epub 2019/04/11. doi: 10.1128/mBio.00459-19. PubMed PMID: 30967466; PMCID: PMC6456755.
23. Huang H, Zeqiraj E, Dong B, Jha BK, Duffy NM, Orlicky S, Thevakumaran N, Talukdar M, Pillon MC, Ceccarelli DF, Wan LC, Juang YC, Mao DY, Gaughan C, Brinton MA, Perelygin AA, Kourinov I, Guarne A, Silverman RH, Sicheri F. Dimeric structure of pseudokinase RNase L bound to 2-5A reveals a basis for interferon-induced antiviral activity. Molecular cell. 2014;53(2):221-34. Epub 2014/01/28. doi: 10.1016/j.molcel.2013.12.025. PubMed PMID: 24462203; PMCID: PMC3974923.
24. Han Y, Donovan J, Rath S, Whitney G, Chitrakar A, Korennykh A. Structure of Human RNase L Reveals the Basis for Regulated RNA Decay in the IFN Response. Science. 2014;343(6176):1244-8. doi: 10.1126/science.1249845.
25. Wreschner DH, McCauley JW, Skehel JJ, Kerr IM. Interferon action--sequence specificity of the ppp(A2'p)nA-dependent ribonuclease. Nature. 1981;289(5796):414-7. Epub 1981/01/29. doi: 10.1038/289414a0. PubMed PMID: 6162102.
26. Han Y, Donovan J, Rath S, Whitney G, Chitrakar A, Korennykh A. Structure of human RNase L reveals the basis for regulated RNA decay in the IFN response. Science. 2014;343(6176):1244-8. Epub 2014/03/01. doi: 10.1126/science.1249845. PubMed PMID: 24578532; PMCID: PMC4731867.
27. Daou S, Talukdar M, Tang J, Dong B, Banerjee S, Li Y, Duffy NM, Ogunjimi AA, Gaughan C, Jha BK, Gish G, Tavernier N, Mao D, Weiss SR, Huang H, Silverman RH, Sicheri F. A phenolic small molecule inhibitor of RNase L prevents cell death from ADAR1 deficiency. Proceedings of the National Academy of Sciences of the United States of America. 2020;117(40):24802-12. Epub 2020/09/23. doi: 10.1073/pnas.2006883117. PubMed PMID: 32958664; PMCID: PMC7547215.
28. Drappier M, Michiels T. Inhibition of the OAS/RNase L pathway by viruses. Curr Opin Virol. 2015;15:19-26. Epub 2015/08/02. doi: 10.1016/j.coviro.2015.07.002. PubMed PMID: 26231767.
29. Drappier M, Jha BK, Stone S, Elliott R, Zhang R, Vertommen D, Weiss SR, Silverman RH, Michiels T. A novel mechanism of RNase L inhibition: Theiler's virus L* protein prevents 2-5A from binding to RNase L. PLoS Pathog. 2018;14(4):e1006989. Epub 2018/04/14. doi: 10.1371/journal.ppat.1006989. PubMed PMID: 29652922; PMCID: PMC5927464.

30. Colón-Thillet R, Hsieh E, Graf L, McLaughlin RN, Jr., Young JM, Kochs G, Emerman M, Malik HS. Combinatorial mutagenesis of rapidly evolving residues yields super-restrictor antiviral proteins. PLoS biology. 2019;17(10):e3000181. Epub 2019/10/02. doi: 10.1371/journal.pbio.3000181. PubMed PMID: 31574080; PMCID: PMC6772013.
31. McDonnell MM, Crawford KHD, Dingens AS, Bloom JD, Emerman M. APOBEC3C Tandem Domain Proteins Create Super Restriction Factors against HIV-1. mBio. 2020;11(2). Epub 2020/04/30. doi: 10.1128/mBio.00737-20. PubMed PMID: 32345636; PMCID: PMC7188997.
32. Park C, Peng C, Rahman MJ, Haller SL, Tazi L, Brennan G, Rothenburg S. Orthopoxvirus K3 orthologs show virus- and host-specific inhibition of the antiviral protein kinase PKR. PLoS Pathog. 2021;17(1):e1009183. Epub 2021/01/15. doi: 10.1371/journal.ppat.1009183. PubMed PMID: 33444388; PMCID: PMC7840043.
33. Carpentier KS, Esparo NM, Child SJ, Geballe AP. A Single Amino Acid Dictates Protein Kinase R Susceptibility to Unrelated Viral Antagonists. PLoS Pathog. 2016;12(10):e1005966. Epub 2016/10/26. doi: 10.1371/journal.ppat.1005966. PubMed PMID: 27780231; PMCID: PMC5079575.
34. Rahman MM, Liu J, Chan WM, Rothenburg S, McFadden G. Myxoma virus protein M029 is a dual function immunomodulator that inhibits PKR and also conscripts RHA/DHX9 to promote expanded host tropism and viral replication. PLoS Pathog. 2013;9(7):e1003465. Epub 2013/07/16. doi: 10.1371/journal.ppat.1003465. PubMed PMID: 23853588; PMCID: PMC3701710.
35. Ung TL, Cao C, Lu J, Ozato K, Dever TE. Heterologous dimerization domains functionally substitute for the double-stranded RNA binding domains of the kinase PKR. Embo j. 2001;20(14):3728-37. Epub 2001/07/12. doi: 10.1093/emboj/20.14.3728. PubMed PMID: 11447114; PMCID: PMC125533.
36. Beattie E, Tartaglia J, Paoletti E. Vaccinia virus-encoded eIF-2 alpha homolog abrogates the antiviral effect of interferon. Virology. 1991;183(1):419-22. Epub 1991/07/01. PubMed PMID: 1711259.
37. Friedrich I, Eizenbach M, Sajman J, Ben-Bassat H, Levitzki A. A cellular screening assay to test the ability of PKR to induce cell death in mammalian cells. Molecular therapy : the journal of the American Society of Gene Therapy. 2005;12(5):969-75. Epub 2005/08/09. doi: 10.1016/j.ymthe.2005.06.442. PubMed PMID: 16084774.
38. Rothenburg S, Seo EJ, Gibbs JS, Dever TE, Dittmar K. Rapid evolution of protein kinase PKR alters sensitivity to viral inhibitors. Nature Structural &Amp; Molecular Biology. 2008;16:63. doi: 10.1038/nsmb.1529
39. Peng C, Haller SL, Rahman MM, McFadden G, Rothenburg S. Myxoma virus M156 is a specific inhibitor of rabbit PKR but contains a loss-of-function mutation in Australian virus isolates. Proceedings of the National Academy of Sciences of the

United States of America. 2016;113(14):3855-60. Epub 2016/02/24. doi: 10.1073/pnas.1515613113. PubMed PMID: 26903626; PMCID: PMC4833222.
40. Nejepinska J, Malik R, Wagner S, Svoboda P. Reporters transiently transfected into mammalian cells are highly sensitive to translational repression induced by dsRNA expression. PLoS One. 2014;9(1):e87517. Epub 2014/01/30. doi: 10.1371/journal.pone.0087517. PubMed PMID: 24475301; PMCID: PMC3903663.
41. Zhang F, Romano PR, Nagamura-Inoue T, Tian B, Dever TE, Mathews MB, Ozato K, Hinnebusch AG. Binding of double-stranded RNA to protein kinase PKR is required for dimerization and promotes critical autophosphorylation events in the activation loop. The Journal of biological chemistry. 2001;276(27):24946-58. Epub 2001/05/05. doi: 10.1074/jbc.M102108200. PubMed PMID: 11337501.
42. O'Gorman S, Fox DT, Wahl GM. Recombinase-mediated gene activation and site-specific integration in mammalian cells. Science. 1991;251(4999):1351-5. Epub 1991/03/15. doi: 10.1126/science.1900642. PubMed PMID: 1900642.
43. Rothenburg S, Seo EJ, Gibbs JS, Dever TE, Dittmar K. Rapid evolution of protein kinase PKR alters sensitivity to viral inhibitors. Nat Struct Mol Biol. 2009;16(1):63-70. Epub 2008/12/02. doi: 10.1038/nsmb.1529. PubMed PMID: 19043413; PMCID: PMC3142916.
44. Rothenburg S, Chinchar VG, Dever TE. Characterization of a ranavirus inhibitor of the antiviral protein kinase PKR. BMC Microbiol. 2011;11:56. Epub 2011/03/23. doi: 10.1186/1471-2180-11-56. PubMed PMID: 21418572; PMCID: PMC3068933.
45. Lin RJ, Yu HP, Chang BL, Tang WC, Liao CL, Lin YL. Distinct antiviral roles for human 2',5'-oligoadenylate synthetase family members against dengue virus infection. Journal of immunology (Baltimore, Md : 1950). 2009;183(12):8035-43. Epub 2009/11/20. doi: 10.4049/jimmunol.0902728. PubMed PMID: 19923450.
46. Scherbik SV, Paranjape JM, Stockman BM, Silverman RH, Brinton MA. RNase L plays a role in the antiviral response to West Nile virus. J Virol. 2006;80(6):2987-99. Epub 2006/02/28. doi: 10.1128/jvi.80.6.2987-2999.2006. PubMed PMID: 16501108; PMCID: PMC1395436.
47. Li Y, Banerjee S, Wang Y, Goldstein SA, Dong B, Gaughan C, Silverman RH, Weiss SR. Activation of RNase L is dependent on OAS3 expression during infection with diverse human viruses. Proceedings of the National Academy of Sciences. 2016;113(8):2241. doi: 10.1073/pnas.1519657113.
48. Diamond MS, Harris E. Interferon Inhibits Dengue Virus Infection by Preventing Translation of Viral RNA through a PKR-Independent Mechanism. Virology. 2001;289(2):297-311. doi: https://doi.org/10.1006/viro.2001.1114.
49. Whelan JN, Parenti NA, Hatterschide J, Renner DM, Li Y, Reyes HM, Dong B, Perez ER, Silverman RH, Weiss SR. Zika virus employs the host antiviral RNase L protein to support replication factory assembly. Proceedings of the National Academy of Sciences of the United States of America. 2021;118(22). Epub

2021/05/26. doi: 10.1073/pnas.2101713118. PubMed PMID: 34031250; PMCID: PMC8179202.
50. Li Y, Renner DM, Comar CE, Whelan JN, Reyes HM, Cardenas-Diaz FL, Truitt R, Tan LH, Dong B, Alysandratos KD, Huang J, Palmer JN, Adappa ND, Kohanski MA, Kotton DN, Silverman RH, Yang W, Morrisey EE, Cohen NA, Weiss SR. SARS-CoV-2 induces double-stranded RNA-mediated innate immune responses in respiratory epithelial-derived cells and cardiomyocytes. Proceedings of the National Academy of Sciences of the United States of America. 2021;118(16). Epub 2021/04/04. doi: 10.1073/pnas.2022643118. PubMed PMID: 33811184; PMCID: PMC8072330.
51. van den Pol AN, Davis JN. Highly Attenuated Recombinant Vesicular Stomatitis Virus VSV-12′GFP Displays Immunogenic and Oncolytic Activity. Journal of Virology. 2013;87(2):1019. doi: 10.1128/JVI.01106-12.
52. Whelan JN, Li Y, Silverman RH, Weiss SR. Zika Virus Production Is Resistant to RNase L Antiviral Activity. J Virol. 2019;93(16). Epub 2019/05/31. doi: 10.1128/jvi.00313-19. PubMed PMID: 31142667; PMCID: PMC6675901.
53. Rice AD, Turner PC, Embury JE, Moldawer LL, Baker HV, Moyer RW. Roles of vaccinia virus genes E3L and K3L and host genes PKR and RNase L during intratracheal infection of C57BL/6 mice. J Virol. 2011;85(1):550-67. Epub 2010/10/15. doi: 10.1128/jvi.00254-10. PubMed PMID: 20943971; PMCID: PMC3014211.
54. Li Y, Banerjee S, Wang Y, Goldstein SA, Dong B, Gaughan C, Silverman RH, Weiss SR. Activation of RNase L is dependent on OAS3 expression during infection with diverse human viruses. Proceedings of the National Academy of Sciences of the United States of America. 2016;113(8):2241-6. Epub 2016/02/10. doi: 10.1073/pnas.1519657113. PubMed PMID: 26858407; PMCID: PMC4776461.
55. Díaz-Guerra M, Rivas C, Esteban M. Inducible expression of the 2-5A synthetase/RNase L system results in inhibition of vaccinia virus replication. Virology. 1997;227(1):220-8. Epub 1997/01/06. doi: 10.1006/viro.1996.8294. PubMed PMID: 9007077.
56. Wickenhagen A, Sugrue E, Lytras S, Kuchi S, Noerenberg M, Turnbull ML, Loney C, Herder V, Allan J, Jarmson I, Cameron-Ruiz N, Varjak M, Pinto RM, Lee JY, Iselin L, Palmalux N, Stewart DG, Swingler S, Greenwood EJD, Crozier TWM, Gu Q, Davies EL, Clohisey S, Wang B, Trindade Maranhão Costa F, Freire Santana M, de Lima Ferreira LC, Murphy L, Fawkes A, Meynert A, Grimes G, Da Silva Filho JL, Marti M, Hughes J, Stanton RJ, Wang ECY, Ho A, Davis I, Jarrett RF, Castello A, Robertson DL, Semple MG, Openshaw PJM, Palmarini M, Lehner PJ, Baillie JK, Rihn SJ, Wilson SJ. A prenylated dsRNA sensor protects against severe COVID-19. Science. 2021;374(6567):eabj3624. Epub 2021/09/29. doi: 10.1126/science.abj3624. PubMed PMID: 34581622.

57. Xia H, Shi PY. Antagonism of Type I Interferon by Severe Acute Respiratory Syndrome Coronavirus 2. Journal of interferon & cytokine research : the official journal of the International Society for Interferon and Cytokine Research. 2020;40(12):543-8. Epub 2020/12/19. doi: 10.1089/jir.2020.0214. PubMed PMID: 33337934; PMCID: PMC7757701.
58. Hassel BA, Zhou A, Sotomayor C, Maran A, Silverman RH. A dominant negative mutant of 2-5A-dependent RNase suppresses antiproliferative and antiviral effects of interferon. Embo j. 1993;12(8):3297-304. Epub 1993/08/01. PubMed PMID: 7688298; PMCID: PMC413597.
59. Coccia EM, Romeo G, Nissim A, Marziali G, Albertini R, Affabris E, Battistini A, Fiorucci G, Orsatti R, Rossi GB, et al. A full-length murine 2-5A synthetase cDNA transfected in NIH-3T3 cells impairs EMCV but not VSV replication. Virology. 1990;179(1):228-33. Epub 1990/11/01. doi: 10.1016/0042-6822(90)90292-y. PubMed PMID: 2171206.
60. Martinand C, Salehzada T, Silhol M, Lebleu B, Bisbal C. RNase L inhibitor (RLI) antisense constructions block partially the down regulation of the 2-5A/RNase L pathway in encephalomyocarditis-virus-(EMCV)-infected cells. European journal of biochemistry. 1998;254(2):248-55. Epub 1998/07/11. doi: 10.1046/j.1432-1327.1998.2540248.x. PubMed PMID: 9660177.
61. Ostertag D, Hoblitzell-Ostertag TM, Perrault J. Overproduction of Double-Stranded RNA in Vesicular Stomatitis Virus-Infected Cells Activates a Constitutive Cell-Type-Specific Antiviral Response. Journal of Virology. 2007;81(2):503. doi: 10.1128/JVI.01218-06.
62. Stojdl DF, Abraham N, Knowles S, Marius R, Brasey A, Lichty BD, Brown EG, Sonenberg N, Bell JC. The murine double-stranded RNA-dependent protein kinase PKR is required for resistance to vesicular stomatitis virus. J Virol. 2000;74(20):9580-5. Epub 2000/09/23. doi: 10.1128/jvi.74.20.9580-9585.2000. PubMed PMID: 11000229; PMCID: PMC112389.
63. Balachandran S, Roberts PC, Brown LE, Truong H, Pattnaik AK, Archer DR, Barber GN. Essential role for the dsRNA-dependent protein kinase PKR in innate immunity to viral infection. Immunity. 2000;13(1):129-41. Epub 2000/08/10. doi: 10.1016/s1074-7613(00)00014-5. PubMed PMID: 10933401.
64. Edgil D, Polacek C, Harris E. Dengue virus utilizes a novel strategy for translation initiation when cap-dependent translation is inhibited. J Virol. 2006;80(6):2976-86. Epub 2006/02/28. doi: 10.1128/jvi.80.6.2976-2986.2006. PubMed PMID: 16501107; PMCID: PMC1395423.
65. Peña J, Harris E. Dengue virus modulates the unfolded protein response in a time-dependent manner. The Journal of biological chemistry. 2011;286(16):14226-36. Epub 2011/03/10. doi: 10.1074/jbc.M111.222703. PubMed PMID: 21385877; PMCID: PMC3077624.

66. Roth H, Magg V, Uch F, Mutz P, Klein P, Haneke K, Lohmann V, Bartenschlager R, Fackler OT, Locker N, Stoecklin G, Ruggieri A. Flavivirus Infection Uncouples Translation Suppression from Cellular Stress Responses. mBio. 2017;8(1). Epub 2017/01/12. doi: 10.1128/mBio.02150-16. PubMed PMID: 28074025; PMCID: PMC5225315.
67. Donovan J, Rath S, Kolet-Mandrikov D, Korennykh A. Rapid RNase L-driven arrest of protein synthesis in the dsRNA response without degradation of translation machinery. RNA (New York, NY). 2017;23(11):1660-71. Epub 2017/08/16. doi: 10.1261/rna.062000.117. PubMed PMID: 28808124; PMCID: PMC5648034.
68. Diaz-Guerra M, Rivas C, Esteban M. Inducible expression of the 2-5A synthetase/RNase L system results in inhibition of vaccinia virus replication. Virology. 1997;227(1):220-8. Epub 1997/01/06. doi: 10.1006/viro.1996.8294. PubMed PMID: 9007077.

Chapter 3: Species Specificity of Primate Protein Kinase R Inhibition by Tanapox and Yaba Monkey Tumor Virus K3 Orthologs

Dewi Megawati[1], Jeannine N. Stroup[1], Chorong Park[1], Taylor Clarkson[1], Loubna Tazi[1], Greg Brennan[1], and Stefan Rothenburg[1]

1. Department of Medical Microbiology and Immunology, School of Medicine, University of California, Davis, California, USA

Abstract

Yaba monkey tumor virus (YMTV) and Tanapox virus (TPV) belong to the yatapoxvirus genus. These viruses infect many different primate species and cause zoonotic infections in humans. Despite the threat posed to human health, the factors determining the host range of these viruses are poorly understood. In this study, we assessed the role of orthologs of the vaccinia virus PKR inhibitor K3 from YMTV and TPV in influencing viral host range. We used a luciferase-based assay to analyze the ability of TPV and YMTV K3 orthologs, which share 75% amino acid identity, to inhibit PKR variants derived from a panel of 15 different primate species. Our results showed that YMTV and TPV K3 orthologs inhibited PKR in a species-specific manner, and that TPV and YMTV K3 showed distinct PKR inhibition profiles. TPV K3 inhibited PKR from 11 primates, including human, substantially better than YMTV K3, whereas both K3 orthologs inhibited the other four primate PKRs comparably. These general patterns observed in the luciferase-based assay were recapitulated in infection assays in either primate derived

cells or cells stably transfected with different PKRs. Furthermore, we found that the C-terminus of both K3 orthologs governed the observed differential PKR inhibition. Together, these observations demonstrate that yatapoxvirus K3 orthologs inhibit PKR in a species-specific manner, which may contribute to the differential susceptibility of different primate species to yatapoxvirus infection.

SIGNIFICANCE

The possible emergence of smallpox-like diseases through zoonosis of animal poxviruses a major public health concern. Members of the yatapoxvirus genus infect humans and other primates and have caused outbreaks throughout Africa for the past 60 years. In addition, human infections with yatapoxviruses have been reported in animal handlers at primate centers in the United States and among travelers who visited Africa. Despite the threat posed to human health, the factors determining the host range of these viruses are poorly understood. Here, we demonstrate that TPV and YMTV K3 orthologs possess virus and host species-specific PKR activity, which might influence yatapoxvirus host species specificity.

INTRODUCTION

Yatapoxviruses are a small group of chordopoxvirinae known to be pathogenic to primates, including humans. The yatapoxvirus genus includes Yaba monkey tumor virus (YMTV) and Tanapox virus (TPV) (1). A third virus, Yaba-like disease virus (YLDV), is closely related to TPV and can be considered as a different variant of the same virus (2). TPV was first isolated from human skin biopsies during a TPV outbreak in 1957 in Tana

River Valley, Kenya (3, 4). YMTV was first isolated from an outbreak of subcutaneous tumors in monkeys in Yaba, Nigeria, in 1958 (5). Yatapoxvirus genomes are A+T rich ranging in size from 135-145 kb (2, 6-8). YLDV and TPV genomes share 98.68% sequence identity, further evidence suggesting that YLDV and TPV are different strains of the same virus. The genomes of YMTV and YLDV share 75% sequence identity (8). Despite being closely related, TPV and YMTV exhibit differences in disease presentations. TPV infection is characterized by vesicular skin lesions, whereas YMTV infection produces a localized histiocyte-filled tumor (histiocytomas) (9).

While both TPV and YMTV infect a wide range of primates, they appear to exhibit host specificity. Serological surveys have shown that TPV is endemic in African and Malaysian but not Indian Rhesus or New World monkeys (3, 4, 10). Human Tanapox disease is considered endemic to several regions of Africa and causes febrile illness and vesicular skin lesions similar to those produced in non-human primates. Sporadic cases have been identified in 30 locations spanning 6000 kilometers from Sierra-Leone to Tanzania, with larger outbreaks occurring from time to time (11). Similarly, antibodies against YMTV have been found in *Hominidae* and Old World monkeys but not in New World monkeys and Indian rhesus monkeys (10). Following experimental subcutaneous inoculation with YMTV, tumor-like masses were detected in Asian rhesus monkeys, but not in African green monkeys, mangabey monkeys, patas monkeys, mice, rats, rabbits, guinea pigs, hamsters, and South American capuchin monkeys (5, 9, 12), indicating host specificity. In addition, a serological survey of 456 primate sera including 26 chimpanzees, 326 Old World monkeys (African green monkeys, patas monkeys, baboon, colobus, rhesus), and 104 New World monkeys (spider monkeys, squirrel monkeys, owl

monkeys, marmosets, and capuchin monkeys) indicated that antibodies against YMTV were evident in chimpanzees and Old-World monkeys but not in any of the New World monkeys (10). While no natural infection of YMTV in humans has been reported, infection of human volunteers as well as an accidental infection of a laboratory worker have resulted in the development mild histiocytomas (13). Despite the threat posed to human health, the factors determining the host range of yatapoxviruses are poorly understood. In addition, vaccination with vaccinia virus does not appear to protect against yatapoxvirus infections (13, 14). Thus, it is important to study factors that determine the host range of yatapoxviruses.

The host tropism of many viruses is largely determined by the attachment and entry via specific host cell receptors. However, as poxviruses use ubiquitous cell surface receptors for entry, it is believed that evasion of the innate immune response post-entry is a more important determinant of poxvirus tropism (15, 16). Protein Kinase R (PKR) is a prominent host restriction factor against poxvirus infection (Reviewed in (17)). PKR exists in a monomeric inactive form and is activated upon binding to double-stranded RNA (dsRNA) produced during infection by most viruses, which leads to PKR dimerization and autophosphorylation. PKR activation blocks viral replication by inhibiting general protein synthesis through the phosphorylation of the alpha subunit of eukaryotic initiation factor 2 (eIF2α) (18). Phosphorylated eIF2α has a high binding affinity for the regulatory core of guanine nucleotide exchange factor, eIF2B, and prevents eIF2B from catalyzing GDP-GTP exchange to eIF2α (19). As GTP-bound eIF2 is required for translation initiation, the resulting low availability of GTP-eIF2 leads to the shut off of cap-dependent protein synthesis, including that of viral proteins. To overcome the antiviral

effects of PKR activity, most poxviruses encode two PKR inhibitors: orthologs of vaccinia virus (VACV) proteins E3 and K3. E3 binds dsRNA and prevents PKR dimerization, whereas K3 competitively inhibits PKR by acting as a pseudosubstrate for the eIF2α binding site (20-22).

It was previously shown that inhibition of host PKR by K3 orthologs of several poxvirus families is a key determinant of host specificity (21, 23-26). Vaccinia virus lacking the E3L gene (VACV△E3L) but maintaining the K3L gene was unable to replicate in HeLa cells but remained replication competent in BHK21 cells, suggesting a role for K3 in determining host range (21). This finding was supported by our recent studies on leporipoxvirus, capripoxvirus, and orthopoxvirus K3 orthologs. We have demonstrated that M156, Myxoma virus (MYXV) K3 ortholog, specifically inhibited rabbit PKR but failed to inhibit other PKR species (23). Similarly, capripoxvirus K3 orthologs inhibited human, goat, and sheep PKR strongly, but exhibiting only weak inhibition of mouse and cow PKR (24). Our studies on inhibition of PKR from a panel of mammalian species by orthopoxvirus K3 orthologs exhibited distinct inhibition profiles. Importantly, the studies revealed that the phylogenetic relatedness of PKR is a poor predictor of the quality of interactions between PKR and K3 orthologs (26), and therefore, these interactions must be determined experimentally. In this study, we used a luciferase-based assay and infections of mammalian cell lines to examine the ability of TPV and YMTV K3 orthologs to inhibit PKR derived from 15 primate species. Our results demonstrate that TPV and YMTV K3 orthologs have distinct PKR inhibition profiles and that they inhibit primate PKR in a species-specific manner.

MATERIALS AND METHODS

Cell lines

Tert immortalized gibbon fibroblasts, HeLa cells (human, ATCC #CCL-2), HeLa PKR-knock-out, and BSC40 (ATCC CRL-2761) were kindly provided by Dr. Adam Geballe (27). RK13 cells (rabbit) expressing E3 and K3 (designated RK13+E3L+K3L) were previously described (28). The cells were grown in Dulbecco's Modified Eagle's Medium (DMEM, Life Technologies) supplemented with 5% fetal bovine serum (FBS, Lonza) or 10% FBS (for gibbon Tert cells) and 100 IU/ml penicillin/streptomycin (Gibco). RK13+E3L+K3L cell culture medium contained 500 µg/ml geneticin and 300 µg/ml zeocin (Life Technologies). Tetracycline-regulated expression human embryonic kidney 293 cells (Flp-In™ T-REx™ 293, Invitrogen) were grown in 10% FBS DMEM culture medium containing zeocin (10µg/ml) and blasticidin S (15 µg/ml, Gibco). Generation of Flp-In™ T-REx™ 293 PKR^{KO} (T-REx PKR^{KO}) has been previously described (Haller et al. unpublished). To generate stable cells, T-REx PKR^{KO} cells were co-transfected with Flp recombinase expression vector pOG44 (Invitrogen) and pcDNA5/FRT/TO (Invitrogen) encoding either human PKR, titi PKR, colobus PKR, and white cheek gibbon PKR. The surviving cells were selected with hygromycin (50 µg/ml) and blasticidin (15 µg/ml) for ten days. T-REx PKR^{KO} stable cells expressing primate PKR were maintained in culture media containing 50 µg/ml of hygromycin (Invitrogen) and 15 µg/ml of blasticidin S (Gibco).

Plasmids

Variants of primate PKR were kindly provided by Dr. Nels Elde (29). Variants of primate PKR and viral antagonist genes VACV_K3L (YP_232916.1), TPV_K3L (EF420156.1), YMTV_K3L (AY386371.1) were subcloned into the pSG5 expression vector for luciferase-based reporter assays. pGL3 luciferase reporter vector was purchased from Promega. Cloning was done using Gibson assembly techniques. To monitor VACV K3L, TPV K3L, and YMTV K3L gene expressions, these genes were cloned into C-terminus DYK-tagged pSG5 vector for transient transfection assay. The C-terminal regions of the TPV and YMTV inhibitors were swapped and cloned into pSG5 using Gibson assembly to generate hybrid $_{N}$TPV-$_{C}$YMTV and $_{N}$YMTV-$_{C}$TPV K3 orthologs. To generate recombinant VACV expressing TPV K3L and YMTV K3L genes, the yatapoxvirus K3 genes were cloned into p837-GOI-mCherry-E3L as previously described (30). To generate T-REx PKR^{KO} stable cells, human PKR, gibbon PKR, colobus PKR, and dusky titi PKR were cloned into pCDNA5/FRT/TO mammalian expression vector. Flippase recombinase expression vector, pOG44, was obtained from Invitrogen. All DNA sequences were confirmed by Sanger sequencing.

Luciferase-based reporter assays

Luciferase-based assays were performed as previously described (31). Briefly, 5 x 10^4 HeLa PKR^{KO} cells were seeded per well in 24 well plates overnight. The HeLa PKR^{KO} cells were co-transfected with 200ng of the indicated PKR expression vector, 200ng of each viral antagonist expression vector, and 50 ng of pGL3 firefly luciferase expression

vector (Promega). Transfection was done using GenJet (Signagen) with DNA to GenJet ratio of 1:2 as described by the manufacturer's protocol. Cells were lysed with mammalian lysis buffer (GE Healthcare) at 48 hours post-transfection. Luciferase activity was measured using a GloMax luminometer (Promega) by adding luciferin (Promega) reagent to the cell lysates as per manufacturer's recommendations. Data are presented as relative luciferase activity in which all data were normalized to pSG5 empty vector. Experiments were conducted in triplicate for each of the three independent experiments.

Virus and infections

Vaccinia virus variant vP872 (32) was kindly provided by Dr. Bertram Jacobs, VCR4+VACV K3L and VCR4+sheeppox K3L (SPPV K3L) were previously described (24). Generation of VC-R4 from vP872 variant was previously described (30). Generation of chimeric vaccinia virus, VCR4+TPV K3L, and VCR4+YMTV K3L, was done by the scarless integration of the open reading frames of the yatapoxvirus K3L orthologs into the E3L locus (30). The chimeric viruses were plaque-purified two times, and the K3L gene integrations were confirmed by Sanger sequencing. The viruses were purified by zonal sucrose gradient centrifugation, and the virus titer was determined on confluent 12-well plates of RK13+E3L+K3L cells. Plaque assays were performed with confluent 6-well plates of the indicated cell lines, which were infected with 50 plaque-forming units (pfu) of each indicated virus. One-hour post-infection, the media were replaced with DMEM containing 5% FBS, 1% carboxymethylcellulose (CMC), and 100 U P/S. After 48 hours, cells were stained with 0.1% crystal violet, and the excess staining was washed with water. The plates were imaged using an iBright Imaging System (Invitrogen). Virus

infection assays were performed in confluent six-well plates of the indicated cells. The indicated cells were infected with each indicated virus at an MOI of 0.01. Cells and supernatants were collected at 30 hours post infections and subjected to three rounds of freezing at -80°C and thawing at 37°C. Lysates were sonicated twice for 15s, 50% amplitude (Qsonica Q500). For infection of stable cells expressing primate PKR, the indicated cells were seeded in 12 well plates (about 5x 10^5 cells per well). The next day, the cells were treated with 1µg/ml doxycycline for 24 hours and were then infected with indicated viruses at an MOI of 0.01. Cell lysates were collected at 30 hours post-infection, and virus titer was determined by 10-fold serial dilutions on RK13+E3L+K3L cells. Virus infections were performed in triplicate.

PCR of viral genomic DNA

HeLa PKR^{KO} cells were seeded in 10 cm dishes to a confluency of 90-100%. The cells were then infected with indicated viruses at an MOI of 0.1 for 24 hours. Viral genomic DNA (gDNA) extraction was done as previously described (33). About 100ng of the isolated viral gDNA was used as template in a PCR targeting K3L ortholog genes using Phusion High Fidelity DNA polymerase (NEB #M0530L). The forward primer sequence is 5' GACGAACCACCAGAGGATGATG 3' and the reverse primer sequence is 5' AGTACTACAATTTGTATTTTTTAATCTATCTCA 3'. PCR products were gel purified with Monarch DNA Gel Extraction Kit (NEB #T1020) and Sanger sequencing was done to confirm K3L genes insertion.

Immunoblot analyses

To determine the level of eIF2α phosphorylation, about 1×10^6 cells were seeded in six-well plates and were allowed attach overnight. The next day, each cell line was infected with VC-R4 +VACV E3L (Vp872), VC-R4, VC-R4 +VACV K3L, VC-R4 + SPPV K3L, VCR4 +TPV K3L, VCR4 +YMTV K3L at MOI of 3. After an hour of incubation, media were replaced with fresh complete media. At 6 hours post-infection, cells were washed with PBS, lysed with 1% sodium dodecyl sulfate (SDS) in DPBS, and sonicated at 50% amplitude for 5 seconds twice. About 10 µg of proteins were run on 12% SDS polyacrylamide gels and transferred to polyvinyl difluoride (PVDF, GE Healthcare) membranes. Membranes were blocked with 5% (w/v) nonfat milk dissolved in TBST (20M Tris,150mM NaCl, 0.1% Tween 20, pH 7.4) for 1 hour. All antibodies were diluted in TBST containing 5% (w/v) nonfat milk. Membranes were probed with primary antibodies against phospho-eIF2α (Santa Cruz, sc101670) and total eIF2α (Santa Cruz, sc11386) at a dilution of 1:1000 overnight at 4°C. After being washed with TBST three times, membranes were probed with secondary antibodies, specifically horseradish peroxidase-conjugated donkey anti-rabbit (Invitrogen A16023) at a dilution of 1:10,000. The membranes were washed three times for 10 minutes, and proteins were detected with Amersham™ ECL™ (GE Healthcare). Images were taken using the iBright Imaging System (Invitrogen).

To determine the level of K3 orthologs expression in a transient transfection system, $4x10^5$ HeLa PKR^{KO} cells were seeded in a 6-well plate. The next day, the cells were transfected with 1 µg of pSG5 empty vector, DYK tagged VACV K3L, DYK tagged TPV

K3L, DYK tagged YMTV K3L, using Genjet: DNA ratio of 2:1. The cell lysates were harvested at 48 hours post-transfection. About 10 µg of protein was subjected to a western blot with the same conditions as described in the previous paragraph. The membrane was probed with primary antibodies against Flag M2 (Sigma F1804) and beta-actin (Sigma A1978) at a dilution of 1:2000 in SuperBlock blocking buffer (Thermofisher) for 1 hour at room temperature. After washing, membranes were probed with secondary antibody horseradish peroxidase-conjugated donkey anti-mouse (Invitrogen, A16110) at a dilution of 1:10,000 in TBST containing 1% (w/v) nonfat milk.

To determine the expression of PKR of the stable cells, $1.5x10^6$ indicated cells were seeded in a 6-well plate overnight. The cells were induced with 1µg/ml doxycycline (Sigma Aldrich D9891) and lysates were harvested 24 hours post-induction. About 25µg of protein was subjected to a western blot. We detected PKR expression using PKR A12 primary antibodies (Santa Cruz, sc393038), which recognize amino acids 2-27 at the N-terminus of PKR of human origin (Figure 3.6A). Membranes were probed with primary antibodies against PKR at a dilution of 1:1000 in 5%milk and beta-actin (Sigma A1978) at a dilution of 1:2000 in SuperBlock blocking buffer overnight at 4^oC. After washing, membranes were probed with secondary antibody horseradish peroxidase-conjugated donkey anti-mouse (Invitrogen, A16110) at dilution 1:10,000 in TBST containing 1% (w/v) nonfat milk.

To determine the level of K3L orthologs expression by the chimeric vaccinia virus, $8x10^5$ HeLa PKR^{KO} cells were seeded in a 6-well plate. The next day, the cells were infected with VC-R4, VC-R4+VACV K3L, VC-R4+TPV K3L, VC-R4+YMTV KL3 at an MOI

of 3. The protein was collected at 24 hours post-infection. About 12μg of protein was subjected to 12% SDS polyacrylamide gels and transferred to polyvinyl difluoride (PVDF, GE Healthcare) membranes. Membranes were probed with primary antibodies beta-actin (Sigma A1978) at dilution 1:2000 in Thermofisher Supperblock blocking buffer, primary antibodies against TPV K3 (Genscript) at dilution 1:1000 in 5% milk dissolved in TBST, VACV-K3 at dilution 1:500 in 5% milk dissolved in TBST overnight at 4°C. Anti-TPV K3 (cVQVIRTDKLKGYVDVRHIT) and anti-VACV K3 (cKVIRVDYTKGYIDVNYKRM) were custom produced by peptide-KLH conjugate in New Zealand rabbit (GenScript). After being washed with TBST three times, membranes were probed with secondary antibodies horseradish peroxidase-conjugated donkey anti-rabbit (Invitrogen A16023) at dilution 1:10,000 in 1% milk for anti-TPV K3 and anti-VACV K3, secondary antibodies horseradish peroxidase-conjugated donkey anti-mouse (Invitrogen, A16110) at dilution 1:10,000 in TBST containing 1% (w/v) nonfat milk for beta-actin. The membranes were washed three times for 10 minutes, and proteins were detected with Amersham™ ECL™ (GE Healthcare). Images were taken using the iBright Imaging System (Invitrogen).

PKR phylogenetic tree

The amino acid sequences of PKR from a panel of 21 different primate species and rabbit PKR were aligned using Clustal Omega (34). The phylogenetic tree was constructed using the maximum likelihood approach in MEGAX software (35). Five hundred bootstrap replicates were performed to estimate the nodal support at major branch points.

RESULTS

Amino acid differences between Yatapoxvirus K3 orthologs

Inhibition of PKR by K3 has been shown to be a key determinant for influencing poxvirus host range (23-26, 31). This study examined the role of TPV and YMTV K3 orthologs in inhibiting PKR derived from a diverse set of primate species. First, we compared the amino acid sequences of the VACV K3 and yatapoxvirus K3 orthologs by multiple sequence alignment. All three K3 orthologs consist of 88 amino acid residues. TPV and YMTV K3 share 75% sequence identity, with 22 amino acid differences between the two orthologs (Figure 3.1). K3 orthologs from more distantly related genera, such as VACV, have a lower percent identity (35-36% identity) with the yatapoxvirus K3 orthologs (Figure 3.1B).

A

```
VACV_K3      ------MLAFCYSLPNAGDVIKGRVYEKDYALYIYLFDYPHFEAILAESVKMHMDRYVE    53
TPV_K3       MNNHKSKLAFCYAFPTVGTVTKGIVTVKDADFTVFLPEFG-LEALIVNYFSVNANIAEK    58
YMTV_K3      MSRNRSQLAFCYAFPTVGTITKGVVTVEGDSFTVFLPEFG-LHALIVNYLSVNVKRAKK    58

                                                          Helix insert region
VACV_K3      YRDKLVGKTVKVKVIRVDYTKGYIDVNYKRMCRHQ    88
TPV_K3       LSKELSGKTINVQVIRTDKLKGYVDVRHIT-----    88
YMTV_K3      LSEKLSGKTVTVQVIRTDKLKGYVDVRHIE-----    88

                                PKR recognition motif
```

B

Percent identity

	VACV K3	TPV K3	YMTV K3
VACV K3	100.00	36.59	35.37
TPV K3	36.59	100.00	75.00
YMTV K3	35.37	75.00	100.00

Figure 3. 1. Multiple sequence alignment of VACV K3, TPV K3, and YMTV K3 orthologs.
(A). Different residues among TPV and YMTV K3 amino acid sequences are highlighted in red. The regions to the left and right of the dotted line were considered the N-terminal and C-terminal regions of the inhibitors, respectively. The alignment of the PKR recognition and the helix insert region are marked in the black boxes. (B). Percent identities between tested K3 orthologs were calculated from the multiple sequence alignment using Clustal Omega.

Yatapoxvirus K3 orthologs inhibit primate PKR in a species-specific manner

We generated a phylogenetic tree from PKR amino acid sequences from a panel of 21 primate species using rabbit PKR as an outgroup to visualize their relatedness among the primate species. Consistent with previous maximum-likelihood analyses of the primate PKR dataset (29), our phylogenetic tree classified these primate PKRs into three groups: hominoids, Old World monkeys, and New World monkeys (Figure 3.2A). Previously, Elde et al. has studied the interaction of 10 PKR variants from these primate species (orangutan, gorilla, chimpanzee, human, gibbon, African green monkeys, rhesus, woolly, titi, tamarin) with VACV K3 and has shown that these PKR variants exhibited differential susceptibility to VACV K3 in the yeast-based assay (29).

We first confirmed the expression levels of VACV K3, TPV K3, and YMTV K3 tagged with C terminal Flag-epitope tags. Western blot results indicated that vaccinia K3 and TPV K3 were expressed at comparable levels, whereas YMTV K3 was expressed at a slightly higher level (Figure 3.2B). After confirming expression, we quantified their ability to inhibit PKR from 15 different primate species using our established luciferase-based expression assay (23, 31). In this assay, we tested sensitivity of PKR from representatives of hominoids (human, gorilla, chimpanzee, orangutan, white-cheeked gibbon), Old World monkeys (colobus, François leaf, baboon, sooty mangabey, rhesus, talapoin, African green monkey, and patas), New World monkeys (tamarin and titi) (Table 3.1). HeLa PKR^{KO} cells were co-transfected with these different primate PKRs and untagged K3 orthologs from either VACV, YMTV or TPV. All primate PKRs and K3 orthologs were expressed in the pSG5 vector driven by the SV40 promoter.

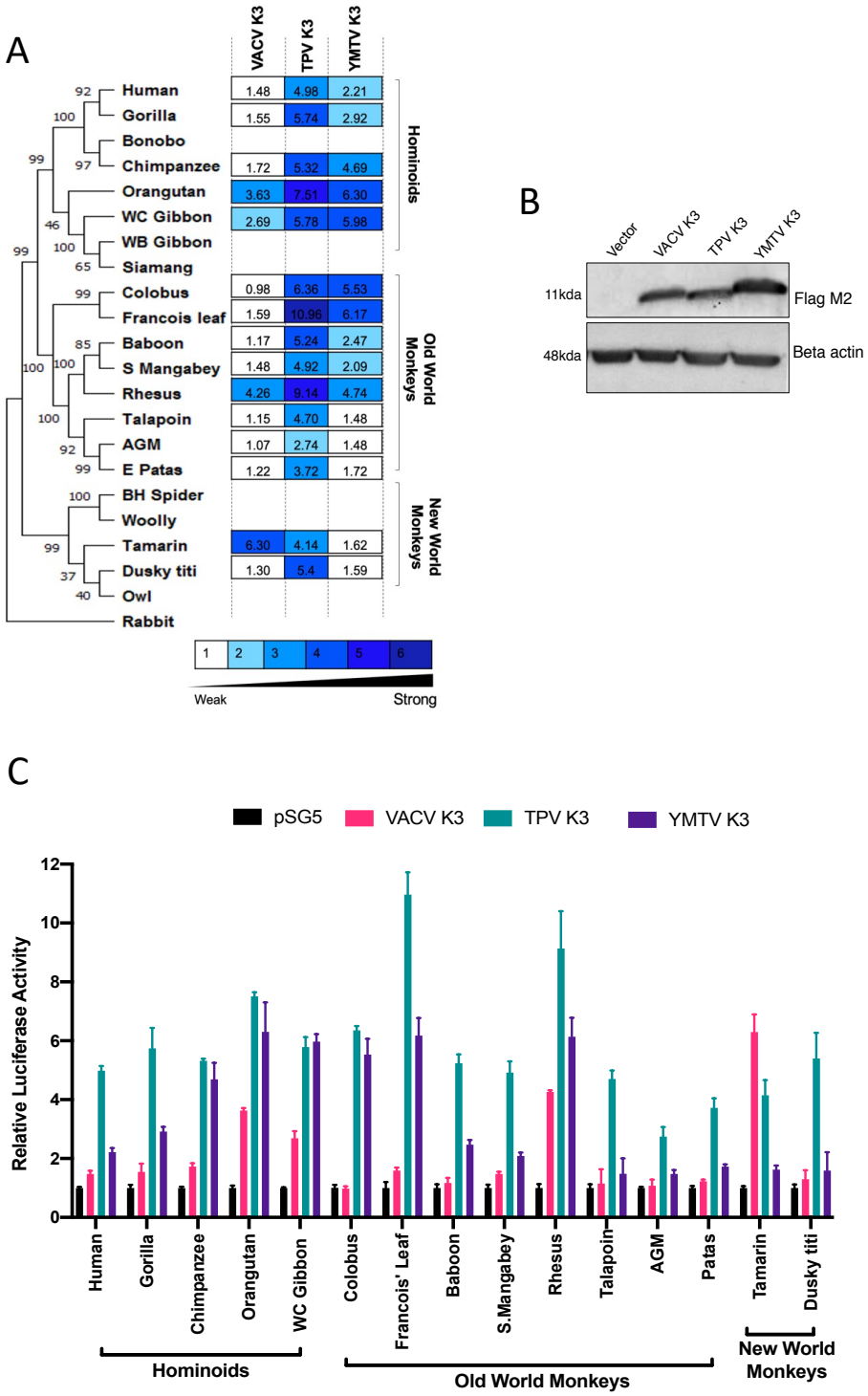

Figure 3. 2. Differential sensitivities of tested PKRs to VACV K3, TPV K3, and YMTV K3 orthologs. *(A). We generated a phylogenetic tree with PKR protein sequences from a panel of 21 primate species and used rabbit PKR as an outgroup. The tree was built by MEGAX program with 500 bootstrap replicates and based on the maximum-likelihood method. Relative sensitivities of PKRs to either VACV K3, TPV K3 or YMTV K3 from multiple luciferase-based reporter assays are shown on a scale from 1 to 6. Scale 1= no or very weak inhibition (≤ 2-fold increase in luciferase readout); 2= weak inhibition (2- to 3-fold); 3=intermediate*

low inhibition (3- to 5-fold); 4=intermediate high inhibition (5- to 7-fold); 5= high inhibition (7- to 10-fold); 6=very high inhibition (≥ 10-fold). (B). HeLa PKR^{KO} cells were transfected with 1μg of either pSG5 empty vector, pSG5 encoding FLAG-tag VACV K3L, FLAG-tag TPV K3L, or FLAG-tag YMTV K3L. Proteins were harvested at 48 hours post-transfection, and K3 expressions were detected with Flag M2 primary antibodies. (C). HeLa PKR^{KO} cells were transfected with expression vectors encoding firefly luciferase (50 ng), with either VACV K3L, TPV K3L, YMTV K3L (200 ng), and PKR (200 ng) from the indicated species. Luciferase activities were measured 48 hours after transfection and normalized to PKR-only transfected cells to obtain relative luciferase activities. Error bars represent the standard deviations from three independent transfections. The luciferase assay results shown are representative of at least three independent experiments.

We found that VACV K3 was an intermediate inhibitor of orangutan PKR and rhesus macaque PKR and a strong inhibitor of tamarin PKR. PKRs from the other tested primates were largely resistant to VACV K3 (Figure 2.2A, C). YMTV K3 and TPV K3 inhibited PKR in a species-specific manner, but the two orthologs showed distinct PKR inhibition profiles. TPV K3 strongly inhibited 9 out of 15 primate PKRs with the strongest inhibited was François leaf monkey PKR. TPV K3 was an intermediate inhibitor of human, sooty mangabey, talapoin, patas, and tamarin monkey PKRs and a weak inhibitor of African green monkey PKR. In contrast, the YMTV K3 ortholog was a weak inhibitor of 9 tested PKRs, an intermediate inhibitor of chimpanzee and rhesus PKRs, and a strong inhibitor of orangutan, white-cheeked gibbon, colobus, and François leaf monkey PKRs. Despite being expressed at a lower level than YMTV K3, TPV K3 inhibited PKR from 13 primates, including humans, substantially better than YMTV K3. In addition, both K3 orthologs inhibited PKR from chimpanzee, orangutan, white-cheeked gibbon, and colobus comparably (Figure 2.2A, B).

Differential PKR inhibition is governed by the C-terminus of yatapoxvirus K3 orthologs

The amino acid sequence alignment of YMTV and TPV K3 orthologs shows 22 amino acid differences between the two orthologs, which are distributed throughout the K3 protein sequence. To investigate which regions are essential for the differential inhibition by yatapoxvirus K3 orthologs, we generated constructs encoding hybrid YMTV-TPV K3 orthologs in which the C-terminal regions of the two inhibitors were swapped. We took advantage of the shared region in the middle part of the gene (FTVFLPEFG) to separate the N-and C- termini by cutting the gene at the FT^V site; there are 11 amino acids difference in each terminus (Figure 3.3A). We analyzed the ability of these hybrid proteins to inhibit human PKR, colobus PKR, and titi PKR using the luciferase assay. The hybrid $_{N}$TPV-$_{C}$YMTV exhibited comparable inhibition levels to the YMTV WT K3 ortholog for each PKR tested (Figure 3.3). Specifically, when the C terminus from YMTV K3 replaced the C terminus of TPV K3, the hybrid $_{N}$TPV-$_{C}$YMTV K3 lost its ability to inhibit human and titi PKR, phenocopying an inhibition profile similar to that of the wild-type YMTV K3 ortholog. Correspondingly, the $_{N}$YMTV-$_{C}$TPV hybrid showed a similar inhibition pattern to the wild-type TPV K3 ortholog. This result suggests that the C-terminus of both K3 orthologs governed differential PKR inhibition.

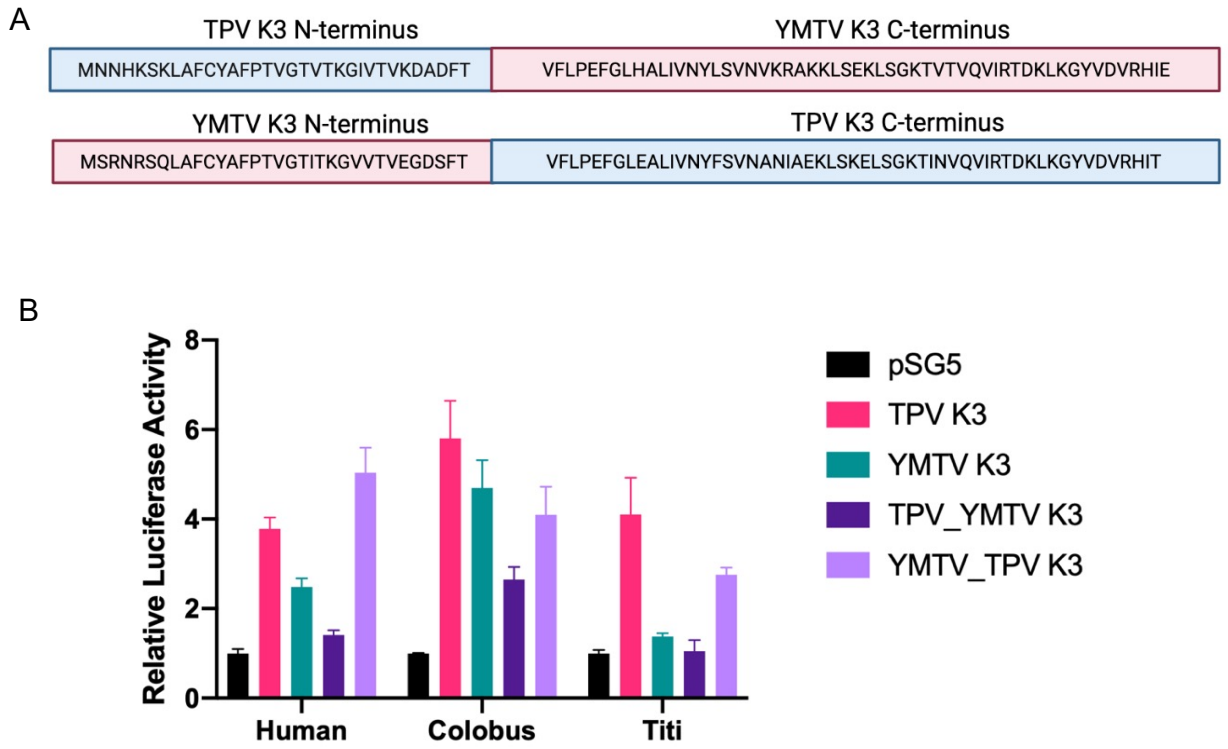

Figure 3. 3. Identification of region of TPV K3 and YMTV K3 orthologs that confer differential PKR inhibition.
(A). Constructs were designed such that the C-terminal regions of the two inhibitors were swapped to generate hybrid proteins. The predicted amino acid sequences of TPV K3 and YMTV K3 hybrid proteins are highlighted in pink and blue, respectively. (B). Human HeLa-PKR^{ko} cells were transfected with expression vector encoding firefly luciferase, indicated PKRs, and either hybrid $_{N}$TPV-$_{C}$YMTV or $_{N}$YMTV-$_{C}$TPV inhibitors. Inhibition of indicated PKRs by TPV K3 and YMTV K3 serve as controls. Luciferase activity was measured 48 hours after transfection. Luciferase light units were normalized to PKR-only transfected cells to obtain relative luciferase activities. Error bars represent triplicate transfections and data are representative of three independent experiments.

Chimeric viruses expressing Tanapox K3 or Yaba Monkey Tumor Virus K3 display cell type specific differences in plaque formation

Next, we investigated whether the ability of TPV K3 and YMTV K3 orthologs to inhibit primate PKR correlates with the ability of the ortholog to rescue replication of a VACV strain that lacks PKR inhibitors in primate-derived cell lines. The VACV strain VC-R4 (VACV△E3L△K3L) is a highly attenuated vaccinia virus variant that can only replicate in

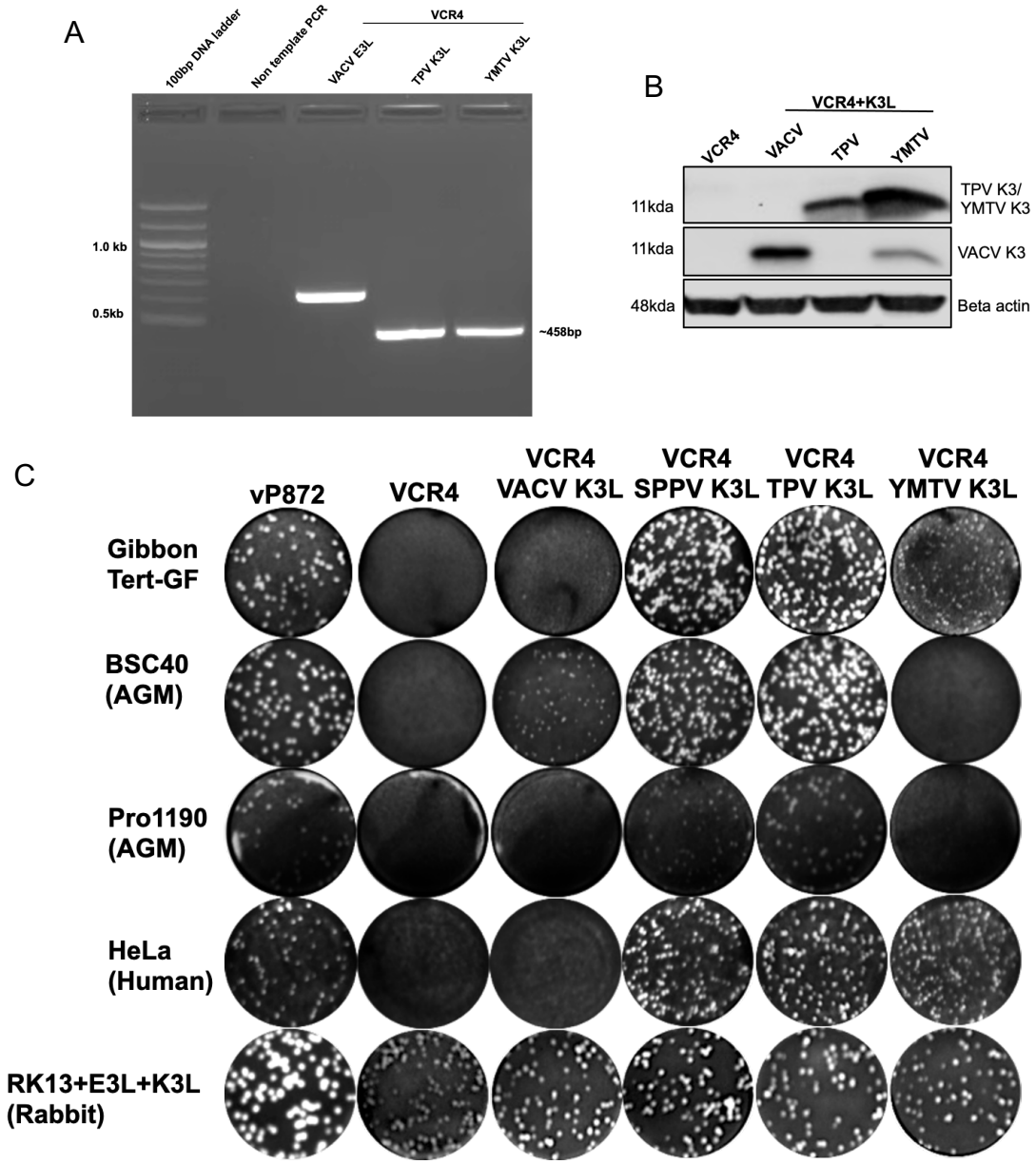

Figure 3. 4. Generation of chimeric VC-R4 expressing yatapoxvirus K3 orthologs.
Integration of K3L ortholog genes was determined by PCR (A) and sequencing (not shown) and immunoblotting (B). (C). Plaque formation of VC-R4 expressing K3 orthologs. A variety of primate-derived cells and RK13+E3L+K3L were induced with 500UI of IFN beta for 24 hours and infected with 50 pfu/ml of the indicated viruses, and plaque formation was visualized with crystal violet at 48 hours after infections.

PKR deficient cell lines or cell lines expressing PKR antagonists (30). To generate VC-R4-TPV K3L and VC-R4-YMTV K3L chimeric viruses, we inserted either TPV K3L or YMTV K3L into VC-R4 at the E3L locus using the scarless integration method as previously described (30). To

confirm K3 ortholog expression, we infected HeLa PKR^{KO} cells with the purified recombinant viruses and performed Western blot. Because there were no antibodies available for the detection of the yatapoxvirus K3 orthologs, we produced custom primary antibodies directed against a peptide from the TPV K3 ortholog, which is identical to the sequence found in YMTV K3, with the exception of the C-terminal amino acid at position 88 (Figure 3.1A). Surprisingly, YMTV K3 was detected at a higher level compared to TPV K3, despite the fact that both K3L orthologs are driven by the same VACV E3L promoter (Figure 3.4B).

We examined the replication of VC-R4-TPV K3L and VC-R4-YMTV K3L in various primate-derived cell lines, including HeLa (human), gibbon Tert-GF (gibbon), BSC40 and PRO1190 (African green monkey), and RK13+K3L+E3L cells (rabbit). We infected these cells with 50 PFU/well of VC-R4, VC-R4+VACV E3L (vP872), VC-R4+VACV K3L, VC-R4+SPPV K3L (sheep poxvirus K3), VC-R4+TPV K3L and VC-R4+YMTV K3L. To see a stronger effect of PKR activation, we induced the cells with 500 units of IFN beta for 24 hours before virus infections, and plaque formation was visualized 48 hours post infection. All viruses formed plaques with comparable sizes in permissive RK13+K3L+E3L cells. As expected, VC-R4 only formed plaques in RK13+K3L+E3L cells, whereas vP872 and VCR4+SPPV K3L formed plaques in all cells tested (Figure 3.4C). VC-R4+VACV K3L developed small visible plaques only in BSC40 cells and to a lesser extent in gibbon cells. Interestingly, VC-R4+TPV K3L infection led to the formation of plaques in all tested cells with comparable size with VCR4+SPPV K3L and vP872. Relative to VC-R4+TPV K3L, VCR4 +YMTV K3L formed smaller plaques in HeLa and gibbon cells and failed to cause plaque formation in both African green monkey cells. In general, based on the plaque assay, TPV K3 rescued VC-R4 replication substantially better in primate-derived cell lines than did YMTV K3.

TPV K3 rescued chimeric virus replication more efficiently than YMTV K3 in primate-derived cell lines.

We next measured virus titers to determine the capacity of yatapoxvirus K3 orthologs to restore the replication of VC-R4. We infected RK13+K3L+E3L and primate-derived cell lines HeLa (human), gibbon tert, BSC40 (African green monkeys), and PRO1190 (African green monkeys) cells with either VC-R4, VC-R4+VACV E3L (vP872), VC-R4+VACV K3L, VC-R4+SPPV K3L, VC-R4+TPV K3L and VC-R4+YMTV K3L at an MOI of 0.01. Cell lysates were collected at 30 hours post-infection, and virus titer was determined in RK13+K3L+E3L cells. Consistent with the plaque assays and luciferase assays, all viruses replicated to comparable titers in RK13+K3L+E3L cells (Figure 3.5). VC-R4 did not replicate in any cells tested (virus titer below 10^3 pfu/ml), except RK13+K3L+E3L cells. VACV K3L rescued VC-R4 virus replication in all cells tested, although the virus yield is about 10-to 100-fold lower than vP872. In HeLa, and gibbon cells, SPPV K3L and TPV K3L both restored the replication of VC-R4 to a level comparable to vP872 virus. In BSC40 and PRO1190 cells, TPV K3L and SPPV K3L rescued VC-R4 replication comparably. Consistent with the plaque assays, VC-R4+YMTV K3L replicated to a similar level as VC-R4+TPV K3L in HeLa cells. However, VC-R4+YMTV K3L replicated less efficiently than VC-R4+TPV K3L in gibbon cells (~11-fold lower), in BSC40 cells (~1394-fold lower), and in PRO1190 cells (~121-fold lower) relative to VC-R4+TPV K3L virus.

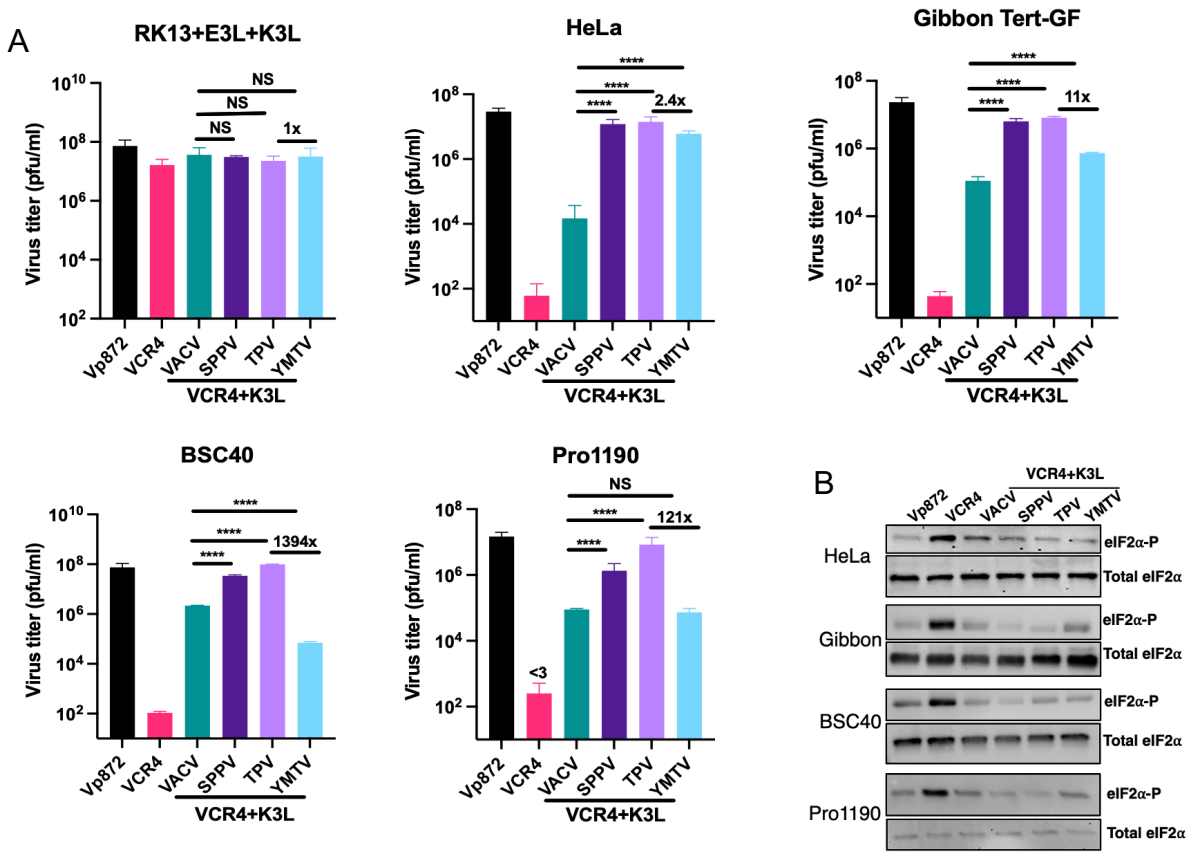

Figure 3. 5. Virus titer of chimeric vaccinia viruses in primate-derived cell lines.
*(A). A variety of primate-derived cells and RK13+E3L+K3L were infected with indicated viruses at an MOI of 0.01. Cell lysates were harvested at 30 hours post infection and virus titers were determined in RK13+E3L+K3L cells. Error bars represent the standard deviations from three independent infections. Fold-changes in virus titer between VC-R4 TPV K3L and VC-R4 YMTV K3L are shown. Data were analyzed by one-way ANOVA followed by Dunnett's multiple comparisons test. Significant values are marked by asterisks (NS=p>0.05, *p<0.05, **p<0.01 ***p<0.001, ****P<0.0001). (B). Phosphorylation of eIF2α after infections with VC-R4 expressing K3 orthologs. Indicated cells were infected with indicated viruses at an MOI of 3. Cells were lysed 6 hours after infection and analyzed by immunoblotting for total eIF2α and phospho-eIF2α.*

Next, we examined the level of phosphorylated eIF2α by Western blot analysis (Figure 3.5B). We infected HeLa (human), gibbon tert, BSC40 (African green monkeys), and PRO1190 (African green monkeys) cells with either VC-R4, VC-R4+VACV E3L (vP872), VC-R4+VACV K3L, VC-R4+SPPV K3L, VC-R4+TPV K3L and VC-R4+YMTV K3L at an MOI of 3. Protein lysates were collected at 6 hours post-infection. Robust phosphorylation of eIF2α was observed in all VC-R4 infected cells, but not in vP872 infected cells. Slightly higher levels of eIF2α phosphorylation was observed in VC-

R4+VACV K3L infected cells than in vP872 and VC-R4+SPPV K3L infected cells. Likewise, a slightly higher level of eIF2α phosphorylation was observed in VC-R4+YMTV K3L infected cells than VC-R4+TPV K3L infected cells, except in HeLa and BSC40 cells, in which the level of eIF2α phosphorylation was comparable. In general, Western blot analyses indicated that the level of eIF2α phosphorylation in the tested cell lines correlated with plaque formation and virus replication, with the exception of BSC40 cells.

Replication of chimeric viruses in T-REx PKR^{KO} stable cells expressing primate PKR.

As each primate cell line might have cell-specific characteristics contributing to the differential virus replication, we generated congenic Flp-In T-REx 293 PKR^{KO} cell lines (T-REx PKR^{KO}, Haller et al, unpublished) expressing a single copy of various primate PKRs (human PKR, white-cheek gibbon PKR, colobus PKR, and dusky titi PKR). The T-REx cells possess a single homology directed integration site; therefore, all cells are congenic and express the PKR genes under doxycycline inducible promoter. This approach allows us to assess the interaction between K3L orthologs and primate PKR by infecting the transgenic cell lines with chimeric VACV expressing K3L orthologs. To analyze expression of PKR in each cell line, we induced the cells with 1μg/ml of doxycycline for 24 hours and performed Western blot analysis with an antibody (A12) generated against a human PKR-derived peptide (Figure 3.6A). Comparable expression of human PKR was

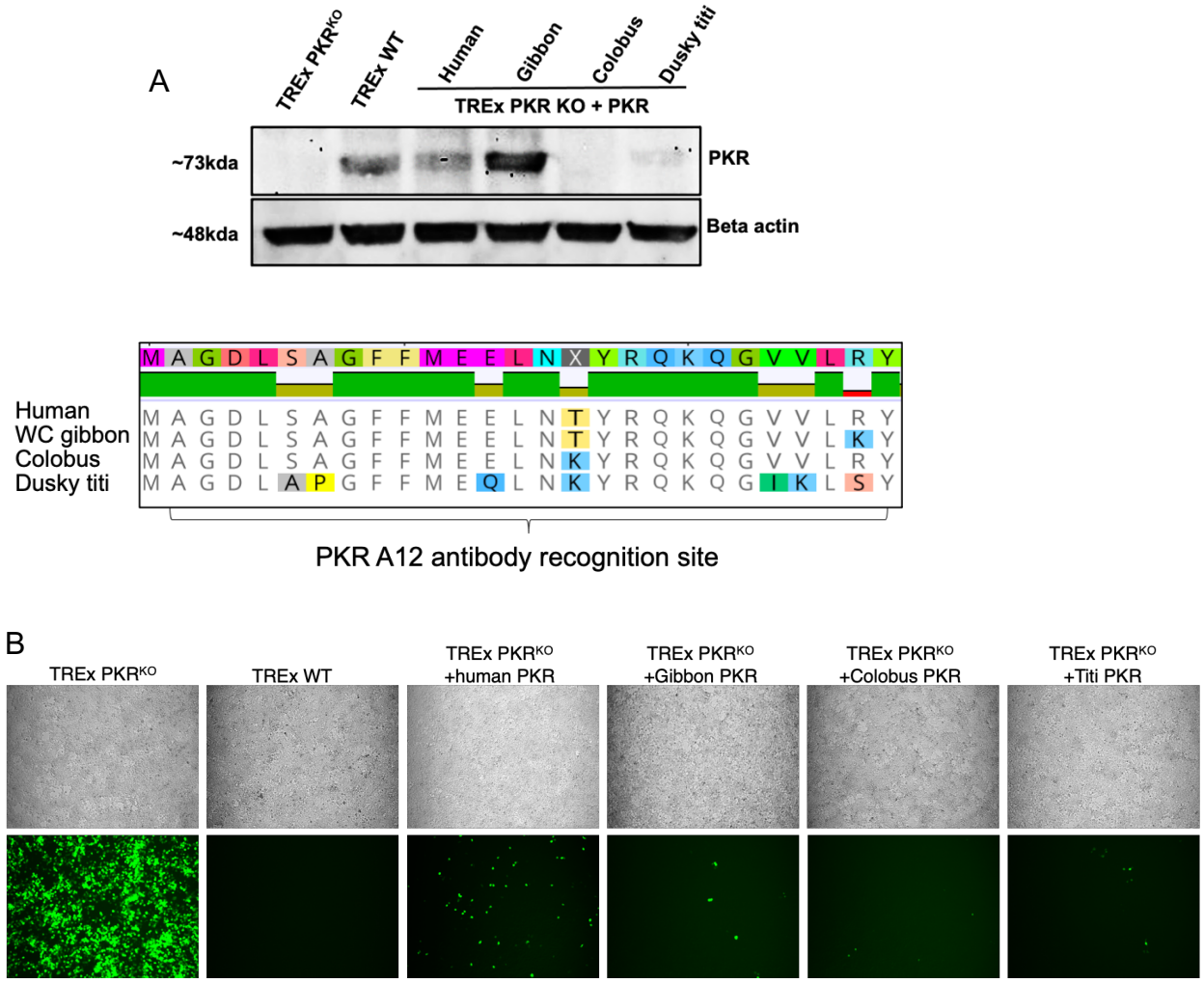

Figure 3. 6. Generation of stable T-REx PKR^{KO} cells expressing primate PKR.
(A). Primate PKR expression was validated by Western blot after 1μg/ml of doxycycline induction for 24 hours. Multiple sequence alignment of the first 27 amino acids of human PKR, white-cheeked gibbon PKR, colobus PKR, and dusky titi PKR is shown. The epitope of PKR A12 primary antibodies is indicated. (B). Infection of stable T-REx PKR^{KO} cells expressing primate PKR variants with VC-R4. Indicated cell lines were treated with 1μg/ml doxycycline for 24 hours, and subsequently infected with VC-R4 MOI of 0.01. EGFP signals in the infected cells were monitored at 48 hours post-infection by fluorescence microscopy.

detected in the parental T-REx cells and the T-REx PKR^{KO}+human PKR cells. A stronger signal was detected in white-cheeked gibbon PKR-expressing cells, whereas only weak signals were detected in dusky titi PKR and colobus-expressing cells. The differences in detection, might be due to real expression differences, or due to the amino acid differences in the epitope detected by the antibody (Figure 3.6A). In order to analyze if

expression of the different PKRs confers antiviral effects we infected T-REx PKR^{KO}, T-REx WT, or T-REx PKR^{KO} expressing either human PKR, gibbon PKR, colobus PKR, or titi PKR cells with VC-R4 at an MOI of 0.01. We observed a robust EGFP signal in T-REx PKR^{KO} cells and considerably less in other cell lines, suggesting PKR was expressed and inhibited VC-R4 replication (Figure 3. 6B).

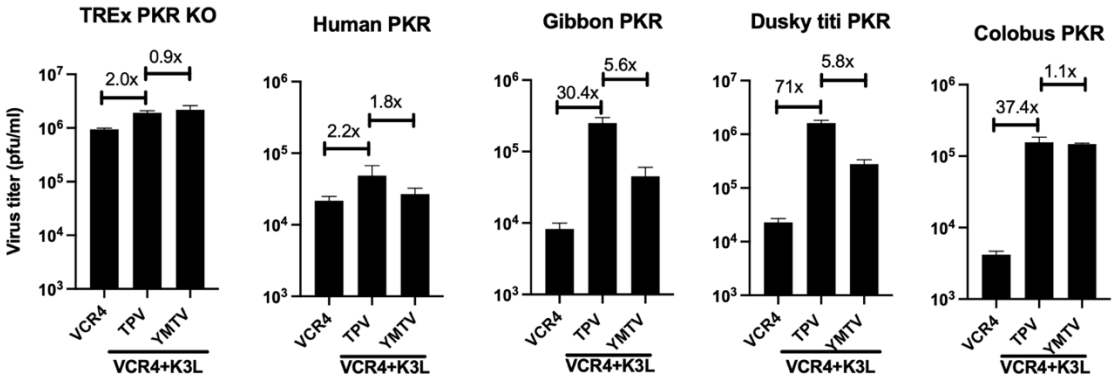

Figure 3. 7. Infection of stable T-REx PKRKO cells expressing primate PKR with chimeric viruses. *The indicated cell lines were infected with VC-R4, VC-R4 TPV K3L, or VC-R4 YMTV K3L viruses at an MOI of 0.01. Cell lysates were harvested at 30 hours post-infection and virus titers were determined in RK13+E3L+K3L cells. Error bars represent the standard deviations from three independent infections. Fold-changes in virus titer are shown.*

We used these PKR-expressing cells to investigate the ability of TPV K3 and YMTV K3 orthologs to restore VC-R4 replication. We infected the T-REx PKR^{KO}, T-REx WT, T-REx PKR^{KO} expressing either human PKR, gibbon PKR, colobus PKR, or titi PKR cells with VC-R4, VC-R4+TPV K3L and VC-R4+YMTV K3L at an MOI of 0.01. The virus titer was determined in RK13+K3L+E3L cells 30 hours post-infection. As expected, VC-R4 only replicated in T-REx PKR^{KO} cell lines, but replicated poorly in T-REx PKR^{KO} cells expressing primate PKR (Figure 7). Insertion of YMTV K3L or TPV K3L failed to rescue VC-R4 replication in T-REx PKR^{KO} containing human PKR. In contrast, the insertion of TPV K3L rescued VC-R4 replication with about 30- to 71-fold higher titer than VC-R4 in

T-REx PKR^{KO} containing gibbon PKR, dusky titi PKR or colobus PKR. In T-REx PKR^{KO} cells expressing gibbon PKR or in dusky titi PKR, VC-R4+YMTV K3L viral titers were about 6-fold lower than that of VC-R4+TPV K3L. In comparison, both K3 orthologs rescued VC-R4 replication at a comparable level in colobus PKR containing cells.

DISCUSSION

Vaccinia virus K3 is a host range factor that acts by inhibiting the host restriction factor PKR. Homology between K3 domain S1 and eIF2α allows K3 to function as a pseudosubstrate of PKR, competitively inhibiting eIF2α phosphorylation (18). This unique interaction between PKR and K3 has been studied using yeast and mammalian cell assay systems (36, 37). Elde et al. (29), previously demonstrated that PKR from Old World monkeys and New World monkeys were generally susceptible to VACV K3, whereas PKR from other hominoids were resistant to VACV K3, indicating species-specific inhibition of primate PKR by VACV K3. We recently described K3 orthologs from leporipoxviruses that specifically infect leporids (rabbits and hares) (23) and capripoxviruses that infect sheep, goats and cattle inhibit their corresponding host PKR in a species-specific manner (24). Our recent studies revealed that K3 inhibition could not be predicted by phylogenetic relatedness of PKR alone (26); thus, this interaction should be examined experimentally. In this study, we examined whether K3 orthologs of the yatapoxvirus genus contribute to host-specific PKR inhibition.

Yatapoxviruses infect primates and can cause zoonotic infections in humans. Here, we analyze how TPV and YMTV K3 orthologs interact with PKR from 15 different primate species in comparison to VACV K3. Our results confirm and extend the results of species-

specific VACV K3 inhibition previously reported in the yeast assays (29) and luciferase-based assays (26). White-cheeked gibbon PKR was largely resistant to VACV K3, whereas VACV K3 strongly inhibited tamarin PKR and rhesus macaque PKR. Interestingly, dusky titi PKR, which was previously shown to be susceptible to VACV K3 in the yeast-based assay, appeared to be largely resistant to VACV K3 in our luciferase-based assays. Although the yeast assay can be used to predict the inhibition of PKR by viral antagonists, yeast expression systems have very different post-translation modifications from mammalian cells, which might affect protein function (38). In general, our data showed that TPV K3 and YMTV K3 exhibited distinct PKR inhibition profiles and that these K3 orthologs inhibited primate PKR in a species-specific manner. All tested primate PKRs were sensitive to TPV K3, although to different degrees. We found a distinct profile of inhibition by YMTV K3 within the Old World monkeys in which sooty mangabey, patas, and African green monkey PKR were largely resistant to YMTV K3 inhibition. In contrast, rhesus macaque PKR was largely sensitive, suggesting an interaction between K3 and PKR cannot be predicted by phylogenetic relatedness. Interestingly, this finding is in line with subcutaneous inoculation studies, showing that YMTV induced tumor formation in rhesus monkeys, whereas no tumors were observed in sooty mangabey, patas, and African green monkeys (5, 9, 12).

TPV K3 and YMTV K3 differ by 22 aa residues in an 88 aa protein (Figure 3.1). K3 orthologs from the orthopoxvirus genus share a higher sequence identity (80.7-98.9%) among their members (26) than do yatapoxvirus K3. We found residues within the C-terminus region govern the differential PKR inhibition by these orthologs (Figure 3.3A). There are two critical conserved motifs in the C-terminus of the K3 orthologs: the PKR

recognition motif and helix insert region (18). The PKR recognition motif of K3 orthologs, which includes residues K74, Y76, and D78, provides important determinants for high-affinity binding to PKR (18). TPV K3 and YMTV K3 orthologs have identical residues in the PKR recognition motif “KGYVD”, one amino acid difference with the typical PKR recognition motif “KGYID” in VACV K3. The helix insert of eIF2α appears to undergo conformational change upon binding to PKR resulting in the Ser51 site of eIF2α becoming fully accessible to the phosphoacceptor binding site of PKR (39). The K3 helix insert region is structurally homologous to the region adjacent to Ser51 in eIF2α (Figure 3.1A). The unique conformation of helix insert region of K3L functions as an inhibitor of PKR activation by preventing PKR trans-autophosphorylation and acting as a pseudosubstrate of PKR (39). In addition, we and others have shown that one or more amino acid residues in orthopoxvirus K3 orthologs are responsible for the differential PKR inhibition and that the amino acid variants are predominantly located in the helix insert region (25, 26). Therefore, it is difficult to predict which residues might be responsible for PKR inhibition. A site-directed mutagenesis experiment could identify the critical residues required for PKR inhibition.

In this study, the function of yatapoxvirus K3 proteins was further examined in the context of virus infection. The E3L and K3L double knockout vaccinia virus strain VC-R4 (VACV△E3L△K3L) can only replicate in PKR deficient cell lines or cell lines that express PKR antagonists. By inserting the K3L from different poxviruses in the E3L locus of VC-R4 we can analyze the chimeric viruses' ability to replicate in PKR competent cell lines. The advantage of using the chimeric virus system is that it allows us to assess the ability of the K3L in rescuing the virus in PKR competent cells. As expected, VC-R4 could not

replicate in all tested cells, except RK13+E3L+K3L cells. VC-R4 expressing SPPV K3L and TPV K3L replicated as efficiently as vP872 in all tested cell lines as shown in plaque assays and virus titer, suggesting that E3 from vaccinia virus and K3 from SPPV and TPV are potent PKR inhibitors for these cell lines. In contrast, the VC-R4+VACV K3L and VC-R4+YMTV K3L formed smaller plaques in all tested cell lines, except in RK13+E3L+K3L where these viruses formed comparable plaque size with other viruses. Together these results indicate that the VACV K3L and YMTV K3L are generally weaker inhibitors for the PKR orthologs that we tested. This result was recapitulated in the virus titer assay. There was 11-fold higher virus titer in VC-R4+TPV K3L infected gibbon-Tert cells than in VC-R4+YMTV K3L infected cells. The difference in virus titer was more pronounced in PRO1190 and BSC40 cells, with about 100-to 1000-fold lower virus titer in VC-R4+YMTV K3L infections. This inhibition generally correlated with the level of eIF2α phosphorylation, with the exception of BSC40 cells, in which no difference in eIF2α phosphorylation was observed, between VC-R4+TPV K3L and VC-R4+YMTV K3L. In contrast, Cao et al. showed expression of YMTV K3L ortholog in VACV△E3L△K3L suppressed eIF2α phosphorylation and restored the virus replication in CV-1 monkey cells (25). Despite being derived from African green monkeys, PRO1190, BSC40, and CV-1 showed somewhat different phenotypes, suggesting cell-specific characteristics might contribute to the differential virus replication.

The colobus PKR and white cheeked gibbon PKR appeared equally sensitive to both yatapoxvirus K3 orthologs in the luciferase-based assay. In the infection assay, the VC-R4+TPV K3L replicated as efficiently as VC-R4+YMTV K3L in T-REx PKR^{KO} expressing colobus PKR, consistent with the luciferase assay. However, we observed a higher virus titer in T-REx PKR^{KO}

expressing white-cheeked gibbon PKR cell lines infected with VC-R4+TPV K3L than did VC-R4+YMTV K3L. This observation also correlated with the formation of larger plaques and higher virus titer in gibbon Tert cell lines infected with VC-R4+TPV K3L compared to VC-R4+YMTV K3L. While the general patterns observed in the luciferase-based assay were recapitulated in the infection assay, we observed some differences in the magnitude of inhibition. The luciferase assay was a good approach for analyzing inhibition of PKR by K3 orthologs; however, currently is not known how strongly the inhibition correlated with a biological effect in infection assay.

Overall, the data presented here to support and extend species-specific PKR inhibition by VACV K3, TPV K3, and YMTV K3 (25, 26, 29). Within primate species PKR, TPV K3 exhibited a broader range of PKR inhibition than did YMTV K3 and VACV K3. VACV K3 appeared to have a narrow range of PKR inhibition within primate species but inhibited a wide range of other mammals PKR (26). It is worth mentioning that the ability of a virus to replicate and disseminate efficiently in its host is dependent on the entire interactome between the host and the virus (40). In addition to K3L, yatapoxviruses encode several host range genes, including E3L, C7L, M11L, Serpins, P28-like, B5R (41). The role of E3L gene of YMTV and C7L of YLDV in host range factors has been previously described (42, 43). However, the role of other genes as host range factors needs to be experimentally confirmed.

Table 3. 1. Accession numbers of genes used for phylogenetic analyses.

Common name	Scientific name	GenBank accession
Human	*Homo sapiens*	NM_002759
Gorilla	*Gorilla gorilla*	EU733258.1
Bonobo	*Pan paniscus*	EU733255.1
Chimpanzee	*Pan troglodytes*	EU733256.1
Orangutan	*Pongo pygmaeus pgmaeus*	EU733259.1
White-cheeked gibbon	*Nomascus leucogenys*	EU733257.1
White-bearded gibbon	*Hylobates albibarbis*	EU733270.1
Siamang	*Symphalangus syndactylus*	EU733271.1
Colobus	*Colobus guereza*	EU733267.1
Francois' leaf	*Trachypithecus francoisi*	EU733268.1
Baboon	*Papio anubis*	XM_009184002.4*
Sooty mangabey	*Cercocebus torquatus atys*	EU733262.1
Rhesus macaque	*Macaca mulatta*	EU733261.1
Talapoin	*Miopithecus talapoin talapoin*	EU733269.1
African green monkeys	*Clorocebus aethiops*	EU733254.1
Patas	*Erythrocebus patas*	EU733260.1
Black-handed spider	*Ateles geoffroyi*	EU733263.1
Woolly	*Lagothrix lagotricha*	EU733266.1
Tamarin	*Saguinus labiatus*	EU733264.1
Dusky titi	*Callicebus moloch*	EU733265.1
Owl monkey	*Aotus trivirgatus*	FJ374685.1
Rabbit	*Oryctolagus cuniculus*	NM_001082213.1

*We identified amino acid differences between our baboon PKR and XM_009184002.4: one synonymous A465G (Q155Q) and four non-synonymous amino acid differences G1490A (E497K), A1498C (K500Q), G1511A (G506T) and A1558G (K520E).

REFERENCES

1. Haller SL, Peng C, McFadden G, Rothenburg S. Poxviruses and the evolution of host range and virulence. Infect Genet Evol. 2014;21:15-40. Epub 2013/10/29. doi: 10.1016/j.meegid.2013.10.014. PubMed PMID: 24161410; PMCID: PMC3945082.
2. Lee HJ, Essani K, Smith GL. The genome sequence of Yaba-like disease virus, a yatapoxvirus. Virology. 2001;281(2):170-92. Epub 2001/03/30. doi: 10.1006/viro.2000.0761. PubMed PMID: 11277691.
3. Downie AW, Taylor-Robinson CH, Caunt AE, Nelson GS, Manson-Bahr PE, Matthews TC. Tanapox: a new disease caused by a pox virus. British medical journal. 1971;1(5745):363-8. Epub 1971/02/13. doi: 10.1136/bmj.1.5745.363. PubMed PMID: 5541925; PMCID: PMC1795031.
4. Jezek Z, Arita I, Szczeniowski M, Paluku KM, Ruti K, Nakano JH. Human tanapox in Zaire: clinical and epidemiological observations on cases confirmed by laboratory studies. Bulletin of the World Health Organization. 1985;63(6):1027-35. Epub 1985/01/01. PubMed PMID: 3011301; PMCID: PMC2536461.
5. Bearcroft WG, Jamieson MF. An outbreak of subcutaneous tumours in rhesus monkeys. Nature. 1958;182(4629):195-6. Epub 1958/07/19. doi: 10.1038/182195a0. PubMed PMID: 13566242.
6. Knight JC, Novembre FJ, Brown DR, Goldsmith CS, Esposito JJ. Studies on Tanapox virus. Virology. 1989;172(1):116-24. Epub 1989/09/01. doi: 10.1016/0042-6822(89)90113-x. PubMed PMID: 2773312.
7. Nazarian SH, Barrett JW, Frace AM, Olsen-Rasmussen M, Khristova M, Shaban M, Neering S, Li Y, Damon IK, Esposito JJ, Essani K, McFadden G. Comparative genetic analysis of genomic DNA sequences of two human isolates of Tanapox virus. Virus Res. 2007;129(1):11-25. Epub 2007/06/19. doi: 10.1016/j.virusres.2007.05.001. PubMed PMID: 17574698.
8. Brunetti CR, Amano H, Ueda Y, Qin J, Miyamura T, Suzuki T, Li X, Barrett JW, McFadden G. Complete genomic sequence and comparative analysis of the tumorigenic poxvirus Yaba monkey tumor virus. J Virol. 2003;77(24):13335-47. Epub 2003/12/03. doi: 10.1128/jvi.77.24.13335-13347.2003. PubMed PMID: 14645589; PMCID: PMC296094.
9. Sproul EE, Metzgar RS, Grace JT, Jr. The pathogenesis of Yaba virus-induced histiocytomas in primates. Cancer research. 1963;23:671-5. Epub 1963/06/01. PubMed PMID: 13978564.
10. Downie AW. Serological evidence of infection with Tana and Yaba pox viruses among several species of monkey. The Journal of hygiene. 1974;72(2):245-50. Epub 1974/04/01. doi: 10.1017/s0022172400023445. PubMed PMID: 4362411; PMCID: PMC2130503.
11. Monroe BP, Nakazawa YJ, Reynolds MG, Carroll DS. Estimating the geographic distribution of human Tanapox and potential reservoirs using ecological niche

modeling. International journal of health geographics. 2014;13:34. Epub 2014/09/27. doi: 10.1186/1476-072x-13-34. PubMed PMID: 25255815; PMCID: PMC4189193.
12. Ambrus JL, Strandström HV. Susceptibility of Old World monkeys to Yaba virus. Nature. 1966;211(5051):876. Epub 1966/08/20. doi: 10.1038/211876a0. PubMed PMID: 4291005.
13. Grace JT, Jr., Mirand EA. Human susceptibility to a simian tumor virus Annals of the New York Academy of Sciences. 1963;108:1123-8. Epub 1963/11/04. doi: 10.1111/j.1749-6632.1963.tb13439.x. PubMed PMID: 14081494.
14. Stich A, Meyer H, Köhler B, Fleischer K. Tanapox: first report in a European traveller and identification by PCR. Trans R Soc Trop Med Hyg. 2002;96(2):178-9. Epub 2002/06/12. doi: 10.1016/s0035-9203(02)90295-6. PubMed PMID: 12055809.
15. McFadden G. Poxvirus tropism. Nature reviews Microbiology. 2005;3(3):201-13. Epub 2005/03/02. doi: 10.1038/nrmicro1099. PubMed PMID: 15738948; PMCID: PMC4382915.
16. Moss B. Poxvirus cell entry: how many proteins does it take? Viruses. 2012;4(5):688-707. Epub 2012/07/04. doi: 10.3390/v4050688. PubMed PMID: 22754644; PMCID: PMC3386626.
17. Jacobs BL, Langland JO. When two strands are better than one: the mediators and modulators of the cellular responses to double-stranded RNA. Virology. 1996;219(2):339-49. Epub 1996/05/15. doi: 10.1006/viro.1996.0259. PubMed PMID: 8638399.
18. Dar AC, Sicheri F. X-ray crystal structure and functional analysis of vaccinia virus K3L reveals molecular determinants for PKR subversion and substrate recognition. Molecular cell. 2002;10(2):295-305. Epub 2002/08/23. PubMed PMID: 12191475.
19. Adomavicius T, Guaita M, Zhou Y, Jennings MD, Latif Z, Roseman AM, Pavitt GD. The structural basis of translational control by eIF2 phosphorylation. Nat Commun. 2019;10(1):2136. Epub 2019/05/16. doi: 10.1038/s41467-019-10167-3. PubMed PMID: 31086188; PMCID: PMC6513899.
20. Romano PR, Zhang F, Tan SL, Garcia-Barrio MT, Katze MG, Dever TE, Hinnebusch AG. Inhibition of double-stranded RNA-dependent protein kinase PKR by vaccinia virus E3: role of complex formation and the E3 N-terminal domain. Molecular and cellular biology. 1998;18(12):7304-16. Epub 1998/11/20. PubMed PMID: 9819417; PMCID: PMC109312.
21. Langland JO, Jacobs BL. The role of the PKR-inhibitory genes, E3L and K3L, in determining vaccinia virus host range. Virology. 2002;299(1):133-41. Epub 2002/08/09. PubMed PMID: 12167348.
22. Langland JO, Jacobs BL. Inhibition of PKR by vaccinia virus: role of the N- and C-terminal domains of E3L. Virology. 2004;324(2):419-29. Epub 2004/06/23. doi: 10.1016/j.virol.2004.03.012. PubMed PMID: 15207627.

23. Peng C, Haller SL, Rahman MM, McFadden G, Rothenburg S. Myxoma virus M156 is a specific inhibitor of rabbit PKR but contains a loss-of-function mutation in Australian virus isolates. Proceedings of the National Academy of Sciences of the United States of America. 2016;113(14):3855-60. Epub 2016/02/24. doi: 10.1073/pnas.1515613113. PubMed PMID: 26903626; PMCID: PMC4833222.
24. Park C, Peng C, Brennan G, Rothenburg S. Species-specific inhibition of antiviral protein kinase R by capripoxviruses and vaccinia virus. Annals of the New York Academy of Sciences. 2019;1438(1):18-29. Epub 2019/01/16. doi: 10.1111/nyas.14000. PubMed PMID: 30644558.
25. Cao J, Varga J, Deschambault Y. Poxvirus encoded eIF2α homolog, K3 family proteins, is a key determinant of poxvirus host species specificity. Virology. 2020;541:101-12. Epub 2020/02/15. doi: 10.1016/j.virol.2019.12.008. PubMed PMID: 32056708.
26. Park C, Peng C, Rahman MJ, Haller SL, Tazi L, Brennan G, Rothenburg S. Orthopoxvirus K3 orthologs show virus- and host-specific inhibition of the antiviral protein kinase PKR. PLoS Pathog. 2021;17(1):e1009183. Epub 2021/01/15. doi: 10.1371/journal.ppat.1009183. PubMed PMID: 33444388; PMCID: PMC7840043.
27. Carpentier KS, Esparo NM, Child SJ, Geballe AP. A Single Amino Acid Dictates Protein Kinase R Susceptibility to Unrelated Viral Antagonists. PLoS Pathog. 2016;12(10):e1005966. Epub 2016/10/26. doi: 10.1371/journal.ppat.1005966. PubMed PMID: 27780231; PMCID: PMC5079575.
28. Rahman MM, Liu J, Chan WM, Rothenburg S, McFadden G. Myxoma virus protein M029 is a dual function immunomodulator that inhibits PKR and also conscripts RHA/DHX9 to promote expanded host tropism and viral replication. PLoS Pathog. 2013;9(7):e1003465. Epub 2013/07/16. doi: 10.1371/journal.ppat.1003465. PubMed PMID: 23853588; PMCID: PMC3701710.
29. Elde NC, Child SJ, Geballe AP, Malik HS. Protein kinase R reveals an evolutionary model for defeating viral mimicry. Nature. 2009;457(7228):485-9. Epub 2008/12/02. doi: 10.1038/nature07529. PubMed PMID: 19043403; PMCID: PMC2629804.
30. Vipat S, Brennan G, Park C, Haller SL, Rothenburg S. Rapid, Seamless Generation of Recombinant Poxviruses using Host Range and Visual Selection. Journal of visualized experiments : JoVE. 2020(159). Epub 2020/06/09. doi: 10.3791/61049. PubMed PMID: 32510495; PMCID: PMC8051324.
31. Rothenburg S, Seo EJ, Gibbs JS, Dever TE, Dittmar K. Rapid evolution of protein kinase PKR alters sensitivity to viral inhibitors. Nat Struct Mol Biol. 2009;16(1):63-70. Epub 2008/12/02. doi: 10.1038/nsmb.1529. PubMed PMID: 19043413; PMCID: PMC3142916.
32. Beattie E, Tartaglia J, Paoletti E. Vaccinia virus-encoded eIF-2 alpha homolog abrogates the antiviral effect of interferon. Virology. 1991;183(1):419-22. Epub 1991/07/01. PubMed PMID: 1711259.

33. Esposito J, Condit R, Obijeski J. The preparation of orthopoxvirus DNA. Journal of virological methods. 1981;2(3):175-9. Epub 1981/02/01. doi: 10.1016/0166-0934(81)90036-7. PubMed PMID: 6268651.
34. Sievers F, Wilm A, Dineen D, Gibson TJ, Karplus K, Li W, Lopez R, McWilliam H, Remmert M, Söding J, Thompson JD, Higgins DG. Fast, scalable generation of high-quality protein multiple sequence alignments using Clustal Omega. Molecular systems biology. 2011;7:539. Epub 2011/10/13. doi: 10.1038/msb.2011.75. PubMed PMID: 21988835; PMCID: PMC3261699.
35. Kumar S, Stecher G, Li M, Knyaz C, Tamura K. MEGA X: Molecular Evolutionary Genetics Analysis across Computing Platforms. Molecular biology and evolution. 2018;35(6):1547-9. Epub 2018/05/04. doi: 10.1093/molbev/msy096. PubMed PMID: 29722887; PMCID: PMC5967553.
36. Kawagishi-Kobayashi M, Silverman JB, Ung TL, Dever TE. Regulation of the protein kinase PKR by the vaccinia virus pseudosubstrate inhibitor K3L is dependent on residues conserved between the K3L protein and the PKR substrate eIF2alpha. Molecular and cellular biology. 1997;17(7):4146-58. Epub 1997/07/01. doi: 10.1128/mcb.17.7.4146. PubMed PMID: 9199350; PMCID: PMC232268.
37. Davies MV, Chang HW, Jacobs BL, Kaufman RJ. The E3L and K3L vaccinia virus gene products stimulate translation through inhibition of the double-stranded RNA-dependent protein kinase by different mechanisms. J Virol. 1993;67(3):1688-92. Epub 1993/03/01. doi: 10.1128/jvi.67.3.1688-1692.1993. PubMed PMID: 8094759; PMCID: PMC237544.
38. Vieira Gomes AM, Souza Carmo T, Silva Carvalho L, Mendonça Bahia F, Parachin NS. Comparison of Yeasts as Hosts for Recombinant Protein Production. Microorganisms. 2018;6(2). Epub 2018/05/02. doi: 10.3390/microorganisms6020038. PubMed PMID: 29710826; PMCID: PMC6027275.
39. Dar AC, Dever TE, Sicheri F. Higher-order substrate recognition of eIF2alpha by the RNA-dependent protein kinase PKR. Cell. 2005;122(6):887-900. Epub 2005/09/24. doi: 10.1016/j.cell.2005.06.044. PubMed PMID: 16179258.
40. Rothenburg S, Brennan G. Species-Specific Host-Virus Interactions: Implications for Viral Host Range and Virulence. Trends in microbiology. 2020;28(1):46-56. Epub 2019/10/11. doi: 10.1016/j.tim.2019.08.007. PubMed PMID: 31597598; PMCID: PMC6925338.
41. Bratke KA, McLysaght A, Rothenburg S. A survey of host range genes in poxvirus genomes. Infect Genet Evol. 2013;14:406-25. Epub 2012/12/27. doi: 10.1016/j.meegid.2012.12.002. PubMed PMID: 23268114; PMCID: PMC4080715.
42. Myskiw C, Arsenio J, Hammett C, van Bruggen R, Deschambault Y, Beausoleil N, Babiuk S, Cao J. Comparative analysis of poxvirus orthologues of the vaccinia virus E3 protein: modulation of protein kinase R activity, cytokine responses, and virus

pathogenicity. J Virol. 2011;85(23):12280-91. Epub 2011/09/16. doi: 10.1128/jvi.05505-11. PubMed PMID: 21917954; PMCID: PMC3209343.
43. Meng X, Chao J, Xiang Y. Identification from diverse mammalian poxviruses of host-range regulatory genes functioning equivalently to vaccinia virus C7L. Virology. 2008;372(2):372-83. Epub 2007/12/07. doi: 10.1016/j.virol.2007.10.023. PubMed PMID: 18054061; PMCID: PMC2276162.